Dynamic Hybrid Materials: Hydrogel Actuators and Catalytic Microsystems

Dynamic Hybrid Materials: Hydrogel Actuators and Catalytic Microsystems

A dissertation presented

by

Lauren Dell Zarzar

to

The Department of Chemistry and Chemical Biology

in partial fulfillment of the requirements

for the degree of

Doctor of Philosophy

in the subject of

Chemistry

Harvard University

Cambridge, Massachusetts

May 2013

Dissertation Advisor: Professor Joanna Aizenberg Lauren Dell Zarzar

Dynamic Hybrid Materials: Hydrogel Actuators and Catalytic Microsystems

Abstract

Dynamic materials which can sense changes in their surroundings and subsequently respond or adapt by autonomously altering their functionality, surface chemistry, transparency, color, wetting behavior, adhesiveness, shape, etc. are primed to be integral components of future "smart" technologies. However, such systems can be quite complex and often require intricate coordination between both chemical and mechanical inputs/outputs as well as the combination of multiple materials working cooperatively to achieve the proper functionality. It is critical to not only understand the fundamental behaviors of existing dynamic chemo-mechanical systems, but also to apply that knowledge and explore new avenues for design of novel materials platforms which could provide a basis for future adaptive technologies.

Part 1 explores the use of environmentally-sensitive hydrogels, either alone or within arrays of high-aspect-ratio nano/microstructures, as chemo-mechanical actuators. Chapters 1 through 7 describe a bio-inspired approach to the design of hybrid actuating surfaces in which the volume-changing hydrogel acts as the "muscle" that reversibly actuates the microstructured "bone". In particular, the different actuation mechanisms arising from variations in how the hydrogel is integrated into the structure array, how chemical signals can be used to manipulate actuation parameters, and finally how such a system may be used for applications ranging from adaptive optics to manipulation of chemical reactions are described. Chapter 8 discusses the use

of responsive hydrogel scaffolds as a means to mechanically compress cells and direct differentiation.

Part II explores dynamic microsystems involving the integration of catalytic sites within intricately structured 3D microenvironments. Specifically, we explore a generalizable and straightforward route to fabricate microscale patterns of nanocrystalline platinum and palladium using multiphoton lithography. The catalytic, electrical, and electrochemical properties are characterized, and we demonstrate high resolution integration of catalysts within 3D-defined microenvironments to generate directed particle and fluid transport.

Contents

Acknowledgements

First and foremost I thank my advisor, Joanna Aizenberg, for her generous support and guidance. Her enthusiasm for science and passion for learning is contagious, and it comes through in the wonderful research group which she has assembled. It was a joy to work with all members of the Aizenberg group throughout the years, but I wish to specifically thank my closer collaborators both from Joanna's group and other groups within Harvard. I thank Philseok Kim for mentoring me during my first year as a graduate student. I am grateful to Alison Grinthal for always being so generous with her time when helping me edit manuscripts. Qihan Liu, Yuhang Hu, and Mathias Kolle were integral in modeling the experimental systems we developed. Phil Kim, Ximin He, Michael Aizenberg, and Ankita Shastri were experimental collaborators on the hydrogel actuator projects, and I always valued their insights and suggestions. I thank Basma Hashmi and Don Ingber for giving me the opportunity to investigate the use of hydrogels as responsive cell scaffolds. I wish to thank my Graduate Advising Committee members, Adam Cohen and Zhigang Suo, for their continued guidance. I also want to acknowledge collaborators outside of Harvard, namely Bryan Kaehr and Jeff Brinker of Sandia National Laboratories, with whom I had the opportunity to collaborate during three summers as part of the National Institute for Nano Engineering initiatives. I am also thankful for the financial support I have received from the National Defense Science and Engineering Graduate Research Fellowship and the National Science Foundation Graduate Research Fellowship.

Last but not least, I sincerely thank my friends and family for their utmost support. Aaron, thank you for putting up with me all those nights after failed experiments, and always reminding me that there's a life outside of the lab. Mom and Dad, thank you for always encouraging me to do what I love, even if it means becoming a professional student!

List of Abbreviations

AAc – acrylic acid
AAm – acrylamide
AFM – atomic force microscopy
APS – ammonium persulfate
BIS – *N,N'*-methylenebisacrylamide
DMSO – dimethyl sulfoxide
DSC – differential scanning calorimetry
EDS – energy dispersive X-ray spectroscopy
EG – ethylene glycol
GMA – glycidyl methacrylate
HAIRS – hydrogel-actuated integrated responsive system
HAR – high aspect ratio
ITO – indium tin oxide
LCST – lower critical solution temperature
MPL – multiphoton lithography
NAS – *N*-acryloxysuccinimide
NIPAAm – *N*-isopropylacrylamide
PAAm – polyacrylamide
PDMS – polydimethylsiloxane
PNIPAAm – poly(*N*-isopropylacrylamide)
PPy – polypyrrole
SEM – scanning electron microscopy
TEM – transmission electron microscopy
VPT – volume-phase transition

List of Figures

Part I: Hydrogel Actuators

Introduction and Background

Design of synthetic systems that sense and respond to environmental stimuli and chemical signals on both a microscopic and macroscopic level has been a longstanding scientific pursuit.[1] But from a biological perspective, the interplay between signaling molecules and/or external stimuli and mechanical reconfiguration is commonplace, indeed fundamental, to nature's ability to self-regulate and adapt. From the nanoscale (the motor-like action of ATPases,[2] the conformational changes of proteins allowing allosteric regulation[3]) to the micro/macroscale (phototropism,[4] proton gradients that drive the beating of flagella,[5] and the motion of bacteria directed by chemotaxis[6]), chemical signals correlated with a structural response, reconfiguration, or movement lie at the heart of many biological processes. Such diversity in the materials systems and mechanisms provides for an equally large range of elegant applications of chemo-mechanical actuators.[7] The beating of cilia in the respiratory tract helps to prevent biofilm formation,[8] while the opening and closing of echinoderm pedicellariae are used for body cleaning and food capture.[9] Cephalopods are artful masters of camouflage, making use of chromatophores that expand and contract to allow the animals to rapidly change color.[10] The widespread demonstrated importance and versatility of such naturally occurring chemo-mechanical systems, particularly their extensive diversity in terms of scale, mechanism, function, and structure, serve as inspiration for the development of "smart" materials that are able to autonomously sense and adapt via self-regulated structural reconfiguration to trigger responsive changes in chemistry, wetting behavior, optical properties, thermal properties, adhesion, mechanical properties, or propulsive forces among others.[1c, 11] Ultimately, understanding and harnessing the power of combining chemically-induced mechanical responses with meaningful

outcomes in terms of structure-function relationships, switchable surface properties, force generation, or directed chemical cascades, will be extremely valuable for designing responsive and adaptive systems.

Researchers have taken various approaches to fabricating biomimetic actuators, among which are biomorph actuators made using Micro Electromechanical Systems (MEMS) technology,[12] magnetically actuated polydimethylsiloxane (PDMS) structures,[13] and artificial cilia or actuators made from responsive gel.[14] However, microscale actuation systems which exhibit reversible chemo-mechanical responses, patternable control of actuation direction, and a high degree of customizability for different applications, have proven difficult to achieve.

Chemo-mechanical Response of Hydrogels

From among the many classes of stimuli-responsive materials, hydrogels in particular have received substantial attention due to their ability to translate a wide range of chemical signals into a mechanical output in the form of the gel's reversible volume change.[15] Responsive hydrogels are cross-linked polymer networks which reversibly swell and shrink in aqueous environments in response to various stimuli including temperature,[16] pH,[17] humidity, light,[18] biomolecules,[19] ionic strength,[20] magnetic[21] and electric fields, redox state,[22] etc. (Figure 1).

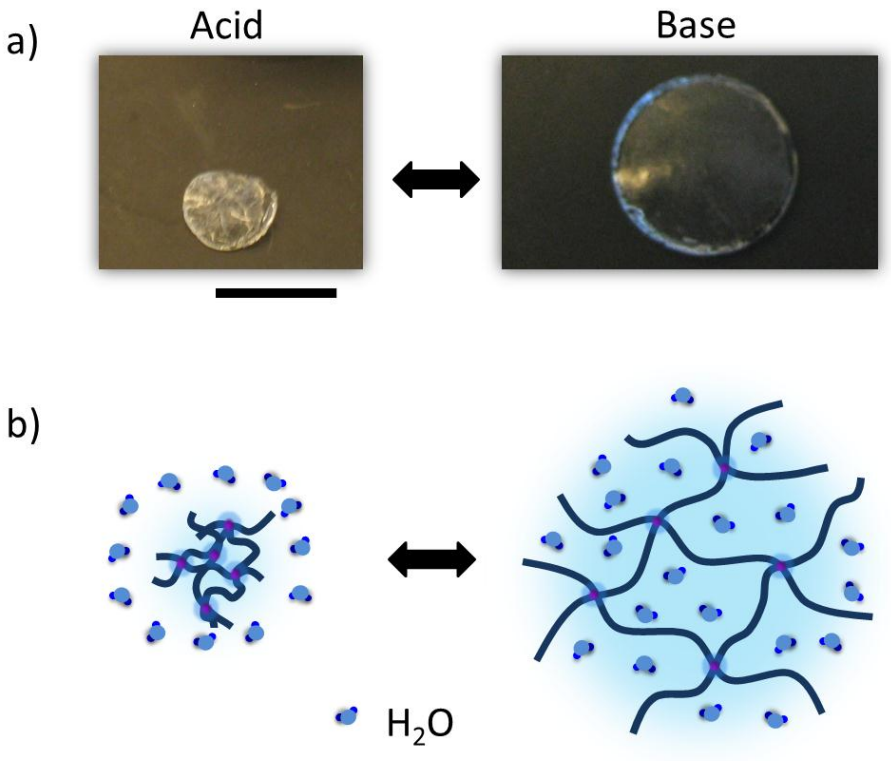

Figure 1. a) A macroscale disk of pH-responsive poly(AAm-*co*-AAc) hydrogel in both contracted and swollen states, exhibiting a large swelling ratio. Scale = 1 cm. b) Schematic of the swelling and deswelling of a cross-linked polymer hydrogel.

The mechanism by which hydrogels translate an external environmental stimulus into a mechanical response depends upon the chemical moieties present in the hydrogel network. The three types of hydrogel primarily discussed herein are humidity-responsive cross-linked poly(acrylamide) (PAAm), pH-responsive cross-linked poly(acrylamide-*co*-acrylic acid) [poly(AAm-*co*-AAc)], and temperature-responsive cross-linked poly(*N*-isopropylacrylamide) (PNIPAAm) (Figure 2). All are cross-linked with *N,N'*-methylenebisacrylamide (BIS). PAAm is only sensitive to the presence or absence of water so to induce volume change it must be dried and rehydrated. When acrylic acid is present, such as in poly(AAm-*co*-AAc), the hydrogel becomes pH-responsive. When the acid is protonated and in its neutral form (at about pH<4.3,

the pK_a of the acrylic acid) the hydrogel is in its contracted state. However, when the pH is raised and the acid becomes deprotonated, the presence of the hydrogen ions in the network generates an increase in osmotic pressure leading to an influx of water molecules causing the hydrogel to swell.[23] Acrylic acid may be replaced by any number of other polymerizable monomers with a different pK_a in order to tune the responsive nature of the gel.

PNIPAAm has the unique property of inverse solubility such that when the hydrogel is heated the polymers undergo an abrupt macromolecular transition from a hydrophilic to a hydrophobic structure.[16] The temperature at which this transition occurs is called the lower critical solution temperature (LCST). PNIPAAm typically has an LCST of 32°C but addition of even small quantities of co-monomers can be used to alter the hydrophobicity of the polymers and tune the LCST; introduction of a more hydrophobic monomer tends to decrease the LCST, while addition of a more hydrophilic monomer tends to increase the LCST.

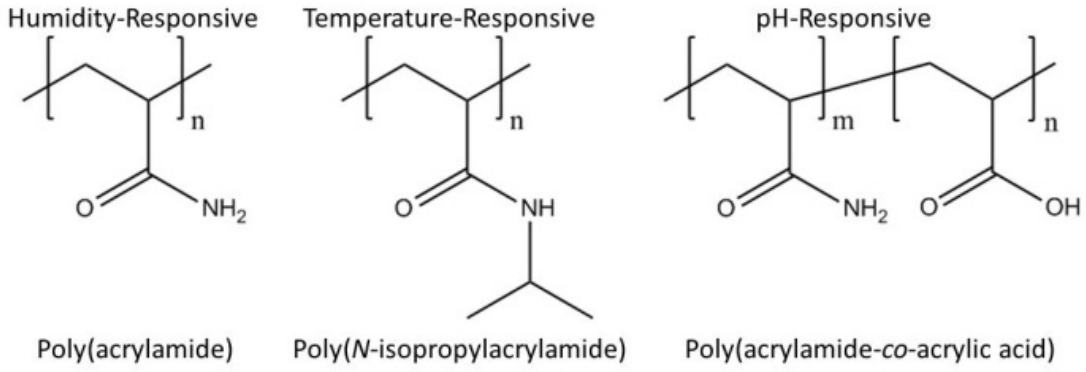

Figure 2. The chemical structures of the three different responsive hydrogels. All are cross-linked with *N,N'*-methylenebisacrylamide.

Introduction to Hydrogel-Actuated Integrated Responsive Systems (HAIRS)

Although hydrogels on their own are effective, highly tunable chemo-mechanical actuators, combining hydrogels with other materials to create composite systems provides routes

to properties and functions not achievable with a single material alone. For example, hydrogels are generally soft and cannot often be molded into intricate, high-aspect-ratio (HAR) structures; if the gels are made stiffer to increase their shape retention, then their swelling ratio may be effectively decreased. Chemically, certain moieties are required in the hydrogel to render it with specific sensitivity, so it may be difficult to tailor other properties (surface chemistry, optical properties) without adding other chemical moieties into the gel thereby disrupting the efficacy of response. However, if the hydrogel is combined with other materials having complementary properties (certain stiffness, surface chemistry, etc.), we may create hybrid systems capable of functioning in ways in which neither material is capable on its own.

In particular, we use the volume change of hydrogels in hydrogel-actuated integrated responsive systems (HAIRS) as that of a "muscle" to move polymeric structures (Figure 3). For instance, when combined with "skeletal" arrays of HAR structures, the hydrogel muscle is able to reversibly reconfigure and bend the embedded nano/microstructures, providing a means to switch surface properties and geometries in response to environmental cues. The interplay between controllable parameters such as the location and type of hydrogel stimulus, the geometry, mechanical properties, and surface chemistry of HAR structures, and the patterning and topography of the hydrogel within the confinement of the structures provides for a highly tunable and customizable chemo-mechanical hybrid system based on just a few individual material components.

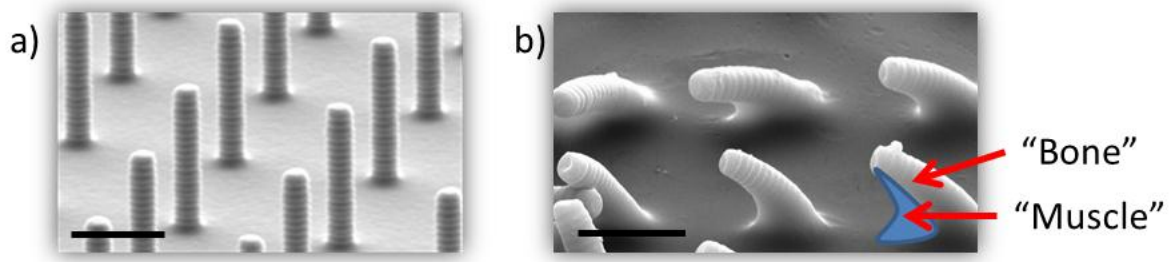

Figure 3. a) HAR post structures before addition of hydrogel. b) Scanning electron micrograph (SEM) showing the surface after addition of hydrogel; the hydrogel "muscle" is dried (contracted) and HAR posts are bent over. If the hydrogel was swelled again the post would stand up. The blue area in b) highlights the location of the hydrogel on each post. Scale = 5 μm.

The first HAIRS consisted of rigid silicon HAR post structures embedded within PAAm.[24] Such systems were demonstrated to have very interesting properties such as reversible wetting behavior.[25] Because silicon structures are stiff, relatively high aspect ratios (>20) should be used to ensure that the structures will be bent significantly by the forces exerted by the gel without breaking. However, the strain induced at the base of the structures during the actuation process still may easily exceed the fracture strain of silicon resulting in broken posts upon hydrogel contraction. So not only are the silicon structures prone to fracture, but they are very expensive and time consuming to produce, setting significant limitations on their application. Therefore, one approach to address these deficiencies is to replace the silicon with polymers, which are far cheaper, softer, and more customizable in terms of their mechanical and chemical properties, and would allow for actuation of HAR structures at the microscale with lower aspect ratios (<10) without breaking.

In the following chapters within Part 1, we examine how HAIRS were transitioned to an all-polymer system and the subsequent optimization, characterization, and application of such

hydrogel–driven actuators. We have identified several different modes of actuation (Figure 4), each leading to a diversity of responses, actuation patterns, and functions. Such actuation modes are dependent on how the hydrogel is physically integrated within the HAR structure array and also upon how the chemical stimulus is applied to the surface. We also explore how integration of the hybrid surfaces within different fluidic environments enables compartmentalized and spatially patterned application of stimuli which further expands the controllability and applicability of the chemo-mechanical response.

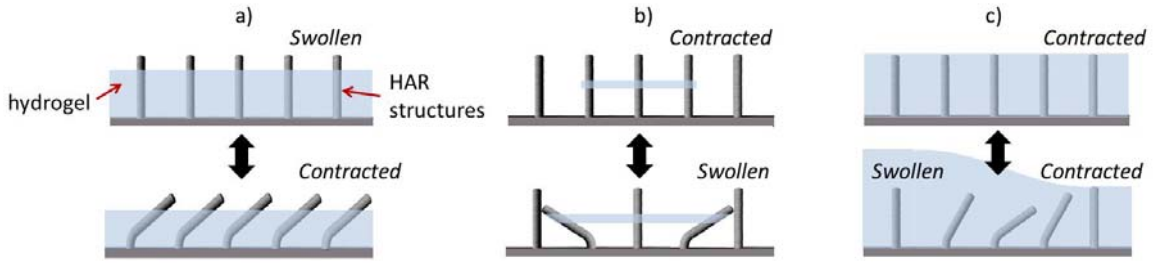

Figure 4. Different modes of HAIRS actuation to be discussed in detail in following chapters. a) Homogeneous expansion and contraction of thin, uniform hydrogel films generates actuation of structures with domains of uniform bending orientation. b) Thin hydrogel films tethered to the middle or tips of the structures and free from attachment to the basal surface generate radial actuation in which structures are pushed outward from the gel center. c) Chemical gradients across the HAIRS surface generate asymmetric forces within the gel thereby actuating the underlying structures in accordance with the gradient location and direction.

Chapter 1: Transitioning to All-Polymer HAIRS

Parts of this chapter have been adapted from: P. Kim, L. D. Zarzar, X. Zhao, A. Sidorenko and J. Aizenberg, "Microbristle in gels: toward all-polymer reconfigurable hybrid surfaces." *Soft Matter*, **6**, 750-755 (2010).

Parts of this chapter have been adapted from: P. Kim, A. K. Epstein, M. Khan, L. D. Zarzar, D. J. Lipomi, G. M. Whitesides and J. Aizenberg, "Structural transformation by electrodeposition on patterned substrates (STEPS): a new versatile nanofabrication method." *Nano Letters*, **12**, 527–533 (2012).

Collaborators: Philseok Kim, Alexander Sidorenko, Joanna Aizenberg

Introduction

HAIRS are composed of two fundamental components: 1) nano/microscale structures which provide the skeletal foundation for the hybrid surface and are to be dynamically reconfigured, and 2) a responsive hydrogel polymerized within the confinement of, and covalently attached to, the structures such that a volume-phase transition (VPT) of the gel induces reconfiguration of the structures. When choosing materials and geometries to be used in HAIRS, there are many parameters which can be tuned for desired properties and functions, a clear advantage of using an all-polymer, highly customizable system.

Choice of HAR Structure Geometry and Material

Upon replacing silicon as used in the first HAIRS systems with polymer HAR structures, an important parameter to consider is the effective stiffness of the structures (S_{eff}) which takes into account both the material modulus and the structure geometry. For two posts with a circular cross-section, the ratio of their effective stiffness is expressed as:

$$\frac{S_{1eff}}{S_{2eff}} = \left(\frac{E_1}{E_2}\right)\left(\frac{l_2}{l_1}\right)^3\left(\frac{d_1}{d_2}\right)^4$$

where E is the modulus, l is the length, and d is the diameter of the post. The silicon posts previously used required a small diameter, d<300nm and a high aspect ratio (l/d >20) for actuation to occur because the material is so stiff (E=200 GPa). If the silicon could be replaced by a polymer having a modulus 2-3 orders of magnitude less, a geometrically stiffer post (microscale with lower aspect ratio) could be used instead. For example, posts made from an epoxy (E=1.5 GPa) with d=1.5 μm, l=10 μm and an aspect ratio of 6.6 would have similar effective stiffness as the silicon nanoposts. Not only would such polymer posts be less prone to breaking, but the fabrication process required to make microposts is far easier than nanoposts.[26]

To fabricate polymer surfaces, structures are replicated from silicon "master structures" via a PDMS replication process as described in detail elsewhere.[27] In brief, the silicon HAR structures are made via photolithography and a Bosch etching process. They are then plasma treated and fluorosilanized to render the surface superhydrophobic. PDMS is then poured over the silicon, cured, and peeled off to create a negative mold. The mold can be back-filled with any number of polymers (epoxies, polyurethanes, etc.). The polymer most often used in this work is a UV-curable epoxy, UVO-114 (Epoxy Technology).

Another advantage of using polymer HAR structures instead of silicon (in addition to the lower cost, less time consuming fabrication, highly-customizable chemical and mechanical

properties) is that there are significantly more routes to altering the HAR structure geometry; to make posts of a different diameter out of silicon, for instance, a new silicon wafer must be etched. However, there are a number of approaches to altering the geometry of polymer replicas.[27-28] One route is to deform the PDMS mold, which is useful for geometries obtained by shearing, stretching, or compression.[27] We more recently reported a complementary method called Structural Transformation by Electrodeposition on Patterned Substrates (STEPS) which can be used to alter structure diameter or wall-thickness (for closed cell structures) even in a gradient fashion which is useful for screening many geometries at once (Figure 5).[28] In STEPS, a conductive polymer, polypyrrole (PPy), is selectively grown on metal-coated areas of a HAR structured polymer to different thickness, thereby altering the geometry. The PPy-coated structures can then be re-replicated into PDMS to create a new mold with an entirely different set of geometric parameters.

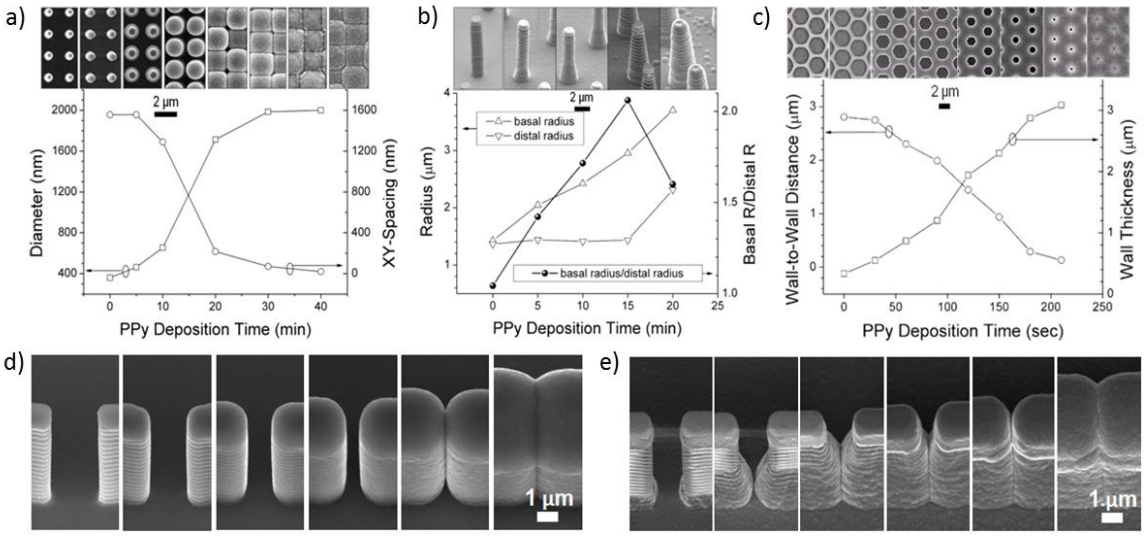

Figure 5. SEM images showing the modification of a parent HAR structure using various STEPS methods. All the images are taken from epoxy replicas of the transformed structures. a) Uniform structural transformation of a nanopost array using metal sputter-coated structures (so

Figure 5 (Continued)… the structures are uniformly coated). The plot shows the gradually increasing diameter of the posts and the decreasing space between adjacent posts as a function of the deposition time. b) Transformation of a straight micropost array into a tapered, conical micropost array by using structures coated using metal evaporation; metal is only continuous at the base of the structures so PPy is deposited first at the basal surface and gradually begins to coat the sides of the structures. The plot shows the basal and distal radius and gradual increase in the ratio between the basal and distal radii of the structures as a function of the deposition time. c) An interconnected honeycomb array undergoing uniform decrease in the size of honeycomb wells and increase in the wall thickness. d, e) Comparison of the gap filling modes on the same parent substrate using sputter-coated metal electrode d), and evaporated metal electrode e). Electrodeposition was performed in an aqueous solution containing 0.1 M sodium dodecylbenzenesulfonate and 0.1 M pyrrole. The deposition voltages are 0.55 V for a) and b), and 0.65 V for c), d), and e). Figure credit: Philseok Kim

For HAIRS to be functional, the hydrogel must be very well attached (preferentially, covalently bonded) to the HAR structures such that when the gel expands and contracts it does not delaminate from the surface nor simply slide up and down the sides of the structures. Epoxy, such as UVO-114, does not have good adhesion to hydrogel so delamination of the hydrogel may occur as soon as the hydrogel swells. In order to surface-functionalize the epoxy such that the hydrogel can covalently bond to the surface, the bi-functional monomer glycidyl methacrylate (GMA) may be mixed into the epoxy pre-polymer to provide surface acrylate groups which can bind to the hydrogel (Figure 6).[26]

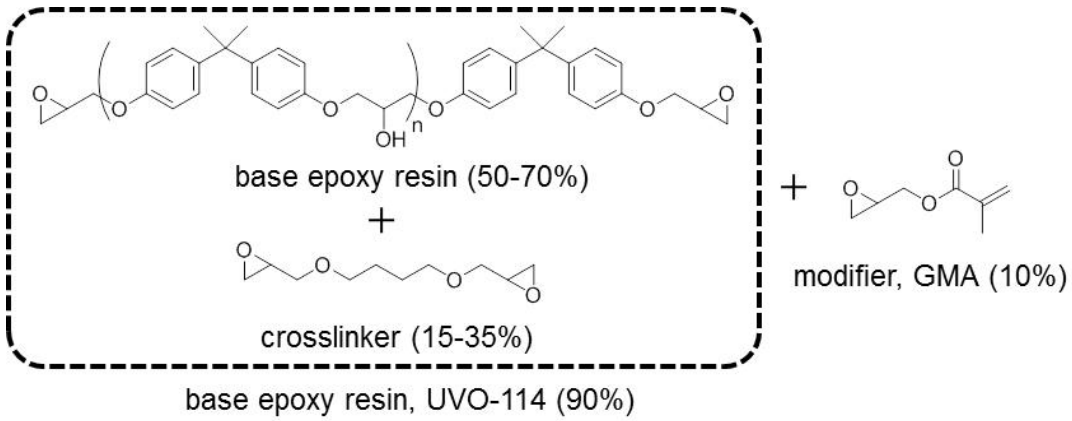

Figure 6. Chemical modification of the UVO-114 epoxy resin with glycidyl methacrylate provides surface acrylate groups on the polymer replicas for hydrogel attachment. Figure credit: Philseok Kim

Choice of Hydrogel

The hydrogel used is also highly variable in its chemical composition depending on the desired stimulus sensitivity, swelling ratio, modulus, etc. The gels primarily described herein are humidity responsive PAAm, pH-responsive poly(AAm-*co*-AAc), and temperature responsive PNIPAAm. However, other types of hydrogels (such as light-responsive hydrogels,[29] self-oscillating gels,[22, 30] biomolecule-responsive gels,[19a, 31] or pH/temperature/humidity-responsive hydrogels of differing chemical composition) could also be incorporated into HAIRS. Hydrogels in general swell and contract reversibly, and therefore the actuation in HAIRS is similarly highly reversible and the actuation can be cycled many times with little system fatigue.

Some parameters to consider when choosing or designing a gel to be used in HAIRS are the swelling ratio and wettability on the HAR structures. If the swelling ratio is too small, not enough force will be generated to induce actuation, while if the swelling ratio is too large (or the gel is too thick) creasing in the hydrogel can occur which might be undesirable. Wettability of

the hydrogel precursor on the structured surface is also significant, because the hydrogel should (for some modes of actuation) be made to cover the base of the structures rather than form a gel layer sitting on top of the structures. Compatibility of the hydrogel solvent and polymer used for structure replication is important as well. For example, solvents like dimethyl sulfoxide (DMSO), which is sometimes used as a solvent for PNIPAAm precursor solutions, can swell epoxy and cause deformation of the underlying HAR structure surface.

Experimental

HAIRS fabrication: All chemicals were used as received. UVO-114 was purchased from Epoxy Technology, (tridecafluoro-1,1,2,2-tetrahydrooctyl)triethoxysilane and glycidyl methacrylate were purchased from Sigma-Aldrich, PDMS (Dow-Sylgard 184) was purchased from Ellsworth.

Silicon masters were made via a Bosch etching process.[32] They were then plasma treated and silanized with (tridecafluoro-1,1,2,2-tetrahydrooctyl)triethoxysilane in a desiccator under vacuum for at least 24 hours. PDMS in a 10:1 ratio of base to hardener was mixed for several minutes then degassed before pouring over the silanized wafer in a petri dish. Further degassing may be needed to remove all the bubbles before curing the PDMS at 70°C for at least 2 hours. After cooling, the PDMS was peeled off of the silicon to yield a negative mold.

To make a polymer replica, a mixture of 9:1 UVO-114:GMA was poured over the PDMS and a glass slide or coverslip was used as a backing. The epoxy was cured under a UV lamp (100 W Blak-Ray with a 385 nm band-pass filter, power at 385 nm: ~10 mW cm^{-2}) for about 20 minutes and peeled off to yield an array of structures identical in shape to the original silicon master.

To measure the modulus of the UVO-114, four-point flexure experiments were performed using a dual column universal materials testing system (Model 5566, Instron) with *ca.* 63 mm long bar specimens with a bending rate of 50 mm/min until a maximum of 4 mm deflection or 500 N applied force. The load force-deflection curve was linearly fitted to find the slope which was subsequently used to find the Young's modulus of the polymers tested.

STEPS protocol: Pyrrole (Sigma-Aldrich) was purified by an alumina column prior to use. An aqueous solution of 0.1 M pyrrole and 0.1 M sodium dodecylbenzene sulfonate (Sigma-Aldrich) was prepared and purged by dry nitrogen for 10 minutes. A gold-coated parent substrate, acting as a working electrode, was placed into the solution. The polypyrrole films were electrochemically deposited using a standard three electrode configuration. An anodic potential of +0.55 V to +0.65V *vs*. Ag/AgCl (saturated with NaCl) was applied under a potentiostatic condition and a platinum mesh was used as the counter electrode. A gradient of the thickness of the deposited polypyrrole film was created by withdrawing the sample at a constant rate from the solution of a total deposition time. Freshly deposited polypyrrole layer was washed with deionized water and dried by either blowing air or critical point drying.

Chapter 2: Incorporating HAIRS into Fluidic Environments

Parts of this chapter have been adapted from: L. D. Zarzar, P. Kim and J. Aizenberg, "Bio-inspired design of submerged hydrogel-actuated polymer microstructures operating in response to pH." *Advanced Materials*, **23**, 1442-1446 (2011).

Parts of this chapter have been adapted from: X. He, M. Aizenberg, O. Kuksenok, L. D. Zarzar, A. Shastri, A. C. Balazs and J. Aizenberg, "Synthetic homeostatic materials with chemo-mechano-chemical self-regulation." *Nature*, **487**, 214-218 (2012).

Collaborators: Ximin He, Joanna Aizenberg

Introduction

With the exception of humidity responsive gels, for which the stimulus is the presence or absence of water, all other responsive hydrogels require a fluidic environment to apply a stimulus. Consequently, development of different approaches for integrating HAIRS within fluidic/microfluidic environments is essential to providing variable routes for patterning and compartmentalizing application of stimuli. A number of different configurations of the hybrid surface and its components (hydrogel and structures) with respect to the environment collectively allow for both horizontal and vertical compartmentalization of the stimulus to enable enhanced control over location, pattern, and rate of stimulus application.

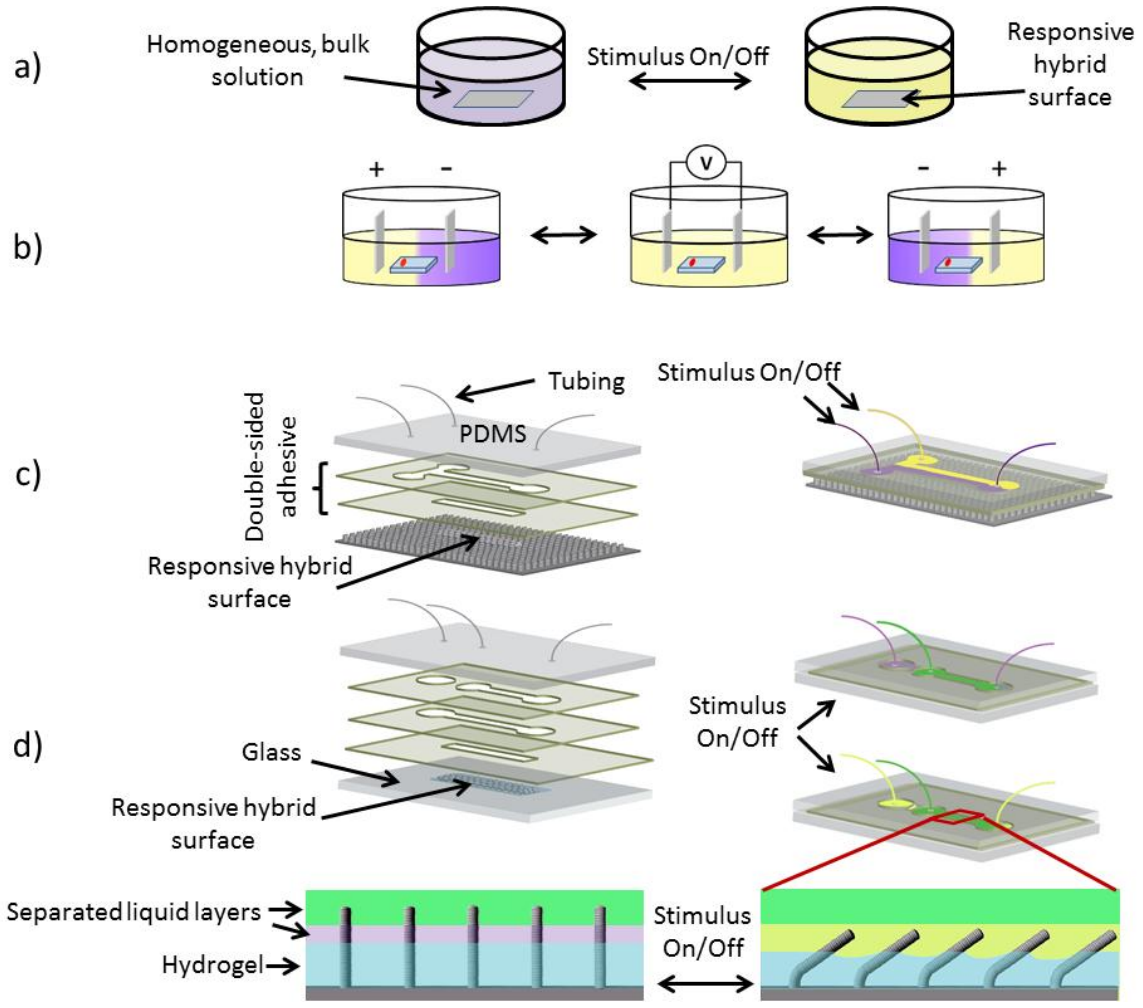

Figure 7. Schematics showing a) application of a bulk, homogenous stimulus to a hybrid surface, b) application of a reversible electrochemically generated pH gradient, c) integration of a hybrid surface into a microfluidic channel designed to apply horizontal laminar flow of different stimuli, and d) integration of a hybrid surface into a microfluidic channel designed to apply vertical laminar flow of two liquids on top of each other. Cross-section of the system in d) shows that the tips of the structures and the gel can be separated into two different environments and structures may be moved in and out of the upper liquid environment via actuation.

Homogenous Environments

The simplest fluidic environment is a bulk solution that can be changed externally, for example, by adding acid and base to induce volume change in a pH-responsive gel or by external heating to induce volume change in a temperature-responsive gel (Figure 7a). Since the solution is generally homogenous, actuation is induced simultaneously over the whole sample.

Electrochemically Generated pH Gradients

In the case of pH-responsive HAIRS, the use of an electrochemically generated pH gradient is advantageous because it allows the pH to be very gradually, controllably, and reproducibly changed over a sample (Figure 7b). Because the hydrogel VPT is fairly abrupt, such small pH changes are necessary to help elucidate the actuation dynamics.[33] The gradients are generated by electrolysis of water at the surface of partially submerged platinum electrodes; the generated hydronium and hydroxide ions subsequently migrate towards the opposite electrode thereby generating a gradient. By changing the initial pH of the solution and the voltage applied, the center and range of the gradient can be tuned.

Microfluidics

For more locally controllable actuation, HAIRS can be integrated within microfluidic systems (Figure 7c,d) with the actuating surface serving as the bottom of the microfluidic channel, laser-cut double sided adhesives defining the walls of the channel, and PDMS as the channel top.

Integration within microfluidic systems provides the ability to compartmentalize different stimuli across the surface, both horizontally (Figure 7c) and vertically (Figure 7d). Horizontal

compartmentalization, in which two solutions flow side by side, creates a well-defined chemical gradient across the surface that can not only be used to pattern where structures are bent or upright, but the gradients themselves can also drive actuation of structures as described in "Chapter 5: HAIRS Responding to Chemical Gradients". Vertical compartmentalization, in which two solutions are layered on top of each other, allows the chemical environment of the hydrogel to be distinct from, and independent of, the environment of the structures' tips. Vertical compartmentalization can be achieved without microfluidics if the two solutions are immiscible and create a stable bilayer, but for entirely aqueous systems laminar flow of two solutions, one on top of another within a microfluidic channel, can be used (Figure 8). The vertical compartmentalization is designed so that the interface of the two solutions falls just below the tips of the structures such that upon actuation the structure tips move in and out of the upper liquid layer (Figure 7d). This configuration can be used to create HAIRS that can switch on and off chemical reactions as described in "Chapter 7: Chemo-mechano-chemical Manipulation of Reactions using HAIRS".

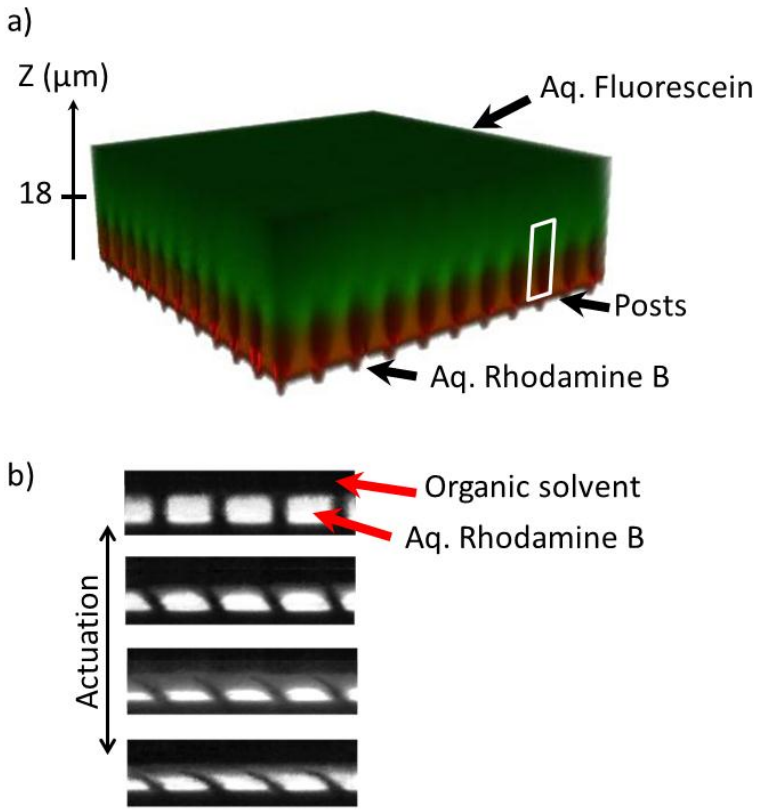

Figure 8. a) Three-dimensional confocal microscope image of a hydrogel-embedded, 18-mm-tall post array in a microfluidic channel immersed in a bilayer liquid labeled with fluorescein and rhodamine B, showing the interface height to be 12 μm. b) Confocal microscopy images of a sample cross-section during actuation in biphasic liquid in a reservoir, where the white colored part is DI water labeled with rhodamine B in bottom layer and the top layer is immiscible organic solvent. Figure credit: Ximin He

Experimental

Generation of reversible pH gradients: Sulfuric acid (H_2SO_4, 95-98%), sodium sulfate (Na_2SO_4), and bromophenol blue indicator were purchased from Sigma-Aldrich and used as received. An electrolyte solution (10 mL; 0.01 M Na_2SO_4, $1x10^{-4}$ M H_2SO_4, and bromophenol blue pH indicator in deionized water) was placed in a petri dish (55 mm diameter). Platinum

electrodes (100 nm Pt with a 10 nm Ti adhesion layer sputter coated on a glass slide) were placed vertically in the solution at a distance of 3 cm apart. The electrodes were held in place at their sides by plastic rungs that were glued with two-part epoxy to the bottom of the petri dish. A voltage of 15 V was applied to the electrodes with a DC power supply (Hewlett Packard, Model E3611A) and the switching of the input polarity in order to reverse the pH gradient direction was done manually.

Building Microfluidic Channels: Microchannels were created by using a VersaLaser laser cutter to cut T-channel patterns, inlets, and rectangular patterns (typically <1 cm long and <750 μm wide) into double sided, pressure sensitive adhesive (Graphix, Maple Heights, OH, thickness ≈ 60 μm per sheet). Two or more adhesive sheets were used together for the channel depending on the depth of channel desired. The sheets were stacked in the appropriate order to create the desired flow pattern over a HAIRS surface such as shown in Figure 7.

The HAIRS surface should have hydrogel located only within the channel or liquid injected into the channel will wick underneath the adhesive and the device will fall apart. A photomask was laser-cut in the same doubled sided adhesive material and same dimensions as, or slightly smaller than, the channel to be used (Figure 9). Only one of the sheet protectors from the double-sided cut mask was removed and the mask was adhered to a coverslip. The original white, matte back of the mask was then colored with black permanent marker. Approximately 10 μL or less of hydrogel precursor solution was placed on the HAR structures and this coverslip/mask was then placed over the droplet to induce wetting of the solution into the structure array. This process (just with a coverslip and no mask) is described in the Experimental section of "Chapter 3: HAIRS with Thin Films of Hydrogel Actuating in Response to Homogeneous Stimuli". The surface was then cured under a UV lamp (100 W Blak-Ray with

a 385 nm band-pass filter, power at 385 nm: ~10 mW cm^{-2}) until the hydrogel within the exposed channel area was cured but not so long that the area underneath the covered mask portion had also polymerized (typically 4-5 minutes). Inlets and outlets for tubing were punched into PDMS using a Harris Uni-Core 1.2 mm micro-punch and the PDMS was used to seal off the top of the channel. Solution was introduced to the channels using a syringe pump and polyethylene tubing (OD=1.09 mm). Typical flow rates ranged from 10-50 µL per minute. In the case of vertical laminar flow, the flow rates of the two liquids were adjusted so that the position of the liquid interface fell within the desired height range of the structures. In some cases, the epoxy structures themselves were replicated only within the area of the channel such that interfaces of <20 µm could be achieved, despite the fact that the adhesive layers are each 60 µm and the device requires a minimum of two adhesive layers to complete.

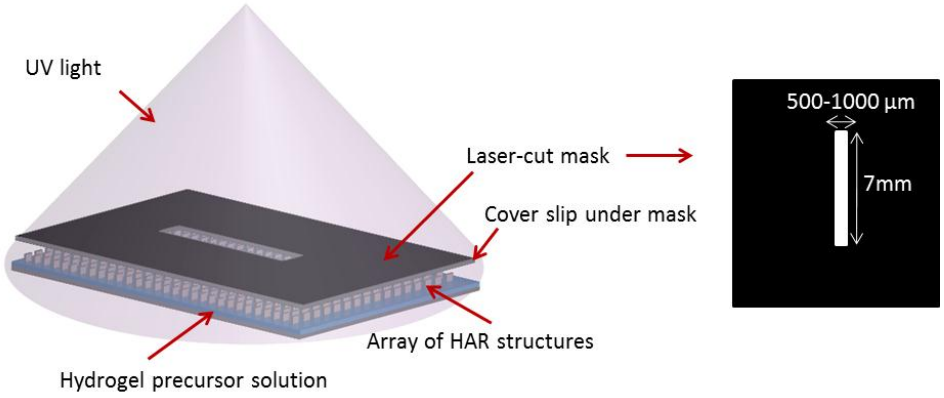

Figure 9. Schematic showing that the hydrogel should be patterned in an area the same size or smaller than the dimensions of the microchannel. The dimensions shown on the mask are variable depending on the size of the channel used.

Chapter 3: HAIRS with Thin Films of Hydrogel Actuating in Response to Homogeneous Stimuli

Parts of this chapter have been adapted from: P. Kim, L. D. Zarzar, X. Zhao, A. Sidorenko and J. Aizenberg, "Microbristle in gels: toward all-polymer reconfigurable hybrid surfaces." *Soft Matter*, **6**, 750-755 (2010).

Parts of this chapter have been adapted from: L. D. Zarzar, P. Kim and J. Aizenberg, "Bio-inspired design of submerged hydrogel-actuated polymer microstructures operating in response to pH." *Advanced Materials*, **23**, 1442-1446 (2011).

Parts of this chapter have been adapted from: P. Kim, L. D. Zarzar, M. Khan, M. Aizenberg, and J. Aizenberg, “Environmentally responsive active optics based on hydrogel-actuated deformable mirror arrays.” *Proc. SPIE*, **7927**, 792705-7 (2011).

Collaborators: Philseok Kim, Alexander Sidorenko, Ashley Taylor, Joanna Aizenberg

Introduction

This mode of actuation, in which a thin film of hydrogel lies at the base of a polymeric HAR structured surface and structure tips may protrude from the gel, is analogous to the first HAIRS systems described using silicon.[24] We expand upon the types of hydrogel used in this

HAIRS system (humidity, pH, and temperature-responsive) as well as vary the shape of the embedded structures themselves and explore how these geometric parameters affect the actuation behavior.

Mode of Actuation

In this mode of actuation the hydrogel is covalently attached to both the HAR structures and the basal surface. With these constraints, the gel cannot expand/contract laterally as it changes volume, so the only option is to increase and decrease in thickness. However, the gel also may not slide up and down the structures, so as it proceeds from the swollen state to the contracted state, the vertical shrinkage generates high downward force on the embedded structures. Ultimately, this force generates instability in the vertically oriented structures and induces them to buckle, or tilt, in similar directions, allowing the gel to contract further and reach an equilibrium state (Figure 10).[34] The structures thus actuate between two orientations upon exposure to a uniform, homogenous stimulus: 1) upright when the hydrogel is swollen and 2) bent when the hydrogel is contracted.[24, 26, 33] A variety of types of gel chemistries all exhibit this same fundamental mechanism. For example, with humidity-responsive hydrogel such as PAAm, structures are upright when the gel is wet and bent when the gel is dry (Figure 10b).[26] For temperature-responsive PNIPAAm, the structures are upright when the temperature is below the LCST of 32°C and bent when the temperature is raised above the LCST.[35] For a pH-responsive hydrogel, poly(AAm-*co*-AAc), the hydrogel transitions between a contracted state where structures are bent and a swollen state where structures are upright, between pH = 4 –5 in accordance with the pK_a of the acrylic acid (Figure 10c).[33]

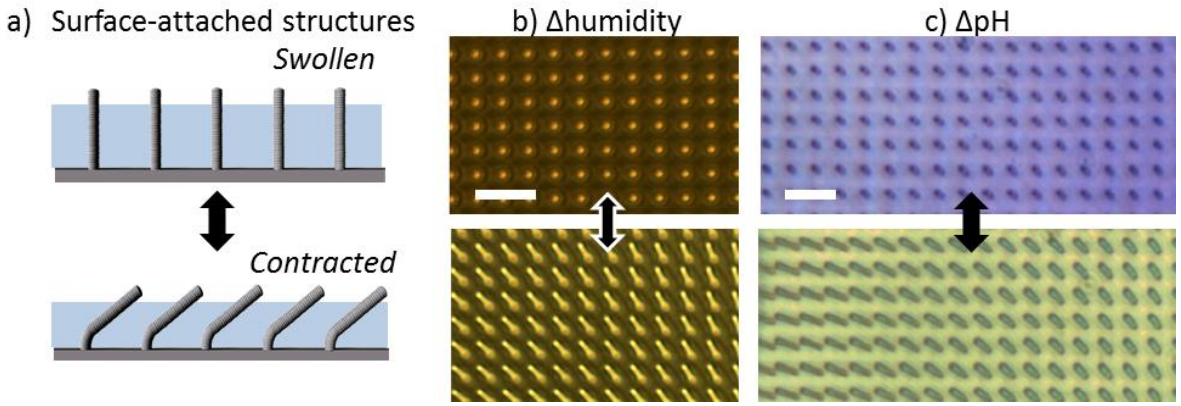

Figure 10. a) HAR structures reversibly bend upon contraction and expansion of a responsive hydrogel. b) Optical micrographs of micropost actuation with a humidity-responsive PAAm and c) pH-responsive poly(AAm-*co*-AAc) hydrogel. Note that the bending direction is uniform within small domains but begins to diverge over short distances. Color in c) arises from pH indicator. Scale = 20 μm.

pH-Responsive Actuation Dynamics

The kinetics of pH-responsive hydrogel volume change depend on a variety of factors including ion exchange rate, solvent diffusion rate, gel thickness, and crosslinking density, and the net result is that swelling and contraction are asymmetric processes where swelling is slower than contraction.[23] This asymmetry in swelling rate lends more dynamic complexity to HAIRS. However, such intricacies of the dynamics of the actuation process can be difficult to observe; even though diffusion of water into and out of the gel may be a relatively slow process and macroscale gels can take days to fully swell or contract, the hydrogels used in HAIRS are generally quite thin (on the order of 10 μm or less) so the actuation is fast (fractions of a second). One way to observe how the swelling/contraction rate is transduced to the bending of the underlying structures is to slow down the rate of pH change significantly, and thus slow down

the volume transition rate. Use of electrochemically generated pH gradients[36] provides for gradual, controllable, and reproducible rates of pH change across a sample, and this method allows us to observe in real time the phase transition of the hydrogel and how it correlates with the rates of actuation.

Such reversible pH gradients were produced in solution by applying a voltage to partially-submerged electrodes. Electrolysis of water produced hydronium and hydroxide ions at the anode and cathode respectively, and their subsequent migration toward the opposite electrode generated a stable pH gradient (see "Chapter 2: Incorporating HAIRS into Fluidic Environments" for details). The VPT of the poly(AAm-*co*-AAc) hydrogel occurs around pH = 4.3 and relatively small changes in pH around this point are needed for actuation. Therefore, we adjusted the initial pH of the electrolyte solution to 4, so that the center of the pH gradient was shifted close to $pK_{a,AAc}$ to reduce the amount of hydronium and hydroxide ions that must be produced in order to vary the pH of the solution in the region of the sample around 4.3 and to trigger actuation.

Using this method, we examined micropost movement both in an un-patterned, flat hydrogel film and in a patterned hydrogel layer with a honeycomb topography that induces microfloret actuation of the embedded microstructures. (HAIRS with topographically patterned hydrogel are discussed in detail in "Chapter 4: HAIRS with Topographically Patterned Hydrogel Responding to Homogenous Stimuli"). Representative results are shown in Figure 11. The pH change is slow enough that the VPT of the hydrogel takes place over a few seconds, and the details of the actuation could be easily recorded. We observed the differences in the rates of actuation corresponding to either contraction or expansion of the hydrogel; there is a sharp and relatively fast actuation transition upon contraction, while actuation is slow and gradual upon

swelling. The actuated polymer microstructures, in essence, function as a self-reporting system for the hydrogel dynamics, visualizing and amplifying important features of the differences in the rates of the swelling and deswelling cycles that might be hard to visualize in the gel by itself. This resultant spatiotemporal difference in the actuation rate and mode may also be advantageous for biomimetic cilia or fins, as an asymmetric beating motion is necessary to generate flow or directional movement.

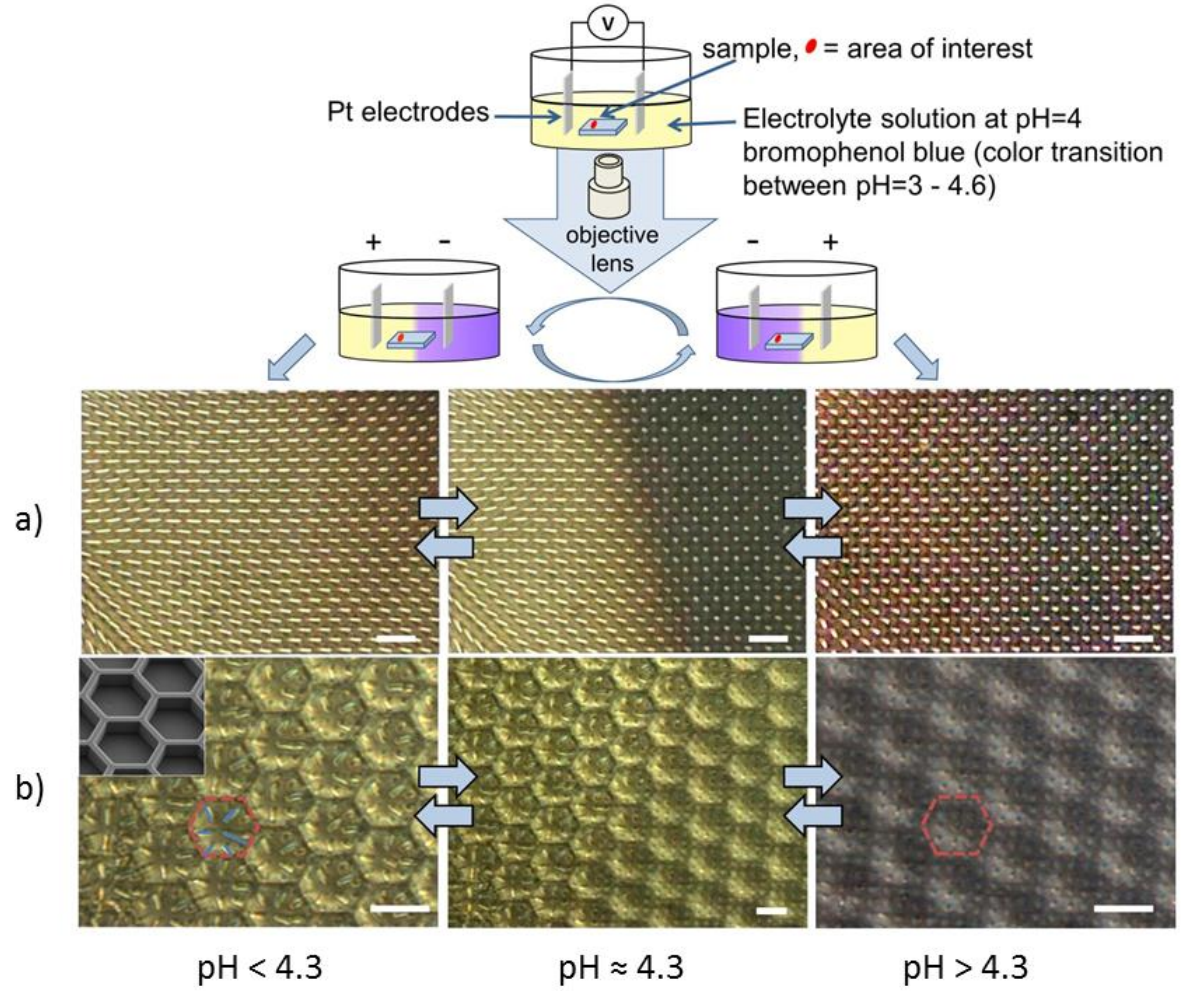

Figure 11. Schematics and optical microscope images of pH-responsive actuation using electrochemically-generated pH gradients. a) Directional actuation using HAIRS incorporating a flat, uniform hydrogel layer, b) opening-microfloret actuation made by confinement using a

Figure 11 (Continued)… honeycomb-patterned surface (inset). (See Chapter 4: HAIRS with Topographically Patterned Hydrogel Responding to Homogenous Stimuli" for details). Left panels: bent microposts (contracted hydrogel). Middle panels: transition state (VPT of the hydrogel); note the sharp boundary between the bent and the upright posts. Right panels: upright microposts (swollen hydrogel). Electric fields of ca. ±0.5 V/mm were used. Note that the color transition of the indicator does not exactly match the pH of the VPT of the hydrogel. Scale = 20 μm.

HAR Structure Geometry Affects Actuation Direction

Although structures generally bend in a reproducible direction with each actuation cycle, it can be more difficult to influence exactly what that bending direction happens to be. For example, symmetrical HAR post structures, which have no geometrically preferred bending direction, are observed to bend in small domains of similar directions that gradually diverge across a surface and are highly sensitive to localized asymmetries in the hydrogel or surface defects (Figure 12). One approach to controlling structure bending direction is to use a HAR geometry with a preferred bending orientation such as an asymmetric fin structure (Figure 13). Such microfins can be used to create large areas (cm^2 at least) of highly uniform directional actuation (Figure 14).

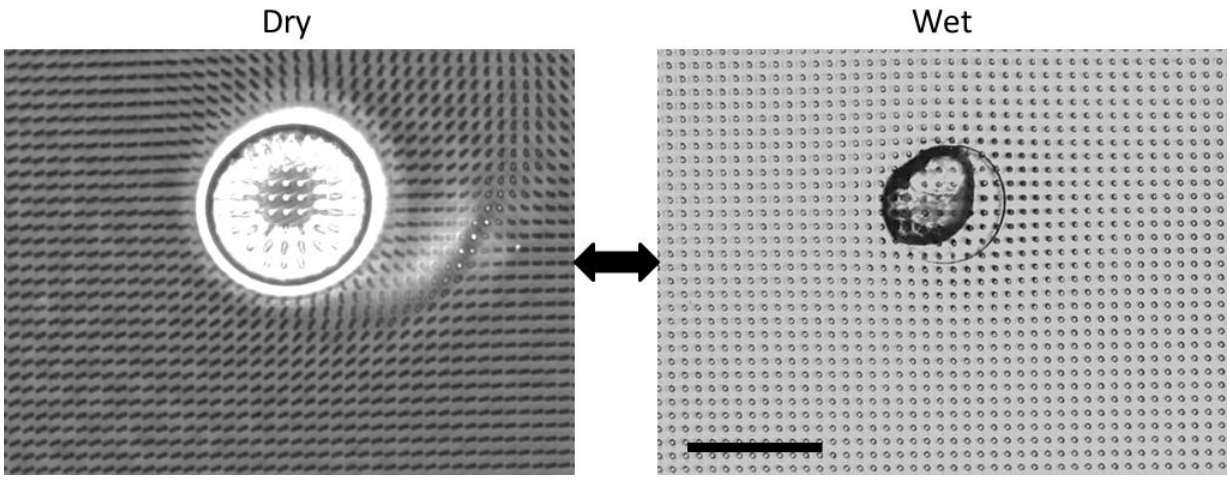

Figure 12. PAAm HAIRS responding to humidity. A local defect significantly influences the direction of actuation of the symmetrical microposts. Scale = 100 µm.

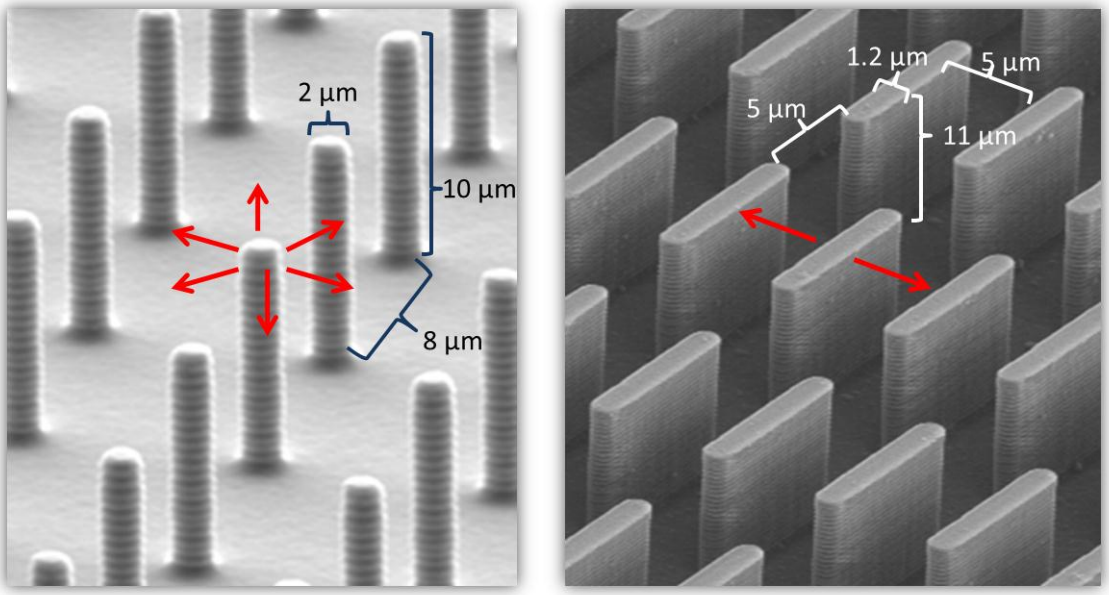

Figure 13. Symmetrical post structures (left) have no geometrically preferred bending direction which makes them very sensitive to local defects in the hydrogel generating domains of different bending directions. Microfins (right) do have a preferred bending axis due to their asymmetric geometry, making it far easier to generate large areas of highly uniform actuation. Red arrows

Figure 13 (Continued)… mark the preferred bending directions. Some exemplary dimensions are included for these specific surfaces, although HAR structures of varying size may be used as well as differently patterned arrays (such as hexagonal arrays of posts, or staggered arrays of microfins).

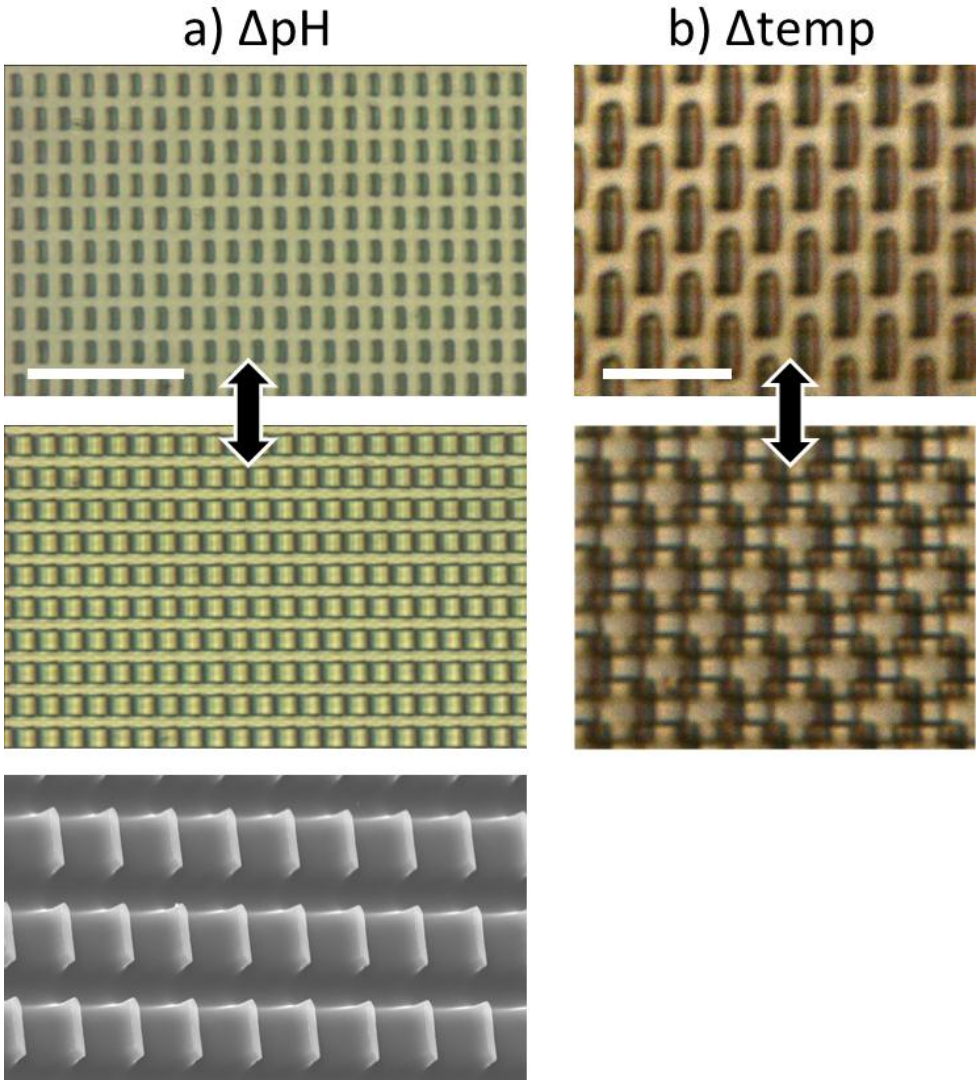

Figure 14. Microfins, due to their anisotropic shape, have a preferred bending direction providing for large areas of highly uniform a) pH and b) temperature-responsive actuation. An SEM of a sample such as shown in a) is aligned beneath; the sample was imaged at 45° from the side to better visualize the hydrogel profile. Each microfin in a) is 10 μm long, 11.5 μm tall, 1.2

Figure 14 (Continued)… μm wide, with spacing of 5μm. Scale = 40 μm. Each microfin in b) is 10 μm long, 2 μm wide, and 15 μm tall. Scale = 20 μm.

Microfluidics to Control Actuation Location

While it has been demonstrated that HAIRS respond to bulk, homogeneous stimuli, it is also interesting to consider how such actuators respond to more localized stimuli, or interfaces of different stimuli. In particular, we investigated how pH-sensitive HAIRS respond to abrupt spatial changes in pH, where both acidic and basic conditions exist within a micrometer-length scale over the sample surface, and particularly whether the actuation is spatially patternable. We created microfluidic systems in which the bottom surface of the channels was made of a hybrid actuation system. Figure 15 shows an example of such a design using a microfin actuating surface: the laminar flow of acid and base allows for spatial control of actuation down to the micron scale. The actuation response is highly localized; the gel contracts and the microfins bend only in areas over which acid is flowing, while neighboring microfins subjected to base remain upright. The transition from bent to upright at the interface of the acid and base streams is sharp and only a few microns wide. Neither flow direction nor rate within the channel influence bending direction. While microfluidics provides a way to spatially control the actuation, the actuators themselves could serve as a sensitive self-reporting system in a device to allow for easy visualization of pH changes.

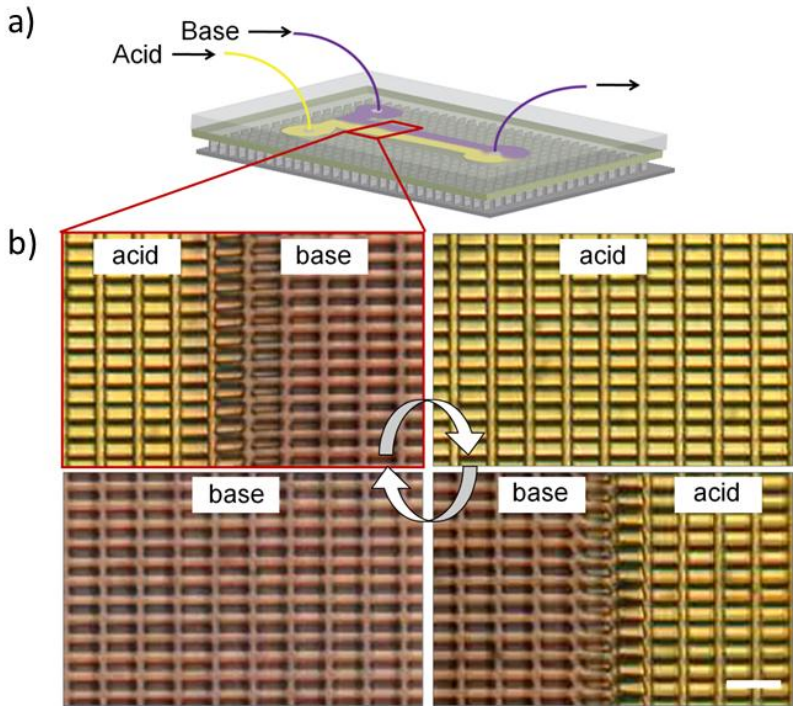

Figure 15. pH-actuated microstructures in microfluidic channels. a) Schematic of the experimental set-up. b) Optical microscope images of microfins within a microfluidic channel and demonstration of spatially controlled actuation using laminar flows of acid and base. As indicated, the images correspond to setups in which acid was supplied in the left channel and base in the right channel; acid in both channels; base in both channels; base in the left channel and acid in the right channel, correspondingly. The color arises from bromophenol blue indicator. Flow is from top to bottom of the images. Scale = 20 μm.

Dynamically-Switchable "Windows"

We used the adaptive function of HAIRS to design reversibly reconfigurable, deformable mirror arrays where the micro-mirrors are metal-coated microfins like those shown in Figure 14. We fabricated an array of micro-mirrors embedded in a humidity or pH-responsive hydrogel layer, which adaptively deforms individual micro-mirrors according to the changes in the

surrounding environment without requiring external input power. Although there are still many remaining challenges to bring this concept to real applications, we envision that this concept of using adaptive materials and systems such as HAIRS may impact the design and utilization of future generation, high-performance adaptive optics for imaging and energy saving applications as well as for new optical applications operating in the presence of environmental stress.

Two methods were used to deposit metal on the sides of the structures and turn the microfin structures into micro-mirrors. Either a thin film of metal (200 nm gold or silver with 10 nm of titanium as an adhesion layer) was shadow evaporated onto an epoxy microfin surface, or metal was sputter-coated on to the PDMS microfin mold to form a conformal coating before epoxy replication as shown in Figure 16.

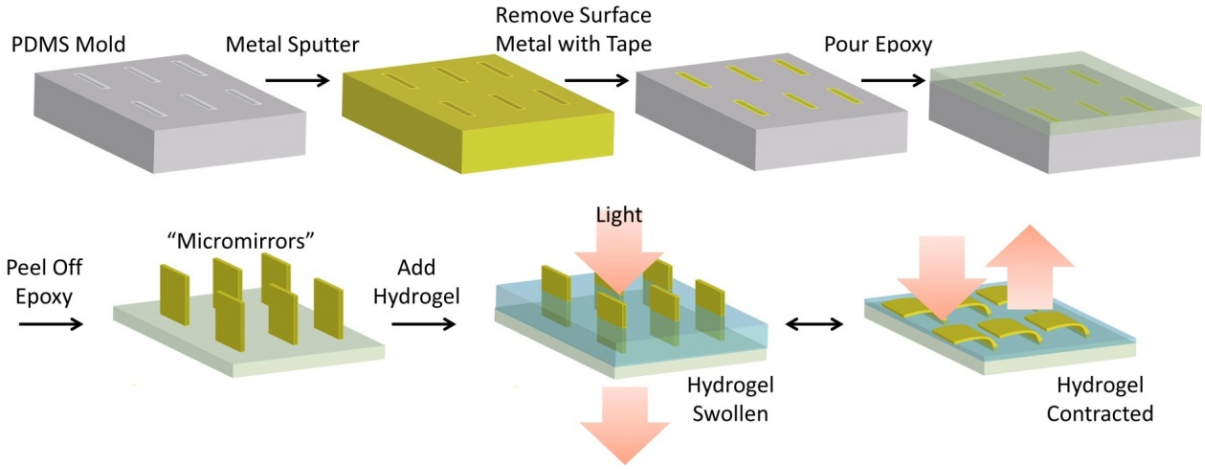

Figure 16. A schematic depicting how metal was transferred only to the sides of the microfins. First, metal is sputter coated on a PDMS mold, and then all the metal on the top surface (not in the wells) is removed with tape. Subsequent replication in epoxy generates transfer of the metal from the PDMS wells to the sides of the replicated epoxy structures due to difference in adhesion. In this way, no metal is deposited on the basal surface as opposed to straightforward shadow evaporation. On the other hand, the films that are transferred with this method are not necessarily as reflective as directly deposited metal films.

Figure 17a,b shows macroscopic and microscopic images of both the high and low transmittance states of both humidity-responsive and pH-responsive HAIRS. It should be noted that the contrast between the two states is not optimally high due to the low ratio of the height of each micro-mirror to the spacing between each, as easily seen in Figure 17b. The contrast ratio can be increased either by using a thin and tall but narrowly spaced micro-mirror array or by using a micro-mirror array with staggered geometry to cover the entire surface when the mirrors are bent. The arrangement of the micro-mirrors can be designed to cover desired fractions of the surface area upon actuation.

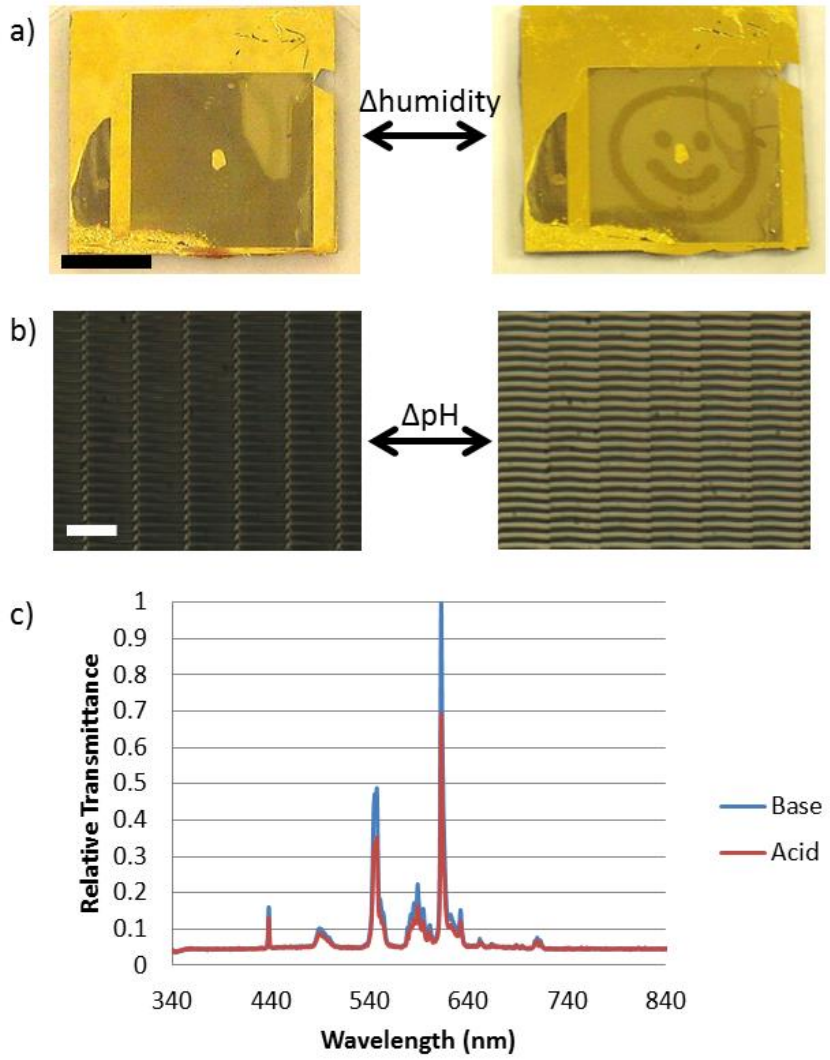

Figure 17. a) Digital photographs of a large area (*ca.* 2 cm x 2 cm) hydrogel-actuated micro-mirror array switching between opaque and transparent states by humidity change. Scale = 1 cm. b) Optical microscope images of a portion of a pH-responsive hydrogel-actuated micro-mirror array. The two images represent the highest light transmission (right, swollen hydrogel) and the lowest light transmission (left, contracted hydrogel). Scale = 25 μm. c) Transmission spectra of a pH-responsive hydrogel-actuated micro-mirror array for low transmittance (acid, red) and for high transmittance states (base, blue). Values are scaled against the maximum transmission attained when the microfins are upright in the hydrogel's swollen state (base).

Experimental

All chemicals and materials were used as received except for *N*-isopropylacrylamide, which was recrystallized from hexane. Silicon masters were fabricated, molded into PDMS, and replicated into epoxy/GMA as described in the experimental section of "Chapter 1: Transitioning to All-Polymer HAIRS".

UV-curable PAAm hydrogel precursor consisted of 40% AAm, 2% BIS, and 1% UV initiator Irgacure 2959 by weight in water.

UV-curable poly(AAm-*co*-AAc) hydrogel precursor consisted of 20% AAm, 20% AAc, 2% BIS, and 1% UV initiator Irgacure 2959 by weight in water.

UV-curable PNIPAAm hydrogel precursor solution consisted of 40% NIPAAm, 2% BIS, and 0.5% UV initiator Darocur 1173 by weight in dimethyl sulfoxide (DMSO).

To create a HAIRS, a drop (<10 μL) of hydrogel precursor solution was placed on a UVO-114/GMA HAR structured surface and a coverslip was placed over the drop to help induce wetting. The surface was then cured for at least 5 minutes under broadband UV illumination until fully polymerized. The coverslip was then removed; if it did not come off easily the sample was soaked in water to loosen it. In the case of PNIPAAm, the sample should be soaked in water for at least a day to remove the DMSO.

Optical imaging and video recording were done on an Olympus IX71 inverted microscope using StreamPix v.3 software and QImaging EXi Blue and Evolution VF cameras. Samples were sputter coated with Pt/Pd for imaging with a JEOL JSM 639OLV scanning electron microscope.

Chapter 4: HAIRS with Topographically Patterned Hydrogel Responding to Homogenous Stimuli

Parts of this chapter have been adapted from: P. Kim, L. D. Zarzar, X. Zhao, A. Sidorenko and J. Aizenberg, "Microbristle in gels: toward all-polymer reconfigurable hybrid surfaces." *Soft Matter*, **6**, 750-755 (2010).

Parts of this chapter have been adapted from: L. D. Zarzar, P. Kim and J. Aizenberg, "Bio-inspired design of submerged hydrogel-actuated polymer microstructures operating in response to pH." *Adv. Mater.*, **23**, 1442-1446 (2011).

Collaborators: Philseok Kim, Xuanhe Zhao (modeling), Zhigang Suo, Joanna Aizenberg

Introduction

Other than using geometric bias in the HAR structure itself, there is little ability to control the bending direction of the structures within a uniform hydrogel film using homogenous stimuli as discussed in Chapter 3. Therefore, we investigated additional approaches to apply bending preference to the system and achieve patternable actuation directions. One such approach is to pattern the hydrogel topography; a thicker gel can act as a "stronger muscle" because it has greater absolute volume change upon expansion and contraction than a thin gel. Therefore, if the thickness of the gel is periodically varied over the HAIRS, then the forces that

the gel exerts on the embedded structures should also be similarly patterned, thereby influencing actuation direction.

Mode of Actuation and Modeling

The first polymeric HAIRS explored with such patterned hydrogel topography was that of the simplest system using humidity-responsive PAAm hydrogel. A numerical model was constructed (by Xuanhe Zhao) for a soft micropost-hydrogel system to visualize the expected bending motion of the posts, when the hydrogel layer that undergoes a VPT has a continuously changing height profile (Figure 18). The model was implemented in the finite-element package, ABAQUS, with a user-defined subroutine, UHYPER, that describes the swelling/deswelling behavior of the hydrogel.[37] The geometry and properties of the polymer microposts were taken as d = 1.5 μm, l = 10 μm, p (pitch) = 8 μm, E = 1.5 GPa) and the swelling ratio of the hydrogel was set to 5 for the simulation. In order to simplify the calculation, a plane strain boundary was assumed for the model. When the hydrogel is in a wet state (Figure 18a), the polymer microposts stand upright. As the hydrogel is drying (Figure 18b-d), the microposts bend toward the regions with thicker gel layers.

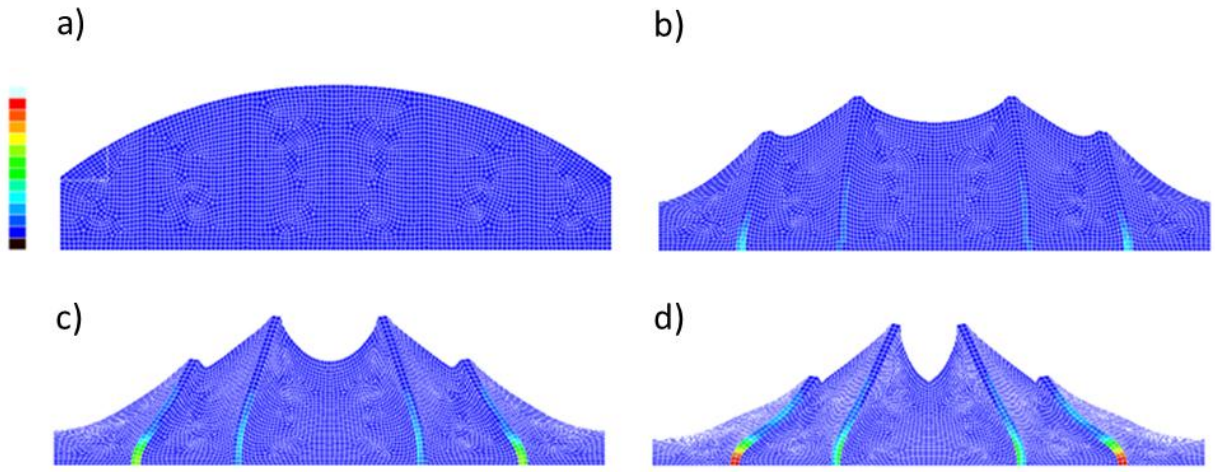

Figure 18 . 2D-finite element simulation results, showing the deformation of soft microposts embedded in a humidity-responsive hydrogel layer with varying thickness. As the hydrogel layer dries (from a) to d)), the microposts are bending toward the area with a thicker hydrogel. The strain is represented as a rainbow scale in each micropost where red - orange areas indicate a larger strain than blue - purple areas. Image credit: Xuanhe Zhao

The patterns achievable by actuation of HAIRS depends upon the swelling properties of the hydrogel and the state in which the hydrogel was polymerized. For example, when using a humidity-responsive hydrogel with patterned topography, the actuation transitions between two states: one is the stress-free state where the hydrogel is swollen and the HAR structures are upright, and the other state is the stressed state in which the gel is dry/contracted and the structures are bent (in the direction towards the thicker gel). However, when a pH-responsive poly(AAm-*co*-AAc) hydrogel is used, there are actually three states between which we can pattern the actuation: swollen (in pH>4.3), intermediate contracted (in pH<4.3), and dry (fully contracted). The hydrogel precursor solution is acidic (pH = 2) which means that the hydrogel is polymerized in the intermediate contracted state — this state is analogous to the "wet" state of

the PAAm hydrogel. Such pH-responsive HAIRS can therefore still undergo humidity-responsive actuation (between intermediate contracted and dry). But additionally, the pH-responsive HAIRS can then be placed in base and the gel will swell significantly beyond its initial volume, adding a third "state" to the actuation. The swelling of the patterned hydrogel has the opposite effect on the HAR structure bending direction in that the structures are now pushed away from (as opposed to pulled towards) the thicker gel in areas of gradient hydrogel thickness. The actuation between these three states is outlined in Figure 19.

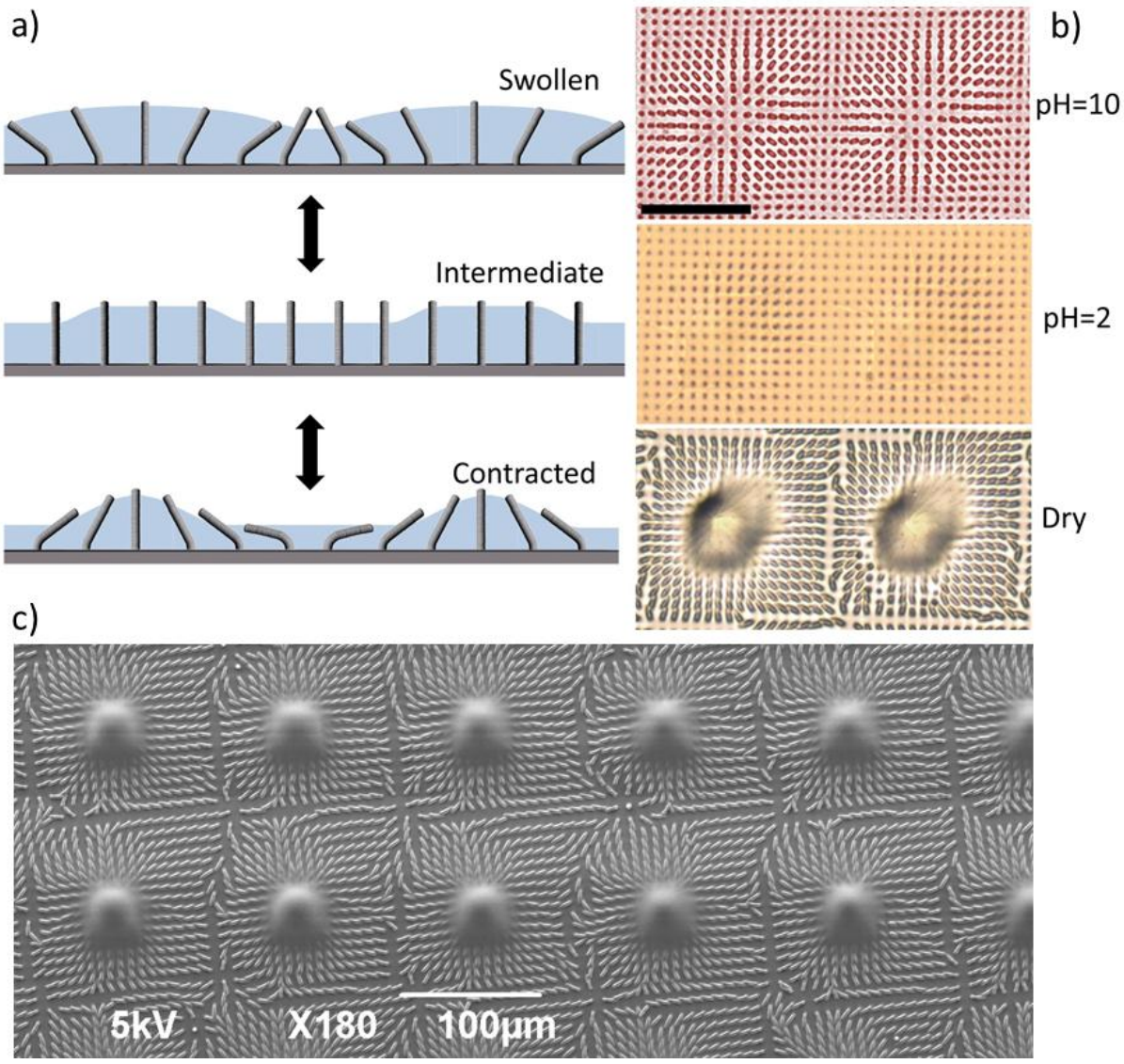

Figure 19. Actuation of HAIRS with topographically patterned hydrogel undergoing transitions between three different volume states. pH-responsive poly(AAm-*co*-AAc) is polymerized in the intermediate state (since the hydrogel precursor is more acidic than the VPT pH), and from there the gel can further swell or contract, generating different actuation patterns. a) Schematic of actuation. b) Optical micrographs of a pH-responsive gel in the fully swollen state (base), intermediate state (acid) and contracted state (dry) in correlation with the schematic patterned using a photomask. Color is from bromophenol blue pH indicator. Scale = 100 µm. c) SEM of HAIRS surface such as in b) in the dry state.

Hydrogel Patterning by Topographical Confinement or a Photomask

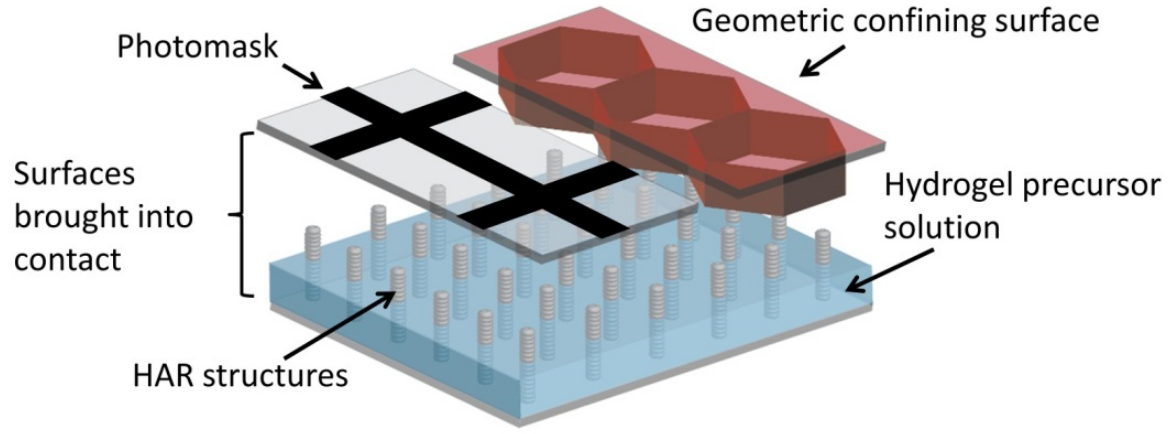

Figure 20. Schematic of fabrication techniques; either a photomask or a 3D-patterned geometric confining surface can be used to control hydrogel topography.

We explored two approaches to patterning the hydrogel topography: photomasking during the hydrogel curing processes and using a patterned confining surface to imprint the topography of the hydrogel during curing (Figure 20). The photomask approach is straightforward; however, care must be taken to control the length of UV exposure and dosage which will affect how much hydrogel is polymerized underneath the masked regions. An example of patterned actuation achieved using the photomask approach is in Figure 19.

In the confining surface approach, a patterned surface (such as an array of honeycombs, posts, bricks, or blades) which does not bind to the hydrogel is placed over the HAR structures and gel precursor solution and the gel is cured in this confined state. The hydrogel topography, and therefore the actuation pattern, is determined by the geometry of the confining surface (Figure 21). However, the hydrogel pattern can also be affected by the wetting behavior of the confining surface. If the confining surface is non-wetting, then the hydrogel precursor solution

will pin to the edges of the topographies (Figure 22a, Figure 23). If the surface is wetting, then the hydrogel precursor solution wets the confining topography and generates patterns shown in Figure 22b. Therefore, with a single geometry of confining surface (such as a honeycomb) we can change the hydrophobicity of the surface using plasma treatment and generate two different actuation patterns (opening and closing microflorets, for example, Figure 22).

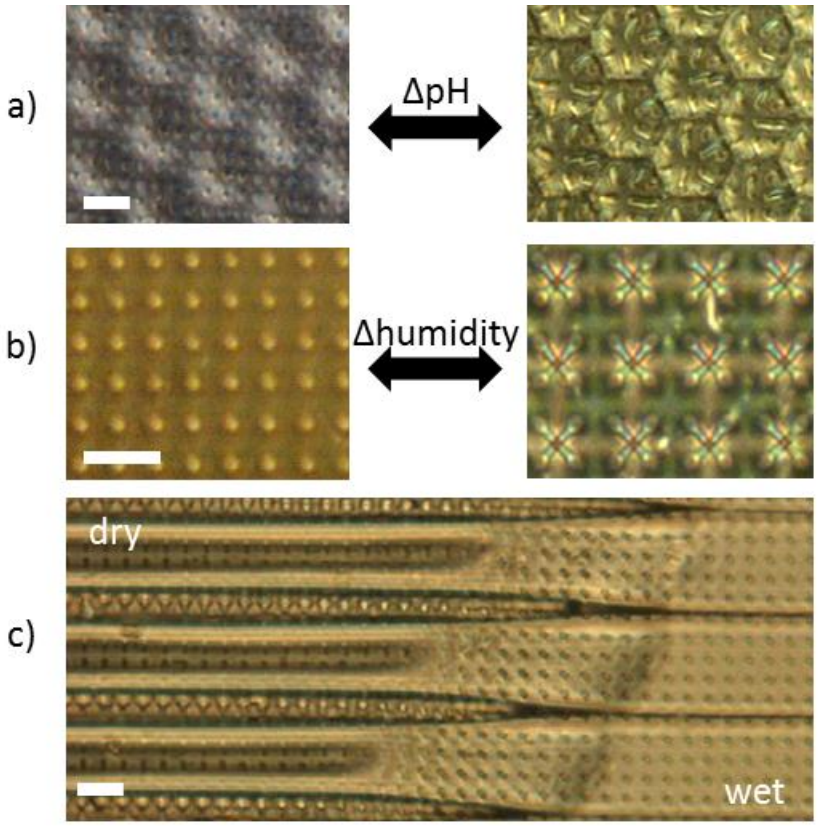

Figure 21. Optical micrographs showing a few different actuation patterns that can be made using patterned confining surfaces. a) pH-responsive "microfloret" actuation made using a honeycomb confining surface. b) "Micro-cross" actuation of microposts made using properly aligned posts as a confining surface. c) "Zipping" actuation made by patterning hydrogel with long blade shapes. The image shows the transition between wet and dry regions. Scale = 20 μm.

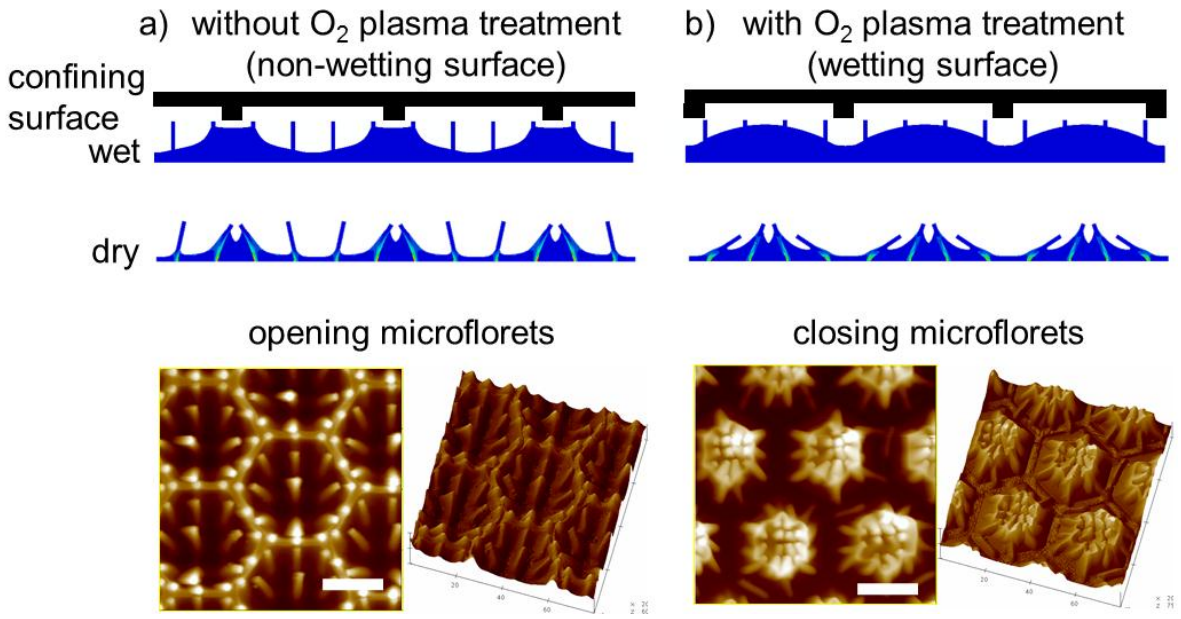

Figure 22. Comparison of finite element simulation and the experimental observations for the formation of a) opening and b) closing microflorets. Top: simulation results comparing the patterns that originate from confining surfaces with different wetting properties. Bottom: Atomic force microscope (AFM) height images (top view and 3D view) of microflorets exhibiting opening and closing actuation upon dehydration. Scale = 20 μm. Figure credit: Philseok Kim

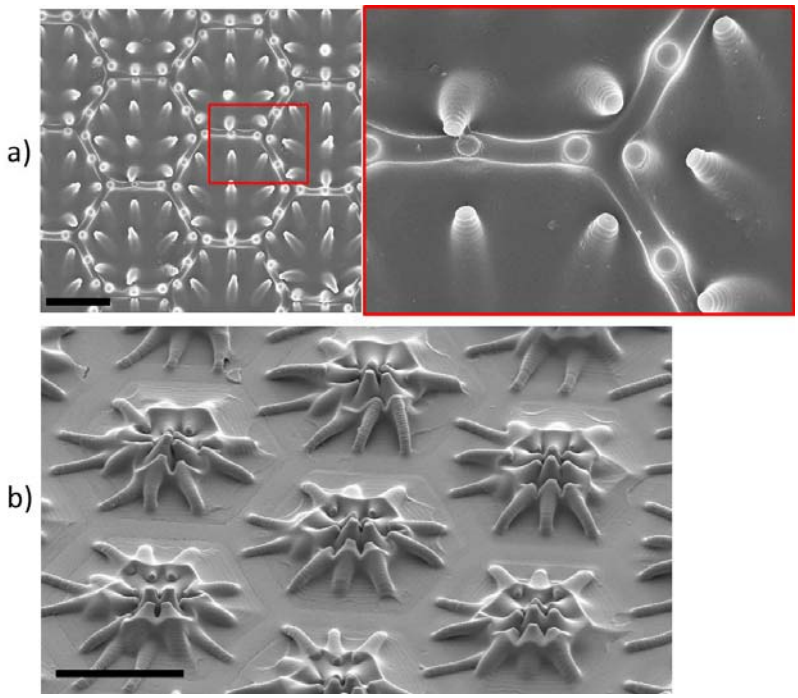

Figure 23. SEM of microposts in AAm hydrogel polymerized under confinement of a) a non-wetting honeycomb pattern similar to the sample shown in Figure 22a and b) a wetting honeycomb pattern similar to the sample shown in Figure 22b. a) The right image (a zoomed-in view of the red box shown at left) shows how the posts slightly protrude from the thinner gel at the center of the honeycomb and bend toward the thicker gel around the perimeter to create an "opening microfloret" pattern. b) The imprinted outline of the honeycomb confining surface is visible on the basal surface around the posts while the hydrogel that remains is in the center of each honeycomb, pulling structures inward creating a "closing microfloret" pattern. Scale = 20 μm.

Experimental

All materials and chemicals were used as received. PDMS molds and UVO-144 epoxy/GMA structures were fabricated as described in the experimental section of "Chapter 1: Transitioning to All-Polymer HAIRS". Hydrogel recipes are described in the experimental

section of "Chapter 3: HAIRS with Thin Films of Hydrogel Actuating in Response to Homogeneous Stimuli".

Confining surfaces were replicated from PDMS molds with a glass slide backing in a similar fashion to the epoxy/GMA HAR structures except that confining surfaces are molded in 100% UVO-114 epoxy to prevent bonding of the hydrogel. If a highly-wetting confining surface was needed, the confining surface was plasma treated with a 100 W plasma cleaner (Model Femto, Diener GmbH, Nagold, Germany) for about 20 seconds.

To make HAIRS with patterned hydrogel topography using a confining surface, a drop (<10μL) of hydrogel precursor was placed on the HAR structures and a patterned confining surface was placed over the droplet to induce wetting. In some cases binder clips held together the confining surface and the HAR structure surface to ensure close contact.

To make HAIRS with patterned hydrogel topography using a photomask, a drop (<10μL) of hydrogel precursor was placed on the HAR structures and a cover slip was placed over the droplet to induce wetting. The photomask (transparency printed by Output City) was placed on top of the coverslip. A commonly used photomask dimension (like that used to create the sample pictured in Figure 19) was an array of squares measuring 130 x 130 μm with line widths of 75 μm. The sample was cured under a fiber optic UV lamp (Blue Wave 200, Dymax Light Curing Systems) for ~20 seconds at a power of 800 μW was measured with a Newport optical power meter, model 1916-c with a Newport 818-ST-UV wand detector.

After curing, the confining surface or cover slip/photomask was removed. If the confining surface did not easily come off the bottom surface, then the sample was soaked in water to induce separation.

Optical imaging and video recording were done on an Olympus IX71 inverted microscope using StreamPix v.3 or ImagePro software and QImaging EXi Blue and Evolution VF cameras. Samples were sputter coated with Pt/Pd for imaging with a JEOL JSM 639OLV scanning electron microscope. AFM images were taken with Veeco NanoMan AFM using Si probes in Tapping Mode under ambient conditions.

Chapter 5: HAIRS Responding to Chemical Gradients

Parts of this chapter have been adapted from: L. D. Zarzar, Q. Liu, X. He, Y. Hu, Z. Suo and J. Aizenberg, "Multifunctional actuation systems responding to chemical gradients." *Soft Matter*, **8**, 8289-8293 (2012).

Collaborators: Qihan Liu, Ximin He, Yuhang Hu, Zhigang Suo, Joanna Aizenberg

Introduction

Localized control over the dynamic movement of nano/microstructures is fundamentally important for actuators and sensors, tunable optics, micromanipulation, and the design of "smart" responsive surfaces.[12, 38] Programming the location of response, the direction of movement, and the extent of structural reconfiguration on the microscale are all important characteristics of tunable, dynamic materials. Natural systems have mastered the ability to use chemical cues, often applied not as a uniform stimulus, but in the form of chemical or electrochemical gradients, to direct the motion of structures from the nanoscale up. For example, the beating of flagella is driven by proton motive force,[5] and the direction of movement of bacteria can be guided by chemotaxis.[6] The ability of a system to respond to a gradient chemical stimulus rather than a homogeneous environment is accompanied by an inherent directionality, allowing for the chemical stimulus to trigger not only the location of response, but also the direction of movement along the gradient.

Although the versatility, tunability, and controllability of artificial responsive actuators would benefit from such directional sensitivity, few systems take advantage of chemical gradients or interfaces to direct the actuation of materials. For instance, chemical gradients have

been used to generate the oriented movement of metallic nanorods, similar in concept to chemotaxis.[39] Recently, there has been significant interest in responsive polymers, such as hydrogels, for chemo-responsive actuators due to their reversible and highly tunable volume change as well as sensitivity to a wide range of stimuli including humidity, temperature, pH, light, and redox state.[1a, 40] Although typically such hydrogels are used and studied in regards to their response to a homogeneous stimulus (i.e. the polymer network is either swollen or contracted in a certain state), introducing localized stimuli or gradients of stimuli across a gel can be advantageous for a number of purposes. Cargo transport, for example, was accomplished using gels that swell and shrink in response to oscillations of the Belousov–Zhabotinsky reaction, transporting particles along with the moving interface between swollen and contracted gel regions.[41] Further exploration of how chemical interfaces and gradients can be used to manipulate hydrogels and induce reversible system directionality is therefore of fundamental interest.

We have previously discussed how within HAIRS asymmetry in the structure geometry itself[33] (Chapter 3) and patterned gel thickness[26] (Chapter 4) provide some control over the bending direction of structures within such systems. However, in such previously described cases,[24-26, 33] the structural actuation responds to homogenous stimuli, and the cycling of gel expansion and contraction results in actuation between pre-programmed configurations inherent to the physical makeup of the surface. To generate a system that is responsive to a far greater range of stimuli scenarios, both in terms of spatial and directional variations, we aimed to use gradient chemical signals to trigger actuation between numerous configurations. Here, we develop a multifunctional actuation system in which microstructures embedded in a pH-responsive gel can undergo multiple actuation scenarios: (i) highly localized, directional

movement of embedded microstructures in response to pH *gradients*, but not to the change in the bulk pH, as in previously described pH-responsive systems,[33] (ii) uniform large-area actuation upon hydration/dehydration. We explore the fundamental mechanisms of such novel behavior, including investigation of how the chemical gradient is translated to the physical structure of the hydrogel and in turn how the system provides the ability to control the direction of bending, location and area of bending, and degree of bending of embedded structures.

Mode of Actuation

HAIRS similar in composition to those described earlier chapters, in which the hydrogel film is covalently attached to both the HAR structures and the base, can be designed to actuate according to a different, complementary mechanism. In this mode, the structures remain standing upright both when the gel is expanded and when it is contracted; the structures show no actuation in the presence of a homogeneous stimulus despite responsive volume changes in the gel. Instead, the structures bend specifically in response to spatial changes, or gradients, in the stimulus. This selectivity is achieved by, for example, polymerizing the hydrogel under conditions such that the structures start out upright when the gel is contracted such that cycles of homogenous, vertical gel expansion and contraction exert no downward force upon the embedded structures. Bending is thus driven specifically by local regions of *lateral* gel expansion and contraction determined by a stimulus gradient (Figure 24).[42]

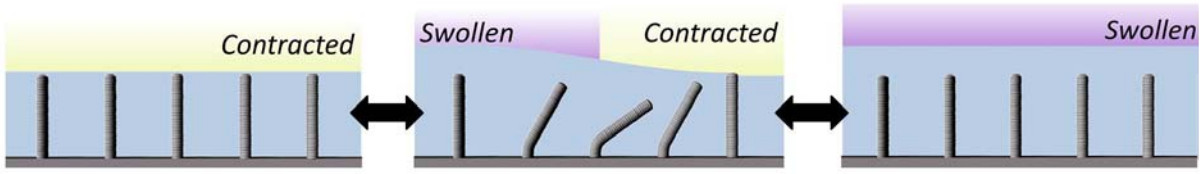

Figure 24. Schematic showing the general mode of actuation for HAIRS responding to chemical gradients. Both when the gel is contracted and swollen the structures remain standing upright. However, under the influence of a chemical gradient which causes neighboring regions to be either swollen or contracted, we observe structures to always bend toward the contracted gel within a transitional region across the gradient. Farther from the gradient the structures remain undisturbed.

Programming Actuation of pH-responsive HAIRS

The hybrid surfaces described in this chapter are HAIRS consisting of high-aspect-ratio flexible microstructures embedded in a pH-responsive poly(AAm-*co*-AAc) hydrogel which has a VPT at pH ≈ 4 – 5 corresponding to the pK_a of acrylic acid (4.3). To fabricate a hybrid surface, hydrogel precursor solution was placed on the structured surface and allowed to spread under confinement of a glass cover slip. The hydrogel was cross-linked by UV-initiated polymerization in this confined state.[33] Since the poly(AAm-*co*-AAc) hydrogel precursor solution is acidic (pH ≈ 2), the *hydrogel is polymerized in a relatively contracted state in terms of volumes achievable by changes in pH.* This is distinct from PAAm or PNIPAAm which are in a relatively swollen state in terms of volume change in response to their respective sensitivity; PAAm is swollen when polymerized, and can shrink significantly upon drying, while PNIPAAm is polymerized at room temperature which is lower than the LCST, so it can shrink significantly

upon increase in temperature. This is an important point when incorporating hydrogels into HAIRS systems.

By controlling the initial position of the structures (bent versus upright) with respect to the initial state of the hydrogel (contracted versus swollen), we could generate a system that will either actuate or remain static in response to the bulk pH change (Figure 25). In particular, we anticipated that if the structures are bent in the initial state of the contracted submerged hydrogel, the structures would actuate into an upright orientation upon the increase in the bulk pH, whereas if the structures are oriented upright in the contracted submerged gel, further gel expansion upon pH increase would not change their orientation. The latter system should, however, show significant actuation upon drying. Indeed, when we generated structures that were bent after the polymerization process, as previously described[33] (Figure 25b, middle), we observed homogeneous pH-responsive actuation because structures could be pushed to the upright position by the hydrogel swelling in basic conditions (Figure 25b, right). Upon drying, the original bent structures show only minimal actuation further down to the surface due to the additional contraction of the gel (Figure 25b, left). When we fabricated surfaces in which the structures in their original state remained upright after hydrogel polymerization by tailoring the initial fabrication and confinement conditions (Figure 25c, middle), we observed vertical expansion of the gel, but no actuation of the microstructures upon increase of pH (Figure 25c, right). In this case, however, significant actuation of the microstructures takes place upon dehydration of the gel between the submerged state and the dry state (Figure 25c, left), as further gel shrinkage upon drying induced structures to buckle. In effect, we were able to shift the homogeneous actuation response from pH to humidity by controlling the initial conditions of the system.

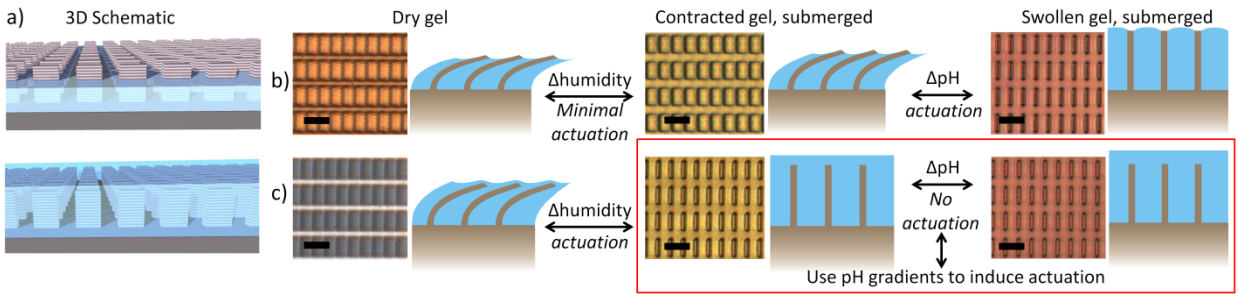

Figure 25. Tuning actuation response with humidity and pH. Each panel contains a top-view optical image along with a schematic side-view cross-section. The coloration in the optical images arises from bromophenol blue pH indicator added to the solution. a) For surfaces in which structures are bent in the contracted state of the gel, we observe pH-responsive actuation, but no actuation between the contracted, submerged state (pH<4.3) and dry. b) For surfaces in which structures are upright in the contracted, submerged state of the gel, we do not observe pH-responsive actuation, but we can still observe humidity-responsive actuation between the contracted state and dry state. The red box highlights the conditions under which we used pH gradients to actuate structures. Scale = 10 μm.

Control of Actuation with pH Gradients

The absence of actuation in response to bulk pH made this particular HAIRS case an ideal test bed for studying the actuation of structures solely in response to pH gradients. We incorporated hybrid surfaces with pH-sensitive hydrogel, but not responsive to homogeneous pH (Figure 25, red box), into microchannels (Figure 26). Hydrogel was cured only in the area of the microchannel using a photomask, and the microchannel itself was made with double sided adhesive sealed at the top with a layer of polydimethylsiloxane (PDMS) as described in the Experimental section of "Chapter 2: Incorporating HAIRS into Fluidic Environments". Aqueous

hydrochloric acid solution (pH = 2) and sodium hydroxide solution (pH = 10) were pumped into the channel creating a sharp pH gradient at the laminar flow interface (Figure 26).

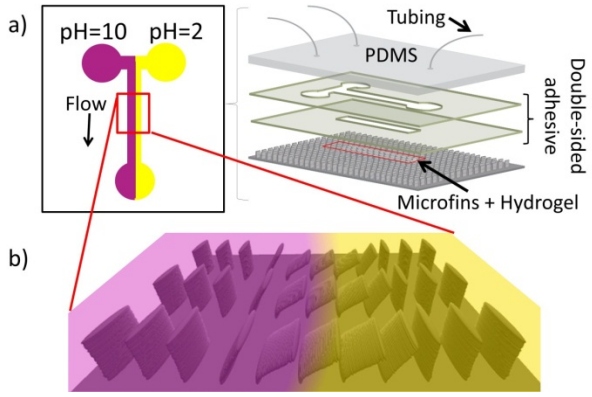

Figure 26. Schematic showing how a) the HAIRS were incorporated into microfluidic systems and b) how the microfins were directionally oriented within the flow.

We investigated the actuation of both microfins (width = 1.2 µm, height = 11.5 µm, length = 10 µm, side to side spacing = 5 µm, front to back spacing = 5 µm) and posts (diameter = 1.5 µm, height = 10 µm, pitch = 8 µm) and observed that structures always bent toward the direction of the acid within a "transition zone" of finite width across the interface, while preserving an upright position farther from the interface, both in the acidic and basic channels (Figure 27). We could reversibly control the bending direction of the structures and the position of the transition zone by changing the location, shape, and gradient direction; for example, as seen in Figure 27a, structures bent in opposing directions simply by reversing the direction of the pH gradient, and in Figure 28 microposts bend according to gradients following a curve.

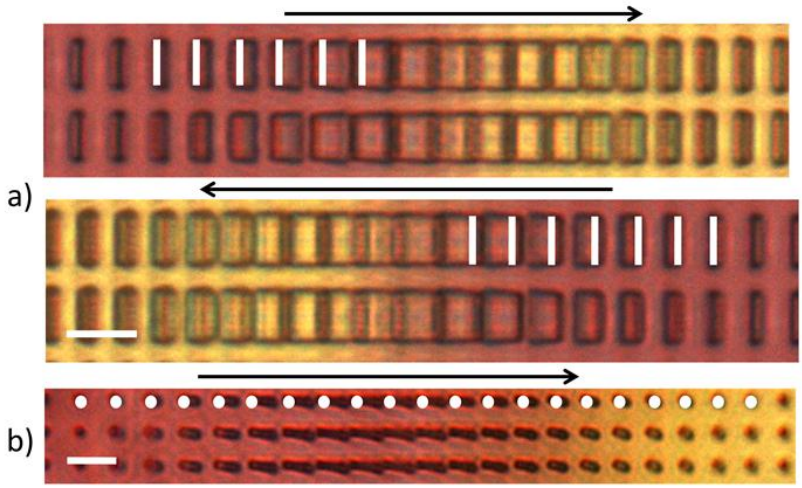

Figure 27. Optical micrographs of microstructures actuating in response to a pH gradient. Structures always bend toward the acid (yellow) across the gradient over a finite width (the "transition zone") before reverting back to the upright orientation. White bars or white dots mark the base of microfins and posts respectively to help visualize the bending direction which is also marked with the black arrows. a) Microfins actuate in response to the pH gradient, and as the gradient direction is reversed, the actuation direction is also reversed. b) Microposts actuate in response to the pH gradient. Color arises from bromophenol blue pH indicator where the yellow is acid (pH=2) and the purple is base (pH=10). Scale = 10 μm.

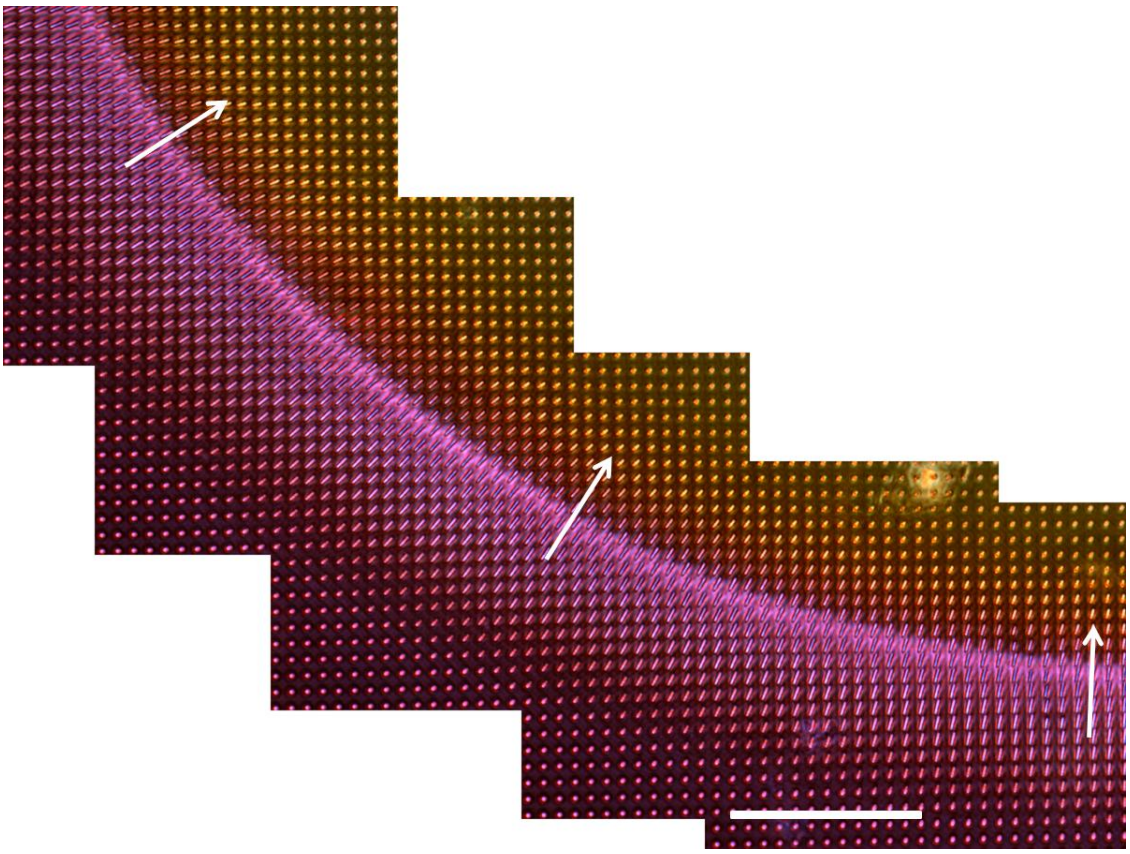

Figure 28. Optical microscope image of microposts actuating in response to a pH gradient that follows a curved shape in a microfluidic channel. The microposts always bend perpendicular to the gradient, as marked by the white arrows. Color is from bromophenol blue indicator where yellow is acid (pH= 2) and purple is base (pH=10). Scale = 100 μm.

Since the gel at this pH interface was able to significantly shear and bend structures in the direction perpendicular to the acid/base interface, we anticipated that this force, when applied across different axes of an asymmetric embedded structure such as a microfin, may also facilitate control over the degree to which structures were bent over. We therefore rotated the hydrogel-embedded microfins within the microfluidic channel so that the pH interface was positioned at different angles relative to the embedded structures. To approximately calculate the degree of structure bending, we assumed that the structures were bent from the substrate base and were not

curved. When the lengths of the structures were oriented parallel to the pH interface (such as in Figure 2c), structures bent to angles of 30-35°; with an interface at a 60° angle, structures' bending angle decreased to 20-25°, and with the interface at an 80° angle, structures bent only 10-15° (Figure 29).

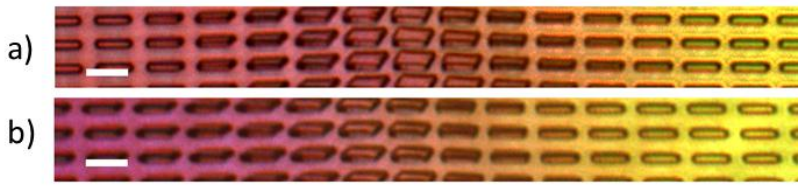

Figure 29. Microfins placed at different angles relative to the laminar flow interface exhibiting different bending angles. a) With the interface at a 60° angle, structures' bending angle is only 20-25°. b) With the interface at an 80° angle, structures bent only 10-15°. Scale = 10 μm.

Furthermore, we observed that even surfaces that *did* actuate in response to homogeneous pH stimulus (such as those shown in Figure 25b, Figure 30a) could still be affected by the pH gradient and induce structures to bend in the opposite direction to what would be normally expected, but only over short distances (Figure 30b). Of course, such backward-bending behavior only took place where the force generated by the pH gradient opposed the buckling-induced actuation direction; in Figure 30b, we saw that when structures already preferentially bent in the direction facing the acid, the actuation pattern was undisturbed, but backward-bending was induced when the preferred bending direction was toward the base. This effect is most prominent when the pH gradient is parallel to the bending axis of the plates (that is, the acid/base interface is perpendicular to the bending axis, as is the orientation in Figure 30). By flowing acid/base in a curve over such a sample (which does actuate in response to homogenous

pH change) we can easily visualize this dependence of the actuation on the direction of the pH gradient (Figure 31).

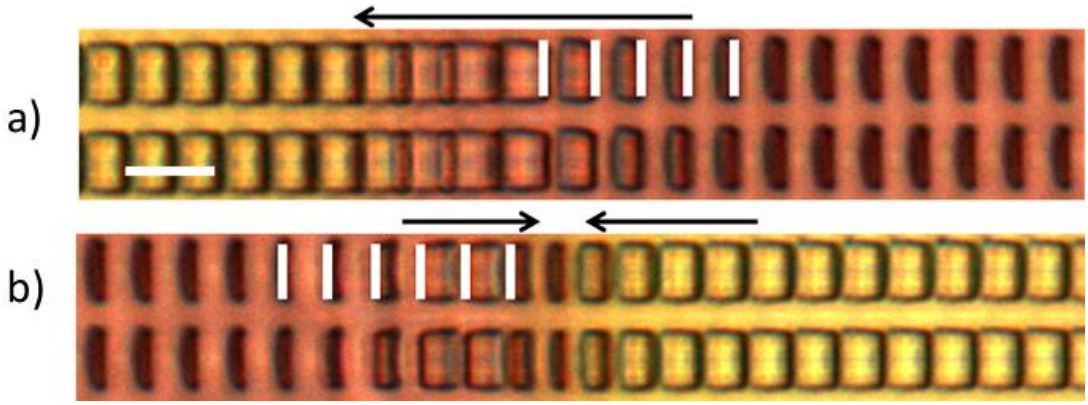

Figure 30. When a sample which actuates in response to homogeneous pH (as shown in Figure 25b) is put in a pH gradient, it exhibits either a) a uniform bending direction corresponding to the bending direction of the original structures (e.g. to the left in the top image, when the acid is flowed on the left side), or b) unique backward-bending at the base/acid interface, when the acid is flowed against the original bending direction, to the right. White bars mark the base of the structures to help visualize bending directions which are also marked with the arrows. Scale = 10 μm.

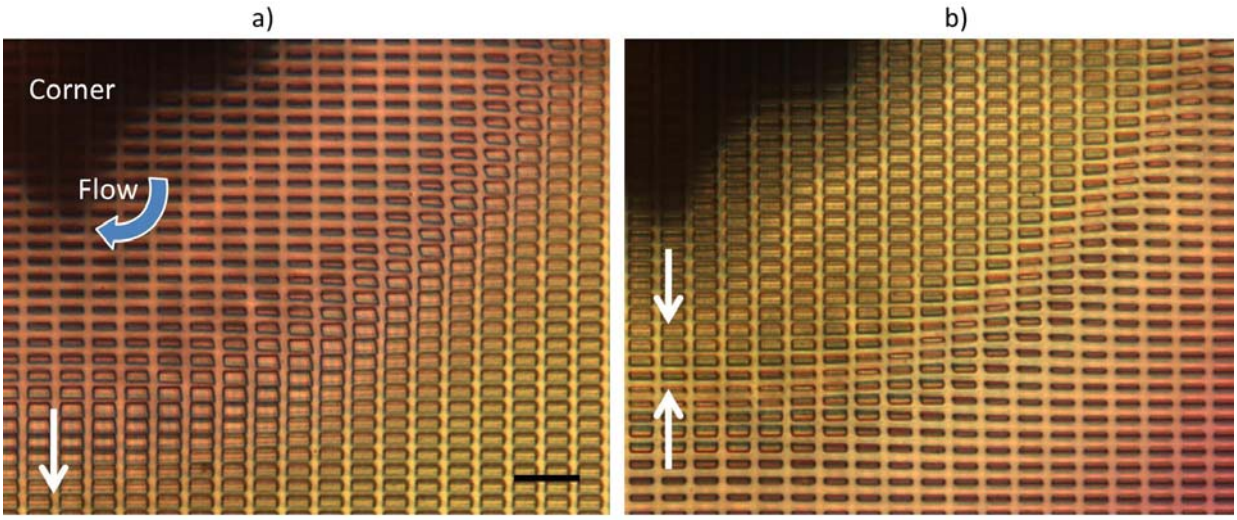

Figure 31. A surface which actuates in response to homogenous pH change (such as in Figure 25b) in a curved microfluidic channel with flow of acid and base to observe the effect the angle of the pH gradient has on the backward bending behavior of the microstructures as shown in Figure 30. a) At all angles of the pH gradient (both parallel and perpendicular to the microfins) in which the acid is in the bottom flow (the direction the fins want to bend), the microfins are always upright in the base and bend uniformly in the acid. b) When the acid is now flowing in the top (opposite to the direction the fins want to bend), we see that when the pH gradient is perpendicular to the microfins' length that there is a great amount of force generated to induce backward bending of the structures. When the gradient is parallel to the microfin length, in the top right corner of b), the force is now along the length of the structures, which induces some shearing, but no significant bending. Color arises from bromophenol blue indicator where yellow is acid (pH = 2) and purple is base (pH = 10). The white arrows mark the structure bending direction. Scale = 20 μm.

The pH gradients used here were quite sharp and spanned only a few microns, but we observed the areas over which the structures bent (the transition zone) to be significantly wider

than the pH gradient itself. We hypothesized that this discrepancy may be due to the fact that the gel cannot immediately conform to the chemical signal due to physical constraints. Thicker gels would then require larger distances to reach their equilibrium swollen and contracted states on either side of the interface than a thinner gel. To test the correlation of gel thickness with transition zone width, we created a surface with increasing hydrogel thickness along the length of the channel. As pictured in Figure 32, we observed that the width of the transition zone indeed increased along with hydrogel thickness even while under the influence of the same pH interface.

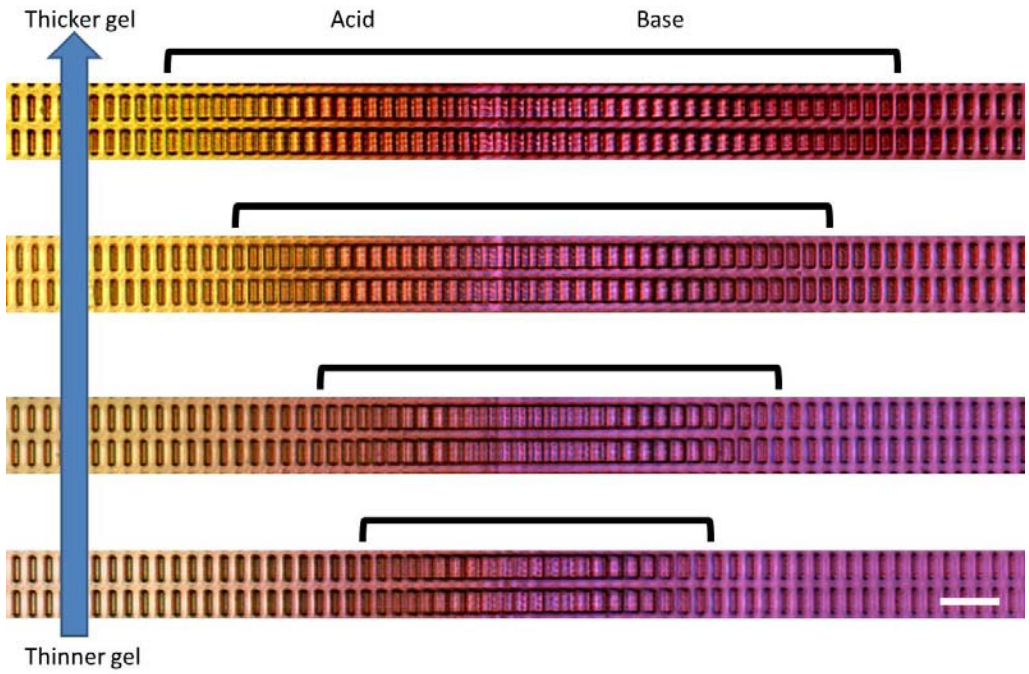

Figure 32. A surface in which there is gradient hydrogel thickness; as the gel thickness increases, the width of the region in which structures bend (indicated by brackets above the micrographs) also increases given the same pH interface. Color arises from bromophenol blue pH indicator. Scale = 20 μm.

We also observe that HAIRS surfaces which respond to chemical gradients also respond to wrinkling patterns in the hydrogel (Figure 33). Surface wrinkling or buckling is a common phenomenon observed during the swelling of hydrogels. As water diffuses into the gel, the outer layers of the gel begin to swell first but the gel is still constrained at the bottom surface and cannot expand laterally to accommodate the stress. Therefore, the swollen surface of the gel is induced to buckle to accommodate the compressive force. In thicker poly(AAm-*co*-AAc) hydrogels we observe these dynamic wrinkling patterns evolving over time until the hydrogel reaches an equilibrium swollen state. The underlying structures, such as microposts, are actuated by the shifting of the gel associated with the dynamic buckling behavior. These dynamics wrinkles have, in essence, the same effect on the structure actuation as the topographies generated by controlled application of pH gradients. The micropost surfaces here can serve as visual vector gradients, providing a read-out of the dynamic behavior of the hydrogel swelling that isn't easily visible by optical microscopy.

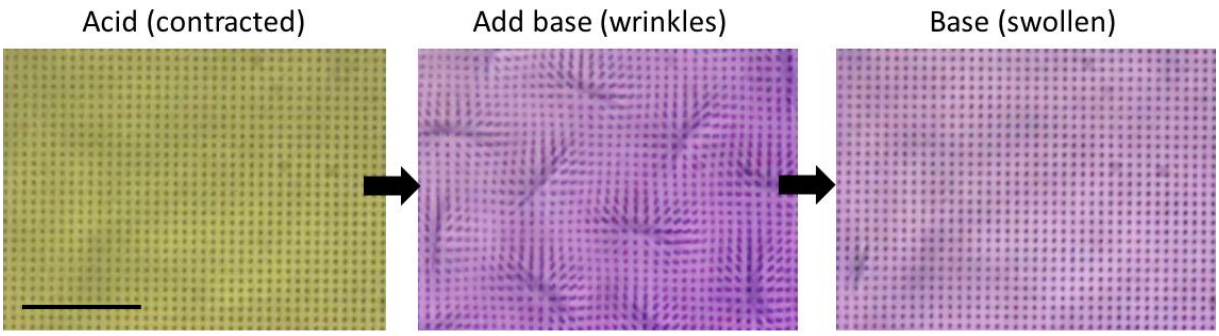

Figure 33. Optical micrographs showing how pH-responsive hydrogel-embedded structures move in response to the dynamic wrinkling patterns which develop in a thicker hydrogel film upon swelling. Both in the fully contracted and fully swollen states the hydrogel appears wrinkle-free and the structures stand upright; while the hydrogel is undergoing the swelling

Figure 33 (Continued)… process and wrinkles form due to compression in the film, the underlying structures are sheared in the directions in which the gel is also shifting. The posts therefore effectively act as vectors allowing visualization of the extent of the hydrogel deformation. Scale = 100 μm.

Confocal Characterization

We used confocal microscopy to quantify the influence of the hydrogel thickness on structure actuation and investigate the hydrogel profile at the pH interface. To visualize both the actuation of the microfins and the topography of the hydrogel at the same time, epoxy microfins were fluorescently dyed with pyrromethene 546 and 1 μm red fluorescent microspheres were adhered to the surface of the hydrogel. Overlaying a confocal Z-stack cross-section showing both the fluorescent microfins and gel-adhered microspheres with a bright field optical image to clearly show the extent of structure actuation (Figure 34) revealed that structure bending in the transition zone correlated to the region over which the thickness profile of the gel was sloped. We could tune the transition zone from widths of <50 μm (less than 10 consecutively bending structures) to nearly 500 μm (~100 consecutively bending structures) simply by changing hydrogel thickness (Figure 35).

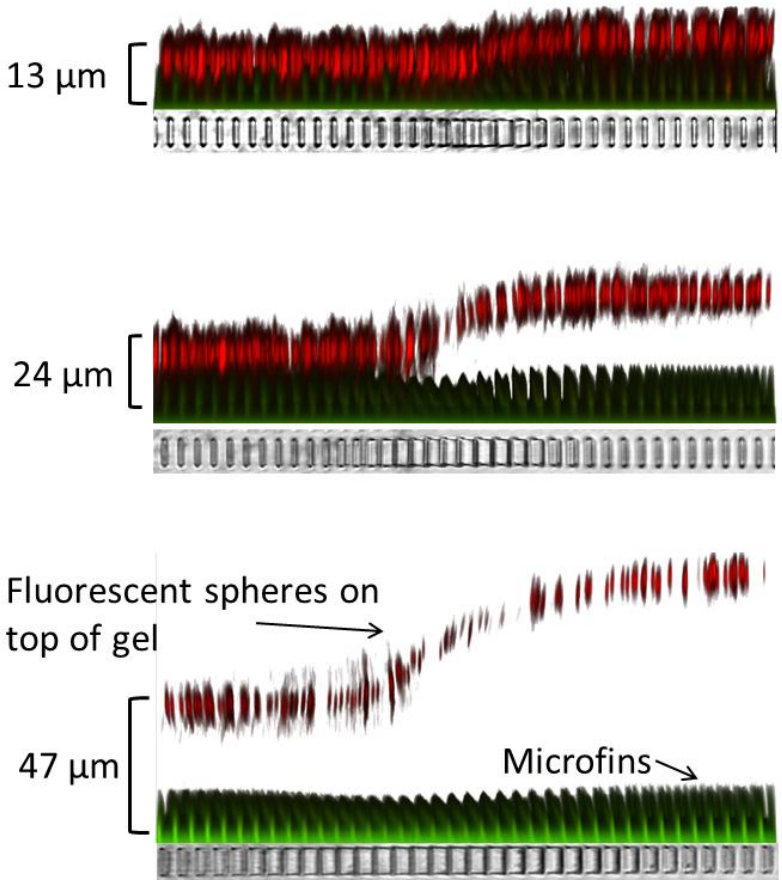

Figure 34. Exemplary confocal Z-stack cross-section of the HAIRS surface with varying thickness of hydrogel while in a microfluidic channel under acid/base laminar flow. Red corresponds to 1µm red fluorescent particles adhered to the hydrogel surface and green corresponds to the microfins. Top-view optical image of the same area is aligned underneath to better visualize structure bending.

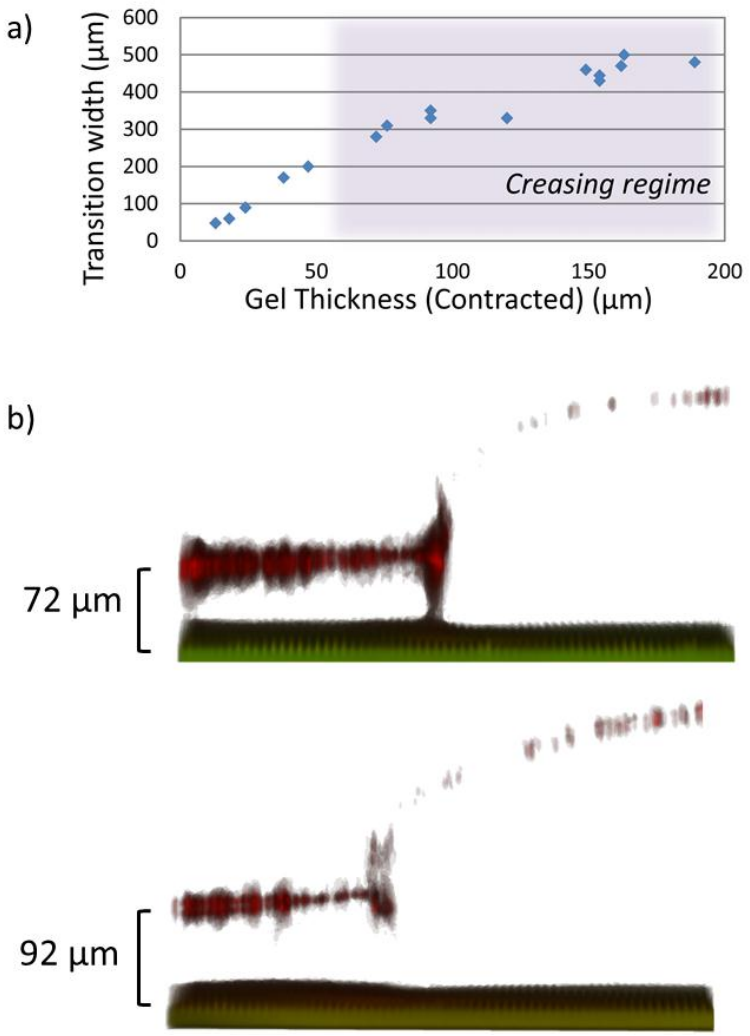

Figure 35. a) Correlation of the transition width with hydrogel thickness (measured in contracted state) indicates a linear relationship for gels <50 µm thick before creasing in the gel occurs and the linear relationship ceases to hold. b) Confocal Z-stack cross sections showing that at greater thickness of hydrogel, creasing is observed at the acid/base interface.

Modeling

To gain insight into the fundamental mechanism of how the pH gradient at the acid/base interface actually causes the bending of the structures, collaborators Qihan Liu and Yuhang Hu modeled the surface deformation using a nonlinear field theory of hydrogels which was

implemented as a user subroutine in the commercial software ABAQUS.[37] The crosslink density of the hydrogel was chosen such that the ratio of the shear modulus of the gel in acidic conditions over that of the epoxy matched the experimentally measured value, $G_{gel}/G_{epoxy}=0.37\text{x}10^{-3}$. Since the behavior of pH-responsive gels can be also understood in terms of the osmotic pressure,[43] we simulated the changes in the pH by prescribing a corresponding change in the osmotic pressure. Under homogeneous pH conditions in which structures are programmed to stand upright in the contracted gel state (Figure 36 top), upon swelling, the gel deforms vertically and increases in thickness; the gel is surface-attached and cannot expand laterally (Figure 36 bottom), and as a result, structures do not actuate. However, under conditions of a sharp pH gradient (Figure 36 middle), we observed that the hydrogel was additionally able to deform horizontally, and this displacement was always in the direction of the acidic region causing structures to be sheared toward the contracted gel. The calculated result is shown in Figure 36, middle, where the gel color indicates the magnitude of horizontal displacement leftward. Our model suggests that the largest horizontal displacement should take place near the acid/base interface and the hydrogel should gradually revert to zero horizontal displacement farther from the interface. This prediction correlates well with the experimental observation of structural bending within a transition zone of finite width. Furthermore, if influence from the embedded structures is neglected, the width of this transition zone should be proportional to the thickness of the gel, which is the only relevant length scale in the system. The experimentally determined correlation between the thickness of the gel and the width of the transition zone appeared to initially follow this predicted linear behavior (Figure 35). At larger gel thicknesses (>50 μm), however, we began to observe that the gel formed creases both along and perpendicular to the interface, and the linear relationship was no longer valid.

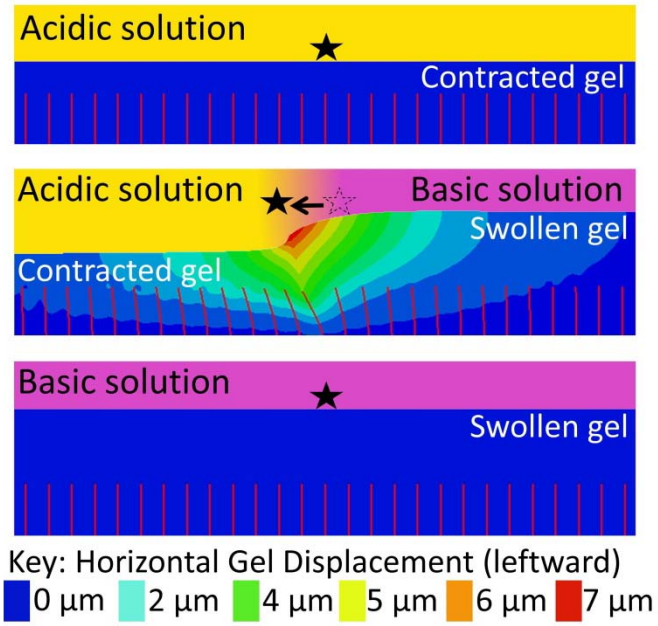

Figure 36. Finite element method (FEM) simulation of the hydrogel and embedded structures in contracted gel (top), across a sharp acid/base interface (middle) and in swollen gel (bottom). The star marks the center of the gel to emphasize the lateral shifting of the hydrogel in the pH gradient case (middle), which is the underlying mechanism for actuation. Gel color indicates the magnitude of leftward displacement. Background color indicates pH (yellow is acidic and purple is basic, correlating with the colors of the pH indicator used). Model credit: Qihan Liu

Conclusions

In summary, we have presented here a novel mechanism for gradient-responsive, hydrogel-driven actuation of microstructures. First, we effectively removed the homogeneous pH response of the hybrid systems made of pH-responsive hydrogel, allowing us to explore the use of gradient pH stimuli to affect tunable actuation via locally generated asymmetries in the hydrogel. We have demonstrated that by using pH gradient stimuli we can achieve a higher level of control over the actuation location, degree of structure reconfiguration, actuation direction,

and general customizability and adaptiveness of the responsive hybrid surfaces. Furthermore, such surfaces now have a built-in actuation response to humidity, providing extended combinatorial sensitivity to multiple stimuli, each with its characteristic actuation pattern. In particular, microstructures embedded in a thick layer of pH-responsive gel similar to the ones in Figure 25c would show either uniform actuation of all microstructures upon dehydration, or a highly localized stripe of actuated microstructures in response to a pH gradient, or no actuation in response to bulk pH change.

Through modeling and simulations we have been able to explain the fundamental mechanism of this new method of hydrogel-driven actuation; lateral displacement of hydrogel occurring at the acid/base interface shears structures always in the direction of this displacement (towards contracted gel) providing the system with highly directional chemical sensitivity. We expect that this new actuation mechanism may prove useful for precise reconfiguration of surface structures, especially for tunable optical systems, or as visual sensors which provide insight into gel dynamics and creasing studies. Furthermore, the mechanism of actuation which we describe here is highly general and not only pH-specific, meaning that this method could be applicable for a range of environmentally-responsive hydrogels. Broadly, the multifunctional dynamic systems developed in this study, in particular the use of non-uniform chemical stimuli within environmentally-sensitive gels to induce structural asymmetry and highly localized reconfiguration (in this case, the use of a pH gradient), coupled with the ability to induce uniform bulk actuation upon application of a different stimulus (in this case, the use of hydration/dehydration), may have far reaching impact on the growing field of "smart", adaptive and multi-responsive systems

Experimental

Sample preparation: GMA-modified epoxy was replicated from PDMS as described in the Experimental section of "Chapter 1: Transitioning to All-Polymer HAIRS". Each microfin was 1.2 μm wide, 11.5 μm tall and separated side-to-side and front to back by 5 μm. Microposts were 1.5 μm in diameter and 10 μm tall with an 8 μm pitch.

To pattern hydrogel within the microfluidic channels, a photomask was used as described in the Experimental section of "Chapter 2: Incorporating HAIRS into Fluidic Environments".

A few microliters of UV-initiated pH responsive hydrogel precursor solution (20% AAm, 20% AAc, 2% bis-AAm, 1% 2-hydroxy-4-(2-hydroxyethoxy)-2-methylpropiophenone, also known as Irgacure 2959, by weight in deionized water) was placed on the GMA-epoxy microstructure sample surface, and a coverslip was placed on top. To make surfaces that actuate in response to bulk pH, the hydrogel layer had to be thin, and the coverslip should touch, or come close to touching, the structures. Upon hydrogel curing, the structures bend over; we hypothesize that the epoxy might be swelling enough such that the structure tips touch the coverslip and are compressed. To make surfaces which do not respond to bulk pH, the hydrogel must be slightly thicker, presumably so that the coverslip never comes in contact with the structures. The thickness of the hydrogel was controlled by using spacers made from layers of tape. The samples were cured under a UV lamp (100W, Black-Ray with no filter) at 5 inches away for 4 minutes, and afterwards, the cover slip mask was removed. The samples were rinsed with water to remove excess precursor solution.

Surfaces were integrated into microfluidic channels as described in the Experimental section of "Chapter 2: Incorporating HAIRS into Fluidic Environments". Typical flow rates ranged from 10-50 μL per minute.

Optical imaging and video recording were done on an Olympus IX71 inverted microscope using StreamPix v.3 software and QImaging Retiga 2000R color camera.

Confocal microscopy: Pyrromethene 546 (Exciton, Inc.) was mixed into the GMA-modified epoxy and used for structure replication. 1 μm red fluorescent carboxylate-modified microspheres (Invitrogen, 2% solids) were diluted 10x in deionized water, and a few drops were let dry on the surface of the hydrogel after sample fabrication but before integration into a microfluidic cell. Confocal microscopy was done on a Leica DMI3000 SP5 TCS in conventional mode.

Chapter 6: Multiphoton Lithography of Hydrogels for 3D Incorporation into HAIRS

Parts of this chapter have been adapted from: L. D. Zarzar, P. Kim, M. Kolle, C. J. Brinker, J. Aizenberg and B. Kaehr, "Direct writing and actuation of 3D-patterned hydrogel pads on micropillar supports." *Angew. Chem. Int. Ed.*, **50**, 9356-9360 (2011).

Collaborators: Philseok Kim, Mathias Kolle, C. Jeffrey Brinker, Joanna Aizenberg, Bryan Kaehr

Introduction

Many biological organisms employ micro- and nanoscale systems to actuate structural components with a high degree of spatial control. The resulting patterned or predetermined movement of the components gives rise to versatile biological materials with locally reconfigurable features and region-specific dynamic properties. HAIRS, similarly, would benefit from the ability to be tailored for scenarios in which highly localized and directed actuation of just a few structures at a time is required.

In previously discussed HAIRS, the hydogel is anchored to a solid basal surface which imposes a serious constraint on the gel's capacity for expansion/contraction, thus limiting the extent of induced actuation of the structural elements and requiring that the hydrogel have a significantly large swelling ratio. Moreover, the previous HAIRS fabrication approaches do not allow the formation of hydrogel islands that would induce localized actuation of selected areas and the associated regional changes in surface properties.

To expand the opportunities for integration of hydrogels in such composite systems including HAIRS, it would be advantageous to tailor not only the chemistry and swelling

properties of the hydrogels but also the size, shape, and placement of the gel in relation to other system components. For example, well-defined, three-dimensionally (3D)-patterned, responsive hydrogel pads placed at the tips of microposts with microscale control would enable nearly unrestricted gel swelling, both in and out of plane, which would actuate the posts locally with more precise control over the movement of individual elements. While extensive research has been devoted to tailoring the swelling, chemical properties, and responsive behavior of hydrogels, less attention has been paid to the development of patterning protocols that would offer area-specific synthesis and 3D control over micro/nanoscale features of the gel. Many routes to defining hydrogel patterns have been explored, including photolithography,[44] soft lithography,[45] and masking techniques;[46] these 2D approaches lack true control over gel features in 3D, limiting their application for localized microactuation.

In this chapter, we discuss an approach to the direct-writing of reversibly swelling pH- and temperature-responsive hydrogel patterns onto polymeric microposts using multiphoton lithography and examine their localized actuation.[47]

Multiphoton Lithography

Multiphoton lithography (MPL) has emerged as a prominent method for the fabrication of intricately 3D-structured materials with nanoscale precision.[48] Pulsed laser light is focused into a photosensitive reagent solution (e.g., photoresist) to initiate photochemical reactions by a multiphoton absorption process. This nonlinear excitation is restricted to regions of high photon density (i.e. proximal to the focal volume of a focused laser beam), enabling photochemical reactions, such as photopolymerization, to be confined to highly resolved 3D volumes on the order of ~ 1 FL (Figure 37). MPL has been commonly used with epoxies[48] and acrylic resins[48-

[49] that tend to be rigid when cured, allowing for creation of detailed and stable structures. However, much less attention has been given to MPL of soft materials such as hydrogels. While MPL has been used to polymerize acrylate-based[14b, 50] and protein-based hydrogels[51], in many cases the stimuli-responsive behavior of these hydrogels has not been investigated and only rarely were the swelling properties reported.[14b, 50c, 51]

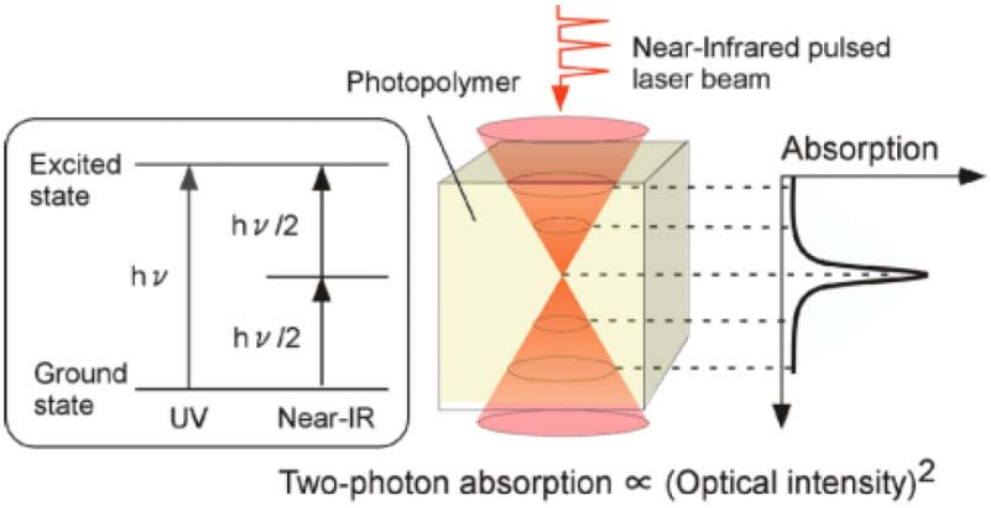

Figure 37. Schematic representing the fundamentals of multiphoton polymerization. Two (or more) photons of lower energy, near-infrared light are absorbed by the UV-sensitive initiator. The rate of two-photon absorption is proportional to the square of the light intensity; therefore the polymerization will be confined to a small volume at the laser focus. Reproduced with permission from John Wiley and Sons, © 2008 WILEY-VCH Verlag GmbH & Co. KGaA, Weinheim.[52]

Mode of Actuation

If the hydrogel is attached only to the structures and not to the basal surface, the gel is far less constrained within the surface plane, generating another distinct chemo-mechanical responsive actuation mode. The driving force behind actuation in this case is lateral gel

expansion and contraction parallel to the surface plane induced by changes in a homogenous stimulus (Figure 38). Structures are actuated radially inward and outward, with structures near the edges of the gel receiving the greatest amount of force and bending the most and structures near the middle receiving less net force and remaining relatively undisturbed. Because the gel expansion is radially outward, the direction the structures are pushed is determined by the overall shape of the gel. Therefore, it is possible to achieve a specific actuation pattern by rationally designing the geometry and placement of the gels on the surface in combination with a corresponding stimulus.

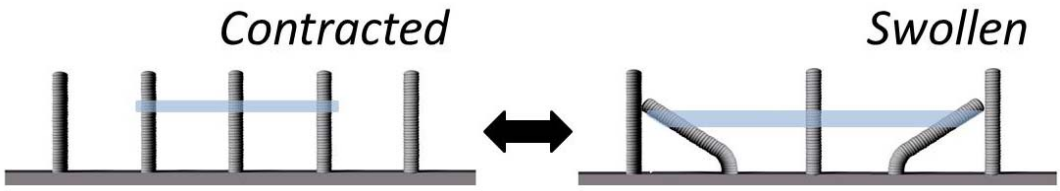

Figure 38. Schematic diagram presenting the general mechanism of actuation resulting from expansion and contraction of hydrogel pads tethered to the sides or tips of structures (but not adhered to the basal surface). The hydrogel is able to more freely change volume laterally, generating localized actuation in which structures move inward and outward from the center of the gel pad.

Patterning Hydrogel Pads on HAR Structures

For this work we used both PNIPAAm and poly(AAm-*co*-AAc) hydrogels; however, the solvent and initiators differ from previous chapters (see the Experimental section of this chapter for details). In a typical experiment, monomer precursors were dissolved in ethylene glycol (40% w/w) in the presence of a UV-curable photoinitiator (1% w/w), such as bis(2,4,6-

trimethylbenzoyl)-phenylphosphine oxide (Irgacure 819), which shows significant absorption around 400 nm to enable two-photon excitation using 750-800 nm pulsed laser light operating at relatively low average powers. The ethylene glycol was exchanged with water after fabrication. As shown in Figure 39a, hydrogel precursor solution is placed on a micropost surface and the laser is passed through an objective lens and into the solution. Polymerization occurs proximal to the laser focus as it is scanned across the sample (Figure 38b), and hydrogel structures of user-defined shapes[53] can be written directly on the bristles at arbitrary distances above the basal surface (Figure 39c).

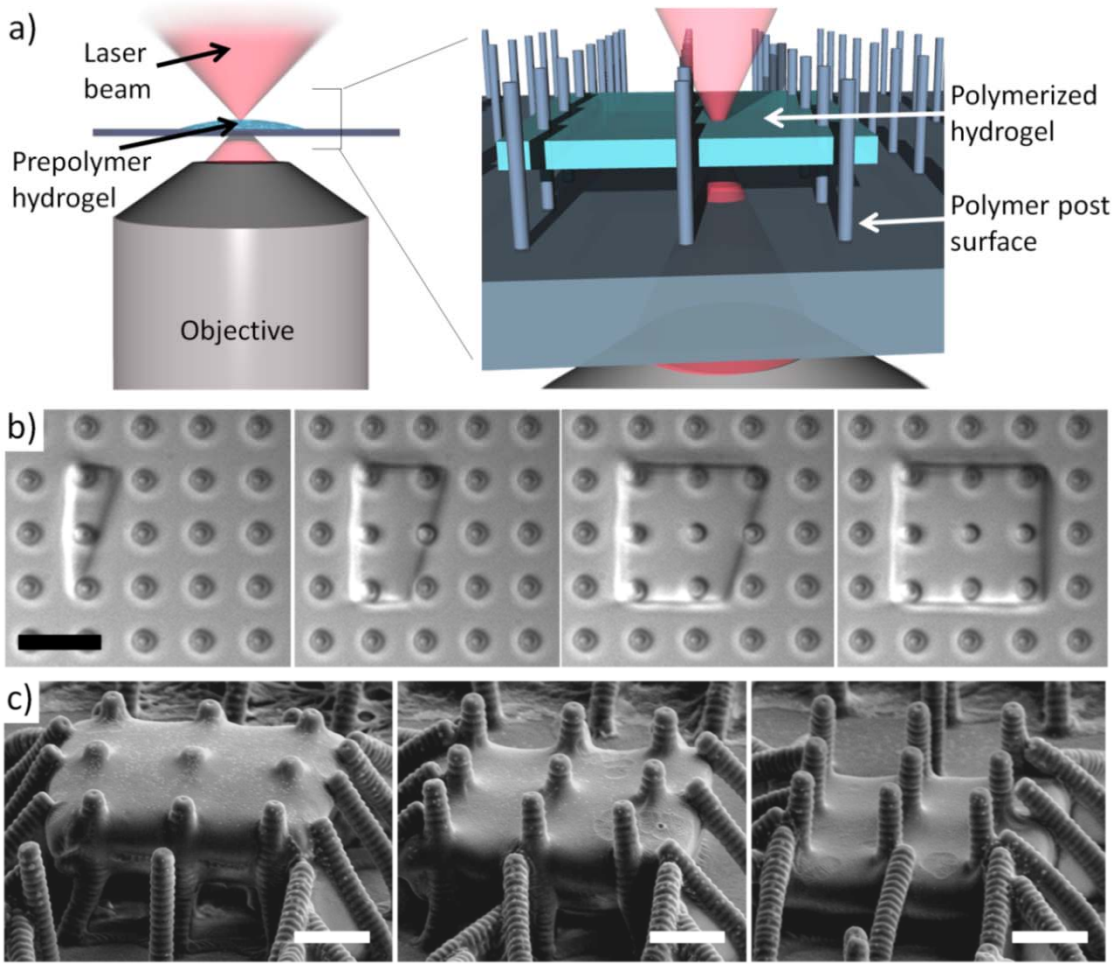

Figure 39. a) Schematic showing the experimental set-up for localized synthesis of MPL hydrogels onto microposts (height = 10 μm, pitch = 8 μm, diameter = 1.5 μm). b) Image sequence of multiphoton-induced polymerization to form a thin hydrogel structure attached to the posts. Scale = 10 μm. c) SEM images show fabricated hydrogel structures placed precisely along the top, middle, and bottom of the posts. The thickness of the hydrogel pads is ~2 μm and is made by two passes of the scanning laser beam. Scale = 5 μm.

Actuation Dynamics, Direction, and Bending Angles

Using the MPL fabrication technique, we patterned both temperature and pH-responsive hydrogel pads on the tops of flexible microposts (Figure 40a). Optical images of a heart-shaped PNIPAAm gel, fabricated at the micropost tips, in the contracted (T > LCST) and swollen (T < LCST) states, reveal that the shape of the gel can influence the bending direction of posts as they are pushed radially outward (Figure 40b). In comparison, a poly(AAm-*co*-AAc) hydrogel patterned in a disk shape exhibits a VPT near the pK_a of acrylic acid (4.3)[23] and actuated the microposts in a similar fashion except that the circular nature of the gel led to a more uniform radial distribution of post bending directions (Figure 40c). These hydrogels (both temperature- and pH-responsive) could be swollen and contracted rapidly (fractions of a second) for dozens or more cycles with little deformation in gel structure. Importantly, suspending the hydrogel on the flexible posts above the substrate surface allows the gel to swell and contract significantly without being constrained by surface attachment. For the thin suspended hydrogel pads, absolute expansion and contraction is greatest along the axes parallel to the surface plane, thus actuating the flexible posts outward or inward. To demonstrate the importance of suspending the gel, we fabricated a pH-responsive gel attached to the basal surface (Figure 40d) but otherwise identical to the gel shown in Figure 40c. The degree of lateral swelling in response to pH is significantly constrained due to the surface attachment, and the actuation of the posts is negligible.

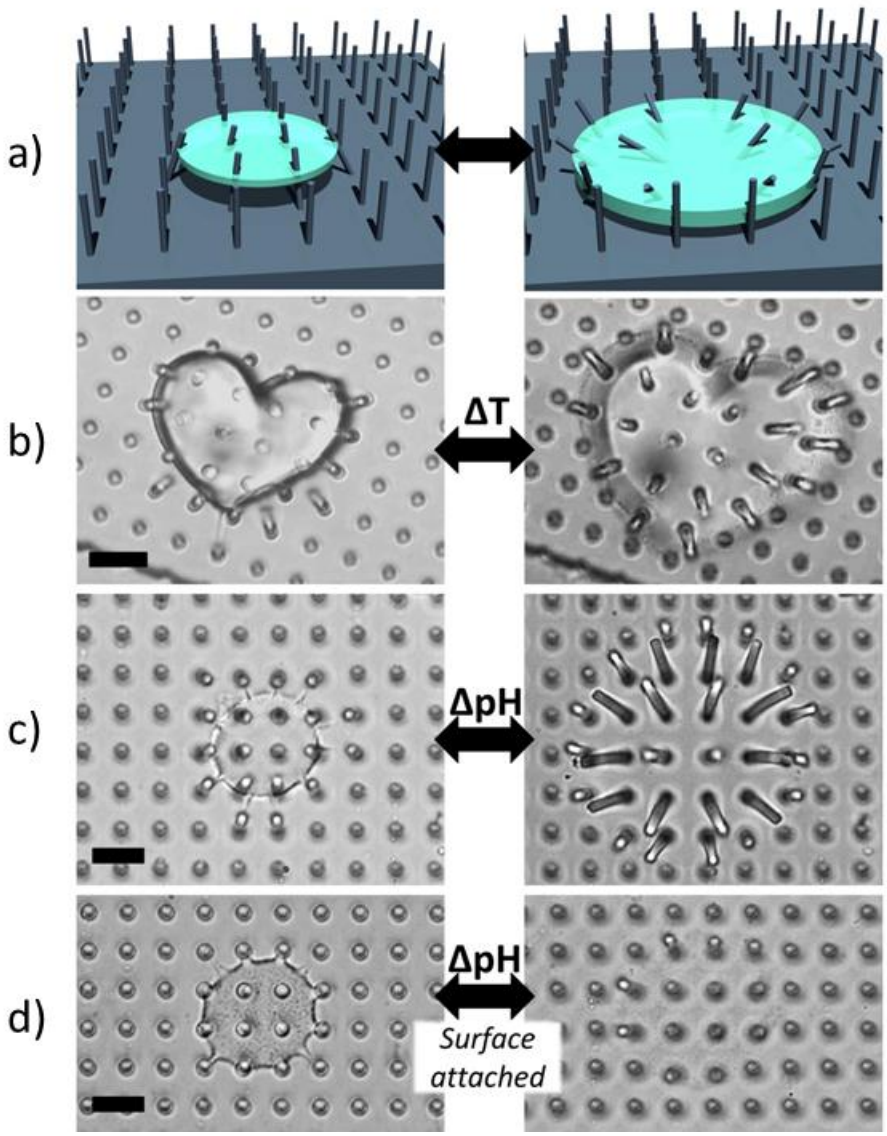

Figure 40. a) Schematic showing the deflection of the flexible posts via tip-attached hydrogel swelling. Optical microscope images of the contracted and swollen states of b) temperature-responsive hydrogel (at T>~30°C and T<~30°C) and c) pH-responsive hydrogel (at pH<4 and pH>5) are shown. d) A thin pH-responsive gel under the same conditions as c), but fabricated at the base of the posts and attached to the basal surface. The attachment to the basal surface prevents the lateral expansion of the gel, and actuation is diminished. Scale = 10 μm.

We envision using these 3D-patterned hydrogels as muscle components to actuate artificial filamentous surfaces (or other flexible structures) with a high level of control. To guide these efforts, we investigated how the swelling of the disk-shaped MPL-patterned poly(AAm-*co*-AAc) hydrogel influences the bending of the epoxy posts across a range of pH values between 2 and 8.8 (Figure 41a). Bending angles for three posts (chosen in a single row across the diameter of the disk) exhibit a sharp VPT between pH = 4–5 in correlation with the expected pH range for the VPT. However, the absolute bending angle in either the swollen or contracted state ultimately depends on the position of each post; for posts located near the outer edge of the hydrogel, bending angles between -20° and >70° were accessible, but for posts near the center of the hydrogel disk, the range was much smaller. Assuming that the primary force exerted upon the posts arises from an outwardly-expanding hydrogel located near the tips, the forces exerted upon the microposts were approximated using $Force = 3\pi DEr^4/(4h^3)$, where E is the Young's modulus of the glycidyl methacrylate-modified epoxy (1.5 GPa),[26] r is the radius of the posts (0.75 μm), h is the height of the posts (10 μm), and D is the distance to which the tip of each post is deflected from its initial position. The forces mapped over the surface plane of the disk in Figure 41b indicate that forces on the order of μN were generated near the edge of the swelled gel—sufficient for microscale manipulations where viscous forces on the order of pN must be overcome.[54] The ability to apply directed forces and dictate filament trajectory via its relative position within the gel provides a foundation to begin to explore actuation schemes over larger distances, for instance, to direct or trap particles with environmental cues using a cilia-like mechanism.

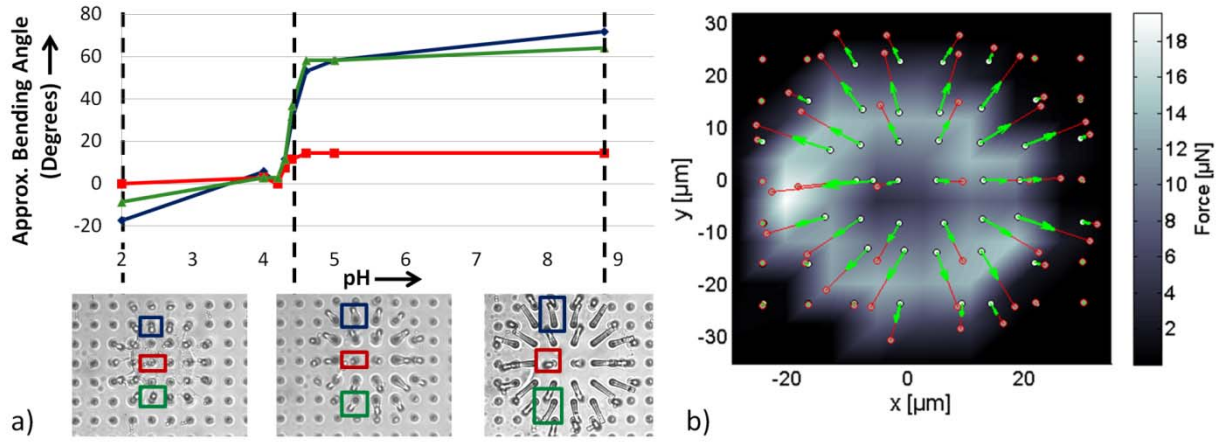

Figure 41. a) Plot of approximate bending angles of posts that support a pH-responsive hydrogel pad as a function of pH, where a negative angle represents the post bending inward toward the center of the gel, and a positive angle represents outwardly bending posts. Posts near the center of the structure (red) show little change in bending. Posts near the edge of the hydrogel (blue and green) bend to very large angles (>70°). b) The displacement of the posts was used to generate a force map of the gel. White circles indicate the initial positions of the tips of the posts when the gel is contracted, and red circles indicate the position of the tips of the posts when the gel is swollen. Red lines connect the initial and final positions. Green arrows symbolize the amount of force normalized to the largest force experienced by a post in the system. The background color map visualizes the extent of the net force exerted on the posts in different areas of the gel. Figure credit for b): Mathias Kolle

Actuation can also be tuned by the laser exposure times (by changing the scan rate or number of scans), which affect the swelling behavior of the gels (Figure 42). Too short an exposure time, and the hydrogel appears weak, or soft – the expansion and contraction cannot generate enough force to actuate structures. Too long of an exposure time and the hydrogel gets

highly cross-linked which leads to a decreased swelling ratio, and little actuation is observed. Therefore by simply tuning the exposure time of the laser, it is possible to affect the relative swelling behavior of the hydrogel; one can pattern the dwell time over a single gel structure such that parts of the hydrogel pad are more densely cross-linked than others.

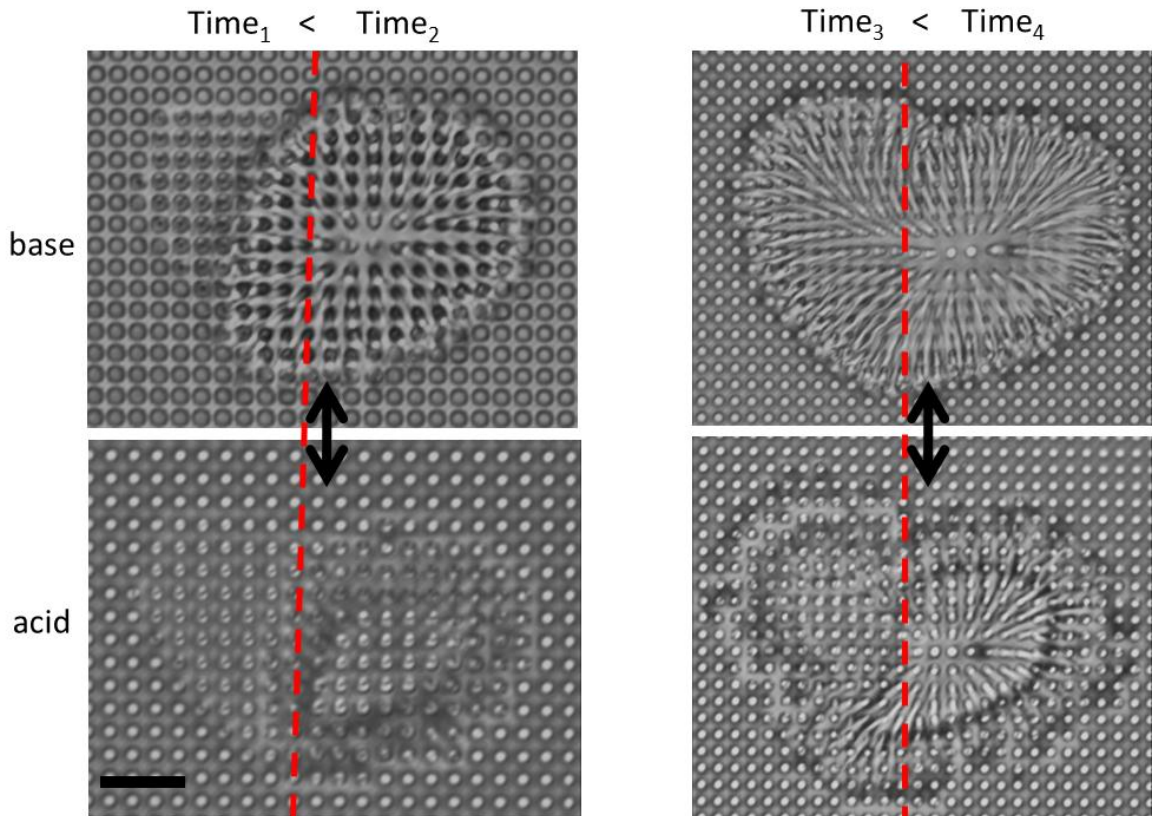

Figure 42. Optical micrographs showing the effects of laser exposure time, tuned by number of scans, on hydrogel properties and actuation behavior. Two heart-shaped hydrogel pads patterned on nanopost substrates (post height = 8 μm, post diameter = 250 nm) in which the two halves of each heart were exposed to different exposure times of the laser. $Time_1$ is the shortest time and $Time_4$ is the longest time. $Time_1$ is not long enough as the hydrogel film is too weak to push the structures outward; $Time_2$ and $Time_3$ exhibit good actuation behavior, but $Time_4$ is too densely cross-linked, and not all of the structures resume an upright position during actuation. Scale = 10 μm.

Actuation can also be achieved using gels made from cross-linked bovine serum albumin (BSA) (Figure 43). These protein gels show volume change in response to pH as changes in the electrostatic interactions within the proteins induce them to unfold or refold.[51] However with too many cycles of pH, or with too extreme of a pH value, the proteins eventually denature and cease to be responsive.

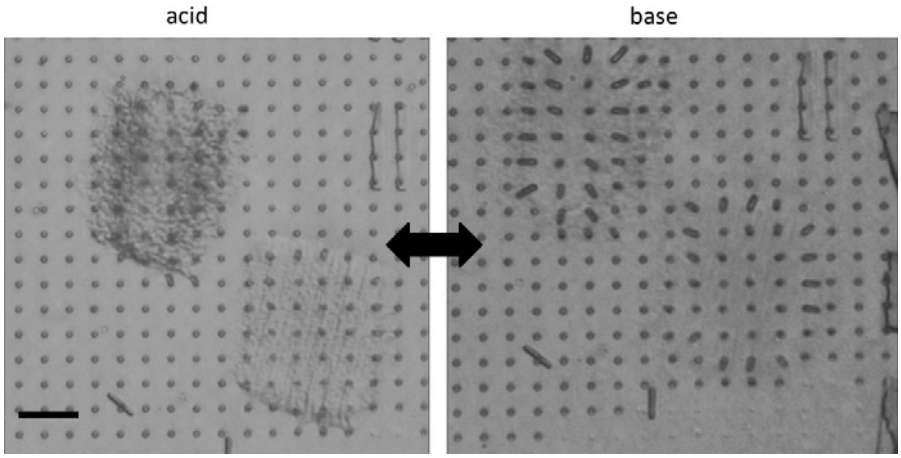

Figure 43. Actuation achieved using BSA hydrogels. The BSA protein eventually denatures and so not many actuation cycles can be achieved. The swelling ratio (and therefore the respective actuation of the posts) is also smaller than what can be achieved by the acrylate-based hydrogels. Scale = 20 μm.

Combinatorial Actuation Responses

The ability to synthesize interacting hydrogels that respond to different stimuli should allow for more complex actuation behaviors not achievable with uniform hydrogel muscles. As shown in Figure 44, the pH-responsive hydrogel and temperature-responsive hydrogel were patterned sequentially as interlocking puzzle pieces. Each hydrogel could be stimulated in an independent manner by changing the combination of pH and temperature. Posts that had a

temperature-responsive hydrogel on one side and pH-responsive hydrogel on the other, near the interface of the gels, could therefore be actuated to four stable configurations; one such post is highlighted in Figure 44. The shape of the hydrogel at the interface (the interlocking part of the pieces) could be compressed or expanded by the response of the neighboring gel. In Figure 44, for example, comparison of (a) to (b) and (c) to (d) illustrates that at constant temperatures but varying pH, the extruding part of the temperature-responsive hydrogel piece is compressed beyond its equilibrium state by an expanding pH-responsive hydrogel. Similarly, upon comparison of (a) to (c) and (b) to (d), we see that the shape of the pH-responsive hydrogel at the interlocking segment is expanded at constant pH but varying temperature. The ability to precisely pattern interacting hydrogels of varying responsivity may provide opportunities for the design of systems exhibiting predictive and programmable responses for different combinations of environmental conditions. Structures may now have more than a single "muscle" that controls actuation and induces complex movement of structural elements.

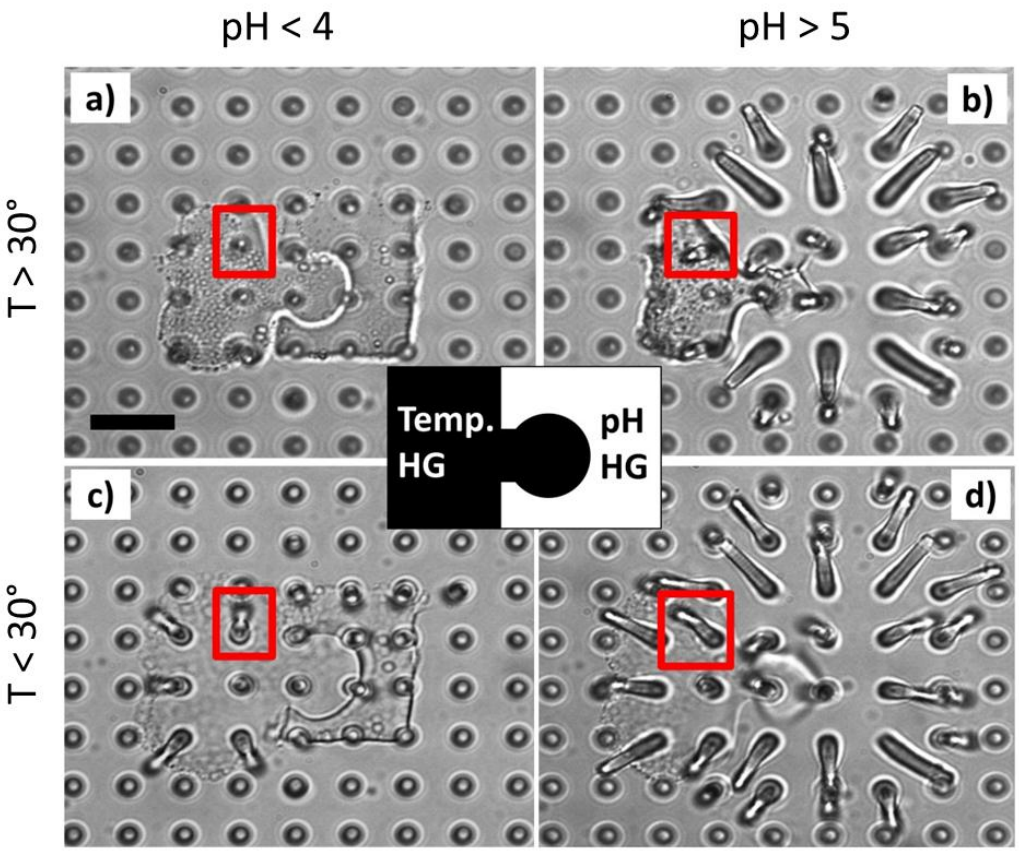

Figure 44. A schematic image showing temperature- and pH-responsive hydrogels fabricated in close proximity as interlocking puzzle piece shapes (center). Optical microscope images at each temperature and pH combination are shown (a-d). The black outline highlights an exemplary post as it is bent at four different angles and directions depending on the combination of conditions. Scale = 10 μm.

Dynamic Optical Response

An important feature of responsive hydrogels is the ability to dynamically adjust and tune the functional density of any chemical moiety in the gel via the VPT. To demonstrate this capability in MPL-generated gels, we co-polymerized a fluorescent, polymerizable rhodamine monomer, methacryloxyethyl thiocarbamoyl rhodamine B, with the pH-responsive hydrogel and

patterned the gel on the microposts (Figure 45). We used poly(AAm-*co*-AAc) because of its large swelling response and rhodamine B because its fluorescence is insensitive to changes in pH over the range needed for the swelling response. Expansion and contraction of the fluorophore-modified hydrogel conferred substantial changes in the fluorescence intensity. In particular, suspending the gel above the substrate surface through attachment along the tips of the posts provided excellent "on/off" behavior of the signal. The significant changes in fluorescence intensity were attributed to the large VPT of the unconstrained hydrogel and its influence on the effective density of the fluorophore within the gel volume. Using multiphoton excitation point measurements, which provide a means to probe a fixed volume of the hydrogel in both its expanded and contracted states, we measured a ~20-fold increase in the density of rhodamine molecules within gels similar to those pictured in Figure 45. As a result, the message in Figure 45a is clearly seen at pH < 4.3 and effectively "erased" at pH > 4.3. Similarly, additional functional components including nanoparticles,[55] peptides,[56] and DNA,[57] can be readily incorporated into these gels and should expand the opportunities for sensors and catalytic systems[58] in which the density and availability of the active sites is tuned via gel response.

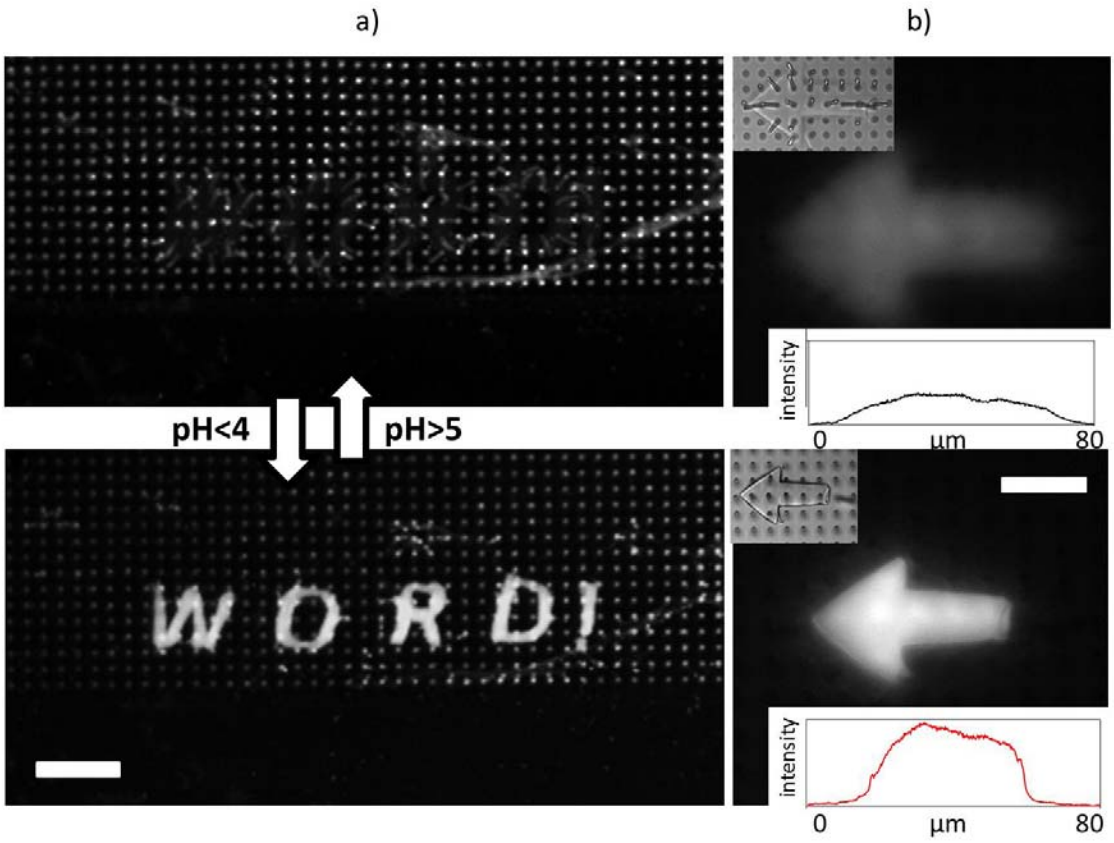

Figure 45. Fluorescence microscope images demonstrating fast and reversible appearance and disappearance of messages due to the change in concentration density of a rhodamine dye which was incorporated into a pH-responsive hydrogel. a) Contraction of the hydrogel in acid increases the fluorescence signal to reveal the message, "WORD!" Scale = 40 µm. b) Contraction of the hydrogel in acid reveals the arrow symbol. Upper insets show differential image contrast images of the gel. Lower insets show the fluorescence intensity profile along the length of the arrow normalized to the bit depth of the fluorescence image. Scale = 20 µm.

Conclusions

In conclusion, we have described a synthetic route to fabricate arbitrary 3D shapes of temperature- and pH-responsive hydrogels using MPL. This procedure allows hydrogels to be

precisely positioned in a suspended state on HAR micropost structures giving rise to significant gel expansion without the surface constraint that typically results from traditional patterning methods in which the gel is attached to the basal surface. The bending angle and actuation direction of microposts are shown to depend on their relative lateral positions (i.e., center versus edge) within the swelling gel, providing a means to direct the movement of post structures with a high degree of tunability. We have shown that this approach makes it possible to pattern interlocking, interacting hydrogels responding to different stimuli and thus to develop unique, complex gel and structural interactions via orthogonal environmental cues. Additionally, hydrogels can be further functionalized, for instance, by introducing a polymerizable fluorophore to generate an optical readout based on the actuation-induced concentration change. MPL-patterned responsive hydrogels incorporating chemical, optical, and catalytic[58] or enzymatic[59] functions will provide great opportunities to develop multi-component chemical reaction, sensing, and diagnostic systems. Although here we describe micro-patterned 3D 'muscle-like' materials integrated with relatively simple micropost components, similar 3D microactuation is achievable for more complex 'skeletal' structures that can be fabricated using common MPL acrylic- and epoxy-based precursors. These studies can be further extended to 3D-patterning of other common responsive gels that are based on similar polymerization chemistry, thus tuning the responsivity of the system for various environments. This synthetic procedure, with its significant capabilities for extensions in structural as well as hydrogel variability, should prove enabling for the exploration of autonomous micro/nano-actuators both inspired by biological systems and those creatively engineered.

Experimental

Substrate and hydrogel preparation: AAm, AAc, BIS, GMA, NIPAAm, EG, and (tridecafluoro-1,1,2,2-tetrahydrooctyl) trichlorosilane were purchased from Sigma-Aldrich (St. Louis, MO). PDMS (Dow-Sylgard 184) was purchased from Ellsworth (Germantown, WI), UV-curable one-component epoxy (UVO-114) was purchased from Epoxy Technology (Billerica, MA), methacryloxyethyl thiocarbamoyl rhodamine B was purchased from Polysciences, Inc., and Irgacure 819 was obtained from BASF. All the chemicals were used as received.

Silicon micropost masters were fabricated using the Bosch process and were replicated in 9:1 (w/w) prepolymer mixture (UVO-114:GMA) on coverslips as described in detail in "Chapter 1: Transitioning to All-Polymer HAIRS". pH-responsive hydrogel prepolymer solution (20% AAm, 20% AAc, 2% BIS, 1% Irgacure 819 by weight in ethylene glycol) and temperature-responsive hydrogel prepolymer solution (40% NIPAAm, 2% BIS, 1% Irgacure 819 by weight in ethylene glycol) were sonicated in the dark for ~5 minutes in a 50°C water bath to assure dissolution of all chemicals and were used immediately. For fluorescently labeled hydrogels, <0.5% by weight of methacryloxyethyl thiocarbamoyl rhodamine B was added. BSA hydrogels were made using a 400 mg/mL aqueous solution of BSA containing 2 mM methylene blue as a sensitizer.

MPL instrumentation and hydrogel polymerization: A mode-locked Ti:sapphire laser (Tsunami, Spectra Physics) operating at ~750 nm with a 60 fs pulse width and 80 MHz repetition rate was used as the light source for two-photon-induced polymerization. Structures were defined using mask-directed MPL as previously described (Figure 46).[53] Briefly, the laser focus was raster scanned with an X/Y open frame scan head (Nutfield Technology) across a digital micromirror device (DMD) that served as a reflectance mask. The laser beam was adjusted to

fill the back aperture of an oil-immersion objective (Nikon 100× Fluar, 1.3 NA) situated on a Nikon inverted microscope. ~100 µL of hydrogel prepolymer solution was placed on the polymer micropost surface and allowed to wet before fabrication. An average laser power of 20-50 mW, measured at the back aperture of the focusing objective, was used to polymerize the hydrogels. After fabrication, all hydrogels were rinsed a minimum of five times in deionized water.

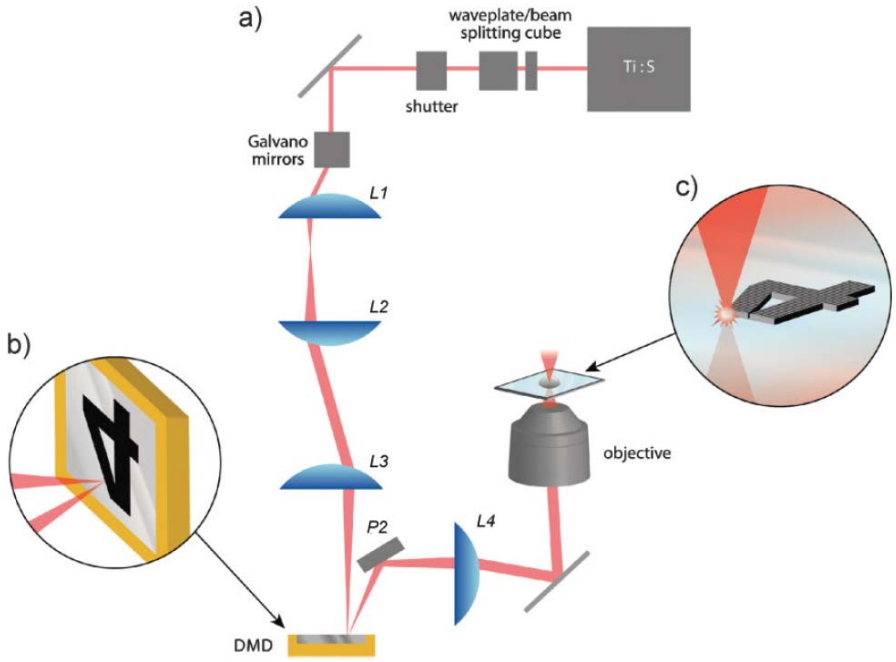

Figure 46. Schematic overview of the MPL set-up.[53] a) The Ti:S laser beam is raster scanned using a pair of galvano-driven mirrors. The relay lenses (L1, L2, and L3; focal lengths 2.5, 10.2, and 15.2 cm respectively) direct the beam onto a DMD. The beam reflects off the DMD and is guided by a periscope (P2) and recollimated using a tube lens (L4, focal length 15.2 cm) before entering the microscope objective. b) Close-up of the beam reflecting off the DMD; the beam is reflected in the "4" shape, which is translated into the "4" pattern generated by polymerization

Figure 46 (Continued)… on the cover slip in c). Image reproduced with permission from John Wiley and Sons, © 2009 Wiley-VCH Verlag GmbH & Co. KGaA, Weinheim.[53]

Sample characterization: Optical imaging was done with the same Nikon inverted microscope setup used for MPL. Optical and fluorescence images and movies were captured using an Andor Ixon EMCCD. Hydrogels were probed by changing either the temperature or pH (using NaOH and HCl) of the solutions.

Determination of dye concentration within poly(AAm-co-AAc) gels: The concentration of rhodamine was estimated using multiphoton-excited (MPE) fluorescence measurements within a swollen and contracted poly(AAm-co-AAc) hydrogel. A mode-locked Ti:sapphire laser beam (10 mW measured at the back aperture of the objective) was focused onto the rhodamine functionalized poly(AAm-co-AAc) gel which was fabricated using MPL. Fluorescence was detected using an Andor Ixon EMCCD over a fixed integration time for the swollen and contracted gel. Over the concentration range of 0.01 – 0.2 mM of rhodamine B, the MPE fluorescence response was observed to scale linearly with the concentration of dye ($R^2 = 0.98$). For a gel fabricated under identical conditions to that presented in Figure 45, the concentrations of the dye in the swollen and contracted states of the gel were determined to be ~0.007 and ~0.170 mM respectively.

Chapter 7: Chemo-mechano-chemical Manipulation of Reactions using HAIRS

Parts of this chapter have been adapted from: X. He, M. Aizenberg, O. Kuksenok, L. D. Zarzar, A. Shastri, A. C. Balazs and J. Aizenberg, "Synthetic homeostatic materials with chemo-mechano-chemical self-regulation." *Nature*, **487**, 214-218 (2012).

Parts of this chapter have been adapted from: X. He, R. S. Friedlander, L. D. Zarzar, and J. Aizenberg, "Chemo-Mechanically Regulated Oscillation of an Enzymatic Reaction." *Chemistry of Materials*, **25**, 521-523 (2013).

Collaborators: Ximin He (primary experimental contributor), Michael Aizenberg, Ronn Friedlander, Olga Kukensok, Ankita Shastri, Anna C. Balazs, Joanna Aizenberg

Introduction

As already exemplified, hydrogel-driven hybrid actuation systems are keen examples of chemo-mechanical (C→M) actuators; the hydrogel provides the chemical sensitivity to a wide range of stimuli, and the embedded HAR structures provide the basis for translation into directed motion. But building from the HAIRS systems described in preceding chapters, we can take the concept a step further and can use the well-characterized mechanical actuation of the hybrid system to induce a programmed chemical output ($C_1 \rightarrow M \rightarrow C_2$) (distinct from the chemistry inside the hydrogel).[35, 60] Such ability would open routes for unique mechanistic control over dynamic chemical reactions, generation of output products including biochemicals, light, heat, or gas, and even the possibility of feedback loops if there is correlation between the chemical output

and the hydrogel sensitivity. Despite its importance in living systems, the concept of chemo-mechanical regulation has not been applied extensively to man-made materials. Synthetic materials typically sense or actuate only along a single chemo-mechanical[24, 61] (C→M) or mechano-chemical[62] (M→C) route, and are generally incapable of integration into feedback mechanisms that necessarily incorporate both pathways ($C_1 \rightarrow M \rightarrow C_2$ or $C \leftrightarrow M$).

The systems described in this chapter are based upon the fundamental HAIRS platform described in "Chapter 3: HAIRS with Thin Films of Hydrogel Actuating in Response to Homogeneous Stimuli"; we take advantage of stimulus compartmentalization so that the surface can be designed to mediate a variety of both chemo-mechanical processes and homeostatic feedback loops, reversibly transducing external or internal chemical inputs into user-defined chemical outputs via the on/off mechanical actuation of microstructures.

Controlling Reaction Dynamics with HAIRS

To synchronize the responsive actuation such that the output reaction can be turned on and off by the movement of the HAR structures, the chemical change driving the actuation ($C_1 \rightarrow M$) must be physically separated from the reaction that produces the chemical output ($M \rightarrow C_2$). This can be achieved by the vertical compartmentalization systems discussed in "Chapter 2: Incorporating HAIRS into Fluidic Environments" either by microfluidic layering with two miscible liquids flowing on top of one another or with a static interface between two immiscible liquids. In this way, the chemical stimulus C_1, which induces the hydrogel to expand or contract to drive actuation, can be introduced to the bottom layer, while the top layer contains reagents that will be acted upon by a catalyst attached to the structure tips (C_2). When structures stand upright, the structure tips enter the reagent environment and the reaction is turned "on";

when the structures bend, their tips exit the reagent layer and the reaction is turned "off" (Figure 47). Because the chemical environments are physically separated, the system allows for the coupling of a wide variety of chemical inputs and outputs which may otherwise be chemically incompatible.

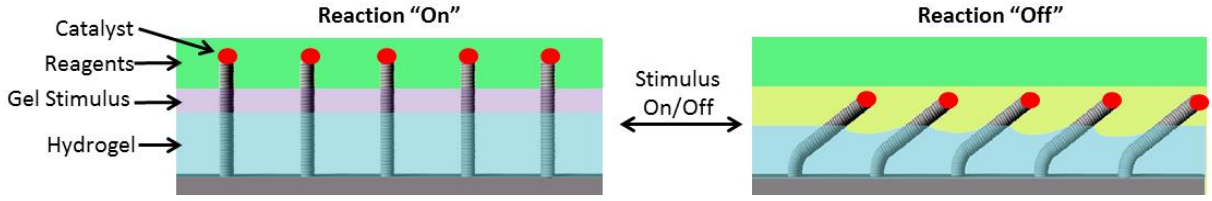

Figure 47. Schematic of HAIRS which can be used to control the on/off switching of a chemical reaction. The separation of the reagents and the gel stimulus is required such that when the structures actuate, the tips (affixed with another reagent or a catalyst) will move in and out of the reagent layer, thereby switching on and off the reaction.

Using a pH-responsive HAIRS integrated into a microfluidic channel with the pH stimulus flowing in the bottom layer and reagents flowing in the top layer, we were able to demonstrate three different output reactions all coupled with pH-driven actuation of the microstructures. First, to determine optical actuation and flow conditions, we performed a simple reversible quenching reaction in which fluorescein, stamped on the tips of the structures, was actuated into and out of an upper liquid containing potassium iodide (Figure 48a). To demonstrate a straightforward catalytic reaction, Pt-coated tips actuated into and out of a dilute solution of hydrogen peroxide, generating intermittent bubbles (Figure 48b). Such HAIRS systems can also be used in sensitive biologically relevant environments, and to exemplify this we also used a similar system to turn on and off an enzymatic reaction which gives off

luminescence, namely the oxidation of luciferin by luciferase (Figure 48c). In this case, because the enzyme is sensitive to pH, we altered the responsiveness of the hydrogel such that the VPT was centered at pH 7 rather than pH 4.3 by adding 10% (w/v) dodecyl acrylate to the pH-responsive hydrogel precursor solution.[63]

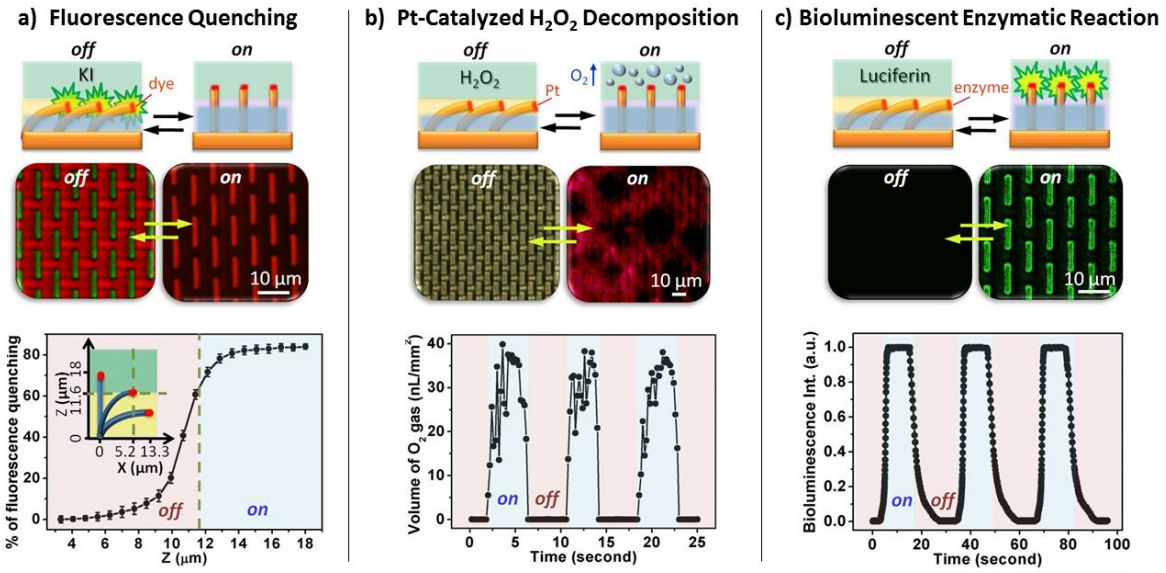

Figure 48. Oscillations in exemplary chemical reactions triggered by pH changes. a) Fluorescence quenching of fluorescein. Top: schematic showing that fluorescein on the tips of the microfins is quenched as they enter a solution of potassium iodide. Middle: confocal micrographs showing that the green fluorescence of fluorescein on the tips of bent fins disappears as they enter the quenching layer. The red fluorescence is from rhodamine in the bottom layer. Bottom: fluorescence intensity as a function of tip position. b) Platinum-catalyzed decomposition of hydrogen peroxide generating oxygen gas. Top: schematic. Middle: optical micrographs showing bubble formation. Color arises from bromophenol blue pH indicator. No bubbles form in the absence of the catalyst, serving as a control. Bottom: time-resolved gas generation synchronous with the action of the fins. c) Bioluminescent enzymatic reaction. Top:

Figure 48 (Continued)… schematic showing how luciferase-coated tips catalyze the light-producing oxidation of luciferin. Middle: confocal micrographs showing the switching on/off the bioluminescent enzymatic reaction. Bottom: oscillations in bioluminescence intensity synchronous with the actuation of the microfins. Figure credit: Ximin He

Feedback Loops

If the chemical output itself can trigger a differential response in the hydrogel and subsequently induce actuation, then it is possible to create a feedback loop within the hybrid system. For example, a temperature responsive PNIPAAm hydrogel can be paired with a variety of possible exothermic output reactions to generate a tunable homeostatic feedback loop that autonomously maintains the surface temperature at a programmed set-point (Figure 49). When the temperature is below the LCST of PNIPAAm (T<32°C) the gel is swollen and the structures stand upright, thereby turning on an exothermic reaction. As the solution heats to above the LCST, the hydrogel contracts, which causes the structures to bend, turning off the reaction to allow a cooling phase. When the solution cools to below the LCST, the cycle starts again, regulating the oscillating temperature within a few degrees of the LCST indefinitely as long as the reagents are replenished (Figure 50).

Such feedback systems are tunable based on parameters such as the responsiveness of the hydrogel, exothermic reaction used, rate of heat production, structure geometry, and the location of the bilayer liquid interface. If the LCST is altered by changing the hydrophobicity of the hydrogel, then the temperature range over which the surface fluctuates will change accordingly; a system in which the exothermic reaction is the hydrosilylation of 1-hexene with triethylsilane and the gel has a LCST=32°C maintains temperatures between 31.0 and 33.8°C, but a system

incorporating a gel with LCST=27.8°C but using the same reaction conditions maintains temperatures of 27.1-29.7°C (Figure 50).

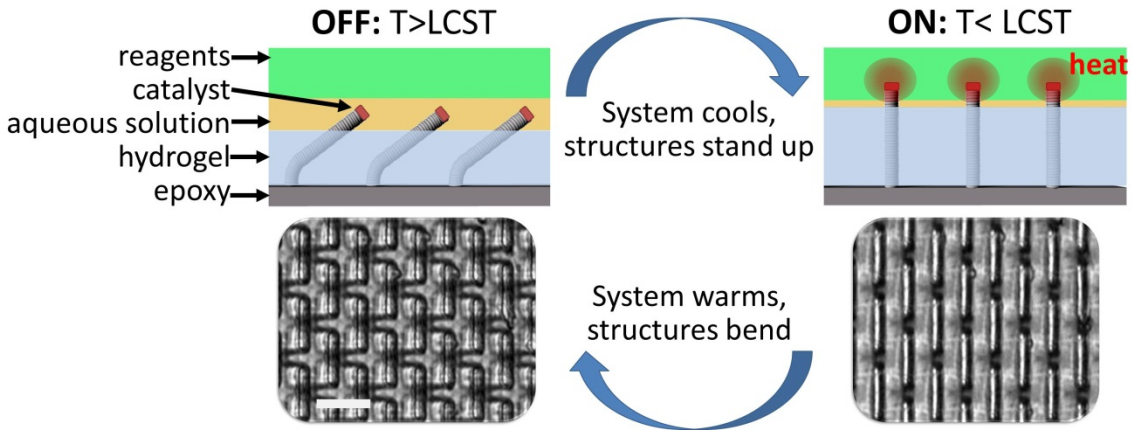

Figure 49. Schematic demonstrating the feedback mechanism of a temperature-regulating hybrid surface. The structure tips are coated with a catalyst which upon entering the reagent layer induces an exothermic reaction. This generated heat raises the surface temperature to above the LCST of the PNIPAAm hydrogel, causing the gel to contract and the structures to bend over, removing the catalyst from the reagent layer and turning off the reaction. The surface cools to below the LCST and the structures stand up again, restarting the feedback cycle. Scale = 10 µm.

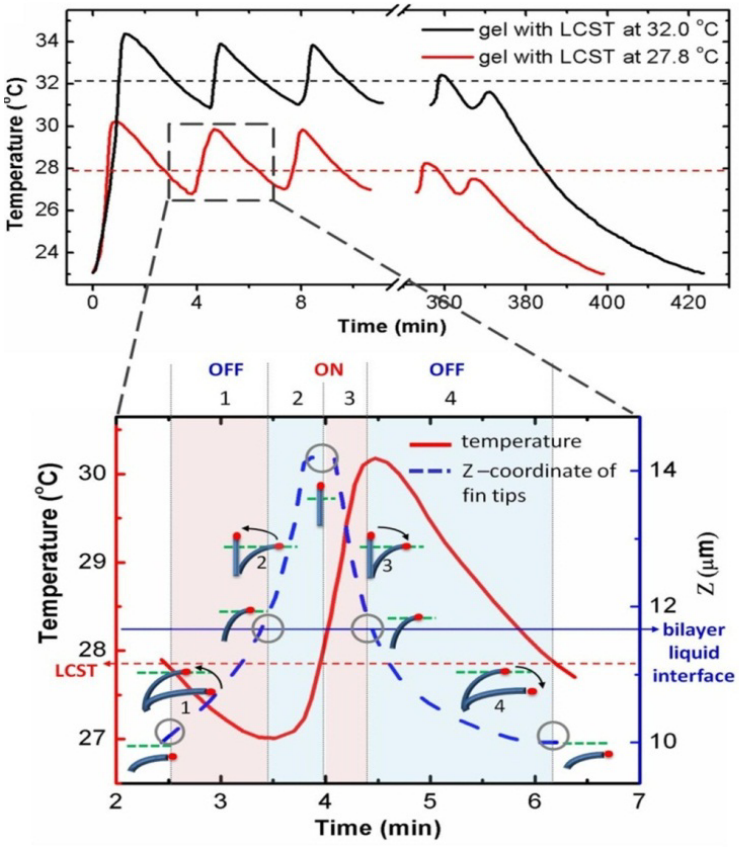

Figure 50. Surface temperature measurements for surfaces with two PNIPAAm-based hydrogels with different LCSTs. As the LCST is changed, the temperature transition for actuation is similarly altered, leading to fluctuations centered at tunable temperatures. Inset shows time-resolved temperature and vertical coordinate (z) of the microfin tips for the system with LCST = 27.8°C. Note that there is a shift between the two curves. Figure credit: Ximin He

A variety of exothermic reactions can be incorporated into such a system, each with its own dynamics and characteristic parameters (Figure 51). Exothermic reactions demonstrated include the hydrosilylation of 1-hexene with triethylsilane or diphenylsilane catalyzed by H_2PtCl_6, the decomposition of cumene hydroperoxide catalyzed by Ph_3CPF_6, and a click reaction between octylazide and phenylacetylene catalyzed by $Cu(PPh_3)_2NO_3$. Each has its own characteristic kinetics and heat generation profiles which ultimately affect the dynamics of the

feedback process. If the heating rate is lower, the amplitude of the temperature fluctuations will decrease and the oscillation period will be lengthened. For example, if reaction (i) in Figure 51 is diluted by 20% for a given HAIRS, we observed an increase in the period from 3.58 min/cycle to 3.85 min/cycle and the temperature fluctuations went from 2.8°C to 2.3°C. Letting the system run for a significant amount of time, thereby depleting reagents, has the same effect. Replacing triethylsilane in reaction (i) with diphenylsilane in (ii), which is more reactive, follows the same trend; a more vigorous reaction led to a higher heating rate, shorter oscillation period, and higher temperature amplitude. Raising the bilayer interface results in smaller temperature fluctuations around a slightly lower temperature, presumably because the catalyst-bearing tips spend less time immersed in the reagent layer. Such geometric and chemical parameters lend the system a high degree of customizability.

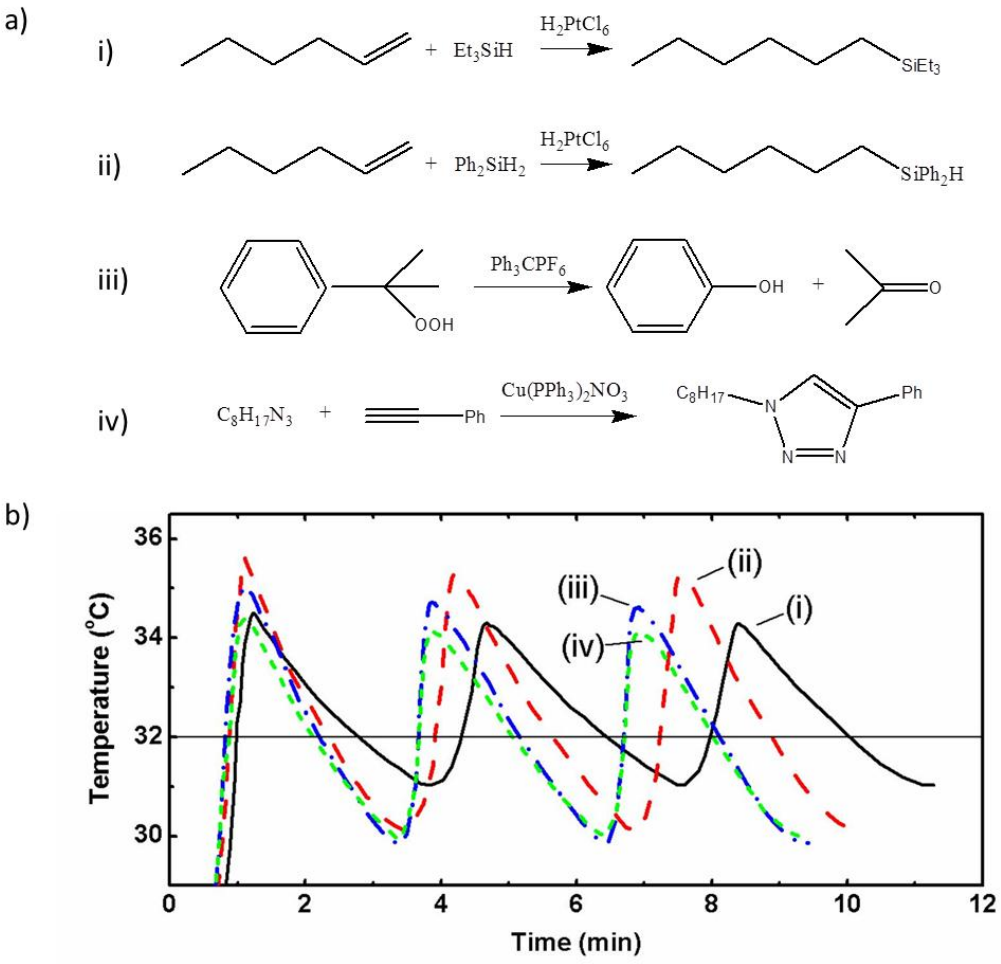

Figure 51. a) Exothermic reactions incorporated into HAIRS with thermal feedback: i) hydrosilylation of 1-hexene with triethylsilane catalyzed by H_2PtCl_6, ii) hydrosilylation of 1-hexene with diphenylsilane catalyzed by H_2PtCl_6, iii) the decomposition of cumene hydroperoxide catalyzed by Ph_3CPF_6, and iv) a click reaction between octyl azide and phenylacetylene catalyzed by $Cu(PPh_3)_2NO_3$. b) Temperature oscillations arising from different exothermic reactions driven by PNIPAAM hydrogel. The labels i-iv correspond to reactions i-iv in a). Figure credit: Ximin He

Conclusions

By compartmentalizing the chemical stimuli and the chemical outputs, either by microfluidic or static techniques, traditional HAIRS have been afforded the capability to chemo-mechanically manipulate reactions. This transition from a chemo-mechanical system, in which an environmental stimulus drives the mechanical movement of the embedded structures, to a chemo-mechano-chemical system in which that mechanical movement can be used to manipulate another chemical output, provides many new opportunities for the generation of self-sustaining, self-regulating materials as well as implications for unique mechanistic control of chemical dynamics and spatiotemporally patterned chemical reactions. Because HAIRS are so customizable, as demonstrated both within this chapter and in preceding sections, they may prove useful for previously difficult sensory and regulatory functions across a wide range of chemical environments, including sensitive biological systems.

Experimental

HARS fabrication: pH and temperature responsive HAIRS were fabricated as described in the Experimental section of "Chapter 3: HAIRS with Thin Films of Hydrogel Actuating in Response to Homogeneous Stimuli". One exception is the pH-responsive hydrogel used in HAIRS for controlling the bioluminescent enzymatic reaction in which case the pH of the VPT must be increased. 10% w/v of dodecyl acrylate was added to the hydrogel precursor solution, and dimethylformamide was used as the solvent.[63] The other exception is that the PNIPAAm hydrogel precursor had 5% of butylmethacrylate added to decrease the LCST of the hydrogel to 27.8°C. The LCST was characterized with differential scanning calorimetry. The microfins used were 2 μm wide, 10 μm long, and 14.5 or 18 μm tall, with spacing of 5 μm in a staggered array.

Tip functionalization: Deposition of fluorescein (100 mg/L in 1:1 v/v water:ethanol), $Cu(PPh_3)_2NO_3$ (50 mg/mL in chloroform), Ph_3CPF_6 (40 mg/mL in ethanol), H_2PtCl_6 (1 mg/mL in water), and luciferase (0.1 μM in HEPES buffer at pH 7.5) was accomplished via PDMS stamping on plasma-treated structure tips overnight to let solvent dry. Unbound reagent/catalyst was rinsed away.

Reagents for exothermic reactions: Cumene hydroperoxide (80% solution), triphenylcarbenium hexafluorophosphate (Ph_3CPF_6), and sodium azide were purchased from Sigma-Aldrich (St. Louis, MO). Phenylacetylene was purchased from Alfa Aesar. Octyl azide was synthesized from octyl bromide **(**Oakwood Products**)** following published procedure.[64] Nitratobis(triphenylphosphine)copper(I), $Cu(PPh_3)_2NO_3$, was synthesized following published procedure.[65]

Bilayer liquids: Stable biphasic interfaces or vertical laminar flow accomplished with microfluidics was used to create the bilayer liquid environments as described in "Chapter 2: Incorporating HAIRS into Fluidic Environments". For fluorescence quenching, the lower phase was either HCl aqueous solution of pH=3 or pH=6 and the upper phase was 0.6 M potassium iodide aqueous solution. For Pt-catalyzed decomposition of hydrogen peroxide, the lower phase was the same as for the fluorescence quenching and the top phase was 0.5% H_2O_2. For the enzymatic reaction, an aqueous solution of 0.01 mM D-luciferin sodium salt with 2 mM $MgCl_2$ and 0.3 mM ATP magnesium salt in 50 mM HEPES pH 7.5 buffer was used in the top fluid layer and alternating flow of pH = 6 sodium citrate buffer and pH=9 sodium tetraborate buffers were used as the bottom layer. For the exothermic cumene hydroperoxide decomposition, the top phase consisted of 40% (v/v) cumene hydroperoxide in toluene and the bottom phase was water. For the exothermic click reaction, the top phase consisted of 1:1 (by mol) octyl azide (2.5 μL)

and phenylacetylene (1.5μL) and the bottom phase was water. For the exothermic hydrosilylation, the top solution was 1-hexene:triethylsilane (or diphenylsilane) at a 1:1 molar ratio. The bottom phase was water.

Chapter 8: Responsive Hydrogel Scaffolds for Mechanical Compression of Cells

Collaborators: Basma Hashmi, Joanna Aizenberg, Donald Ingber

Introduction

Cells and tissues developing *in vivo* experience a myriad of complex stimuli, both chemical and mechanical, which influence their development, differentiation, and function. Recently, there has been increased interest in understanding the effects of different mechanical forces upon cells and tissues and the role that these mechanical forces play in differentiation and organ formation, especially so that this knowledge can be applied to tissue engineering.[66] For instance, cell fate can be controlled by mechanically manipulating cell shape,[67] mitotic spindle orientation can be mechanically controlled by the application of tension to transmembrane integrin receptors,[68] and mechanical stimuli can alter cell lineage commitment.[69] There have been many approaches used to apply and measure forces to cells *in vitro*, including substrate stretching, out-of-plane circular substrate distention, fluid shear systems, micromanipulation, AFM, and magnetic forces.[66, 70] We are interested as to whether the actuation of responsive hydrogels could be similarly engineered to apply directed mechanical forces to cells and induce desired differentiation.

Temperature-responsive PNIPAAm hydrogel is ideal for such a scaffold, as the LCST is near to, or can be tailored to, biologically-relevant conditions (near 37°C). This characteristic of PNIPAAm has made it a popular materials choice for some biological applications, especially drug delivery,[71] cell encapsulation,[72] and injectable scaffolds.[73] Also, PNIPAAm undergoes a relative shift from hydrophilic to more hydrophobic when raised above the LCST, a property that has been used to release cells and tissues from surfaces.[74]

PNIPAAm is often mixed with co-monomers or surface-functionalized with other molecules in order to tune the LCST and the adhesive properties of the hydrogel. Acrylic acid, for example, can be added to increase the LCST from 32°C to closer to 37°C.[75] In many cases the PNIPAAm should be chemically modified with biopolymers or proteins/peptides, such as chitosan,[76] gelatin,[77] or short –RGD– containing peptides,[78] to increase cell affinity. However, chemical additives can also drastically change the LCST and reduce the swelling ratio of the gels, so design of PNIPAAm gels with specific responsive behavior can be a challenge depending on the desired properties and application.

Use of PNIPAAm Hydrogel to Trigger Tooth Differentiation

In the condensed mesenchyme, cells become closely packed together and begin to differentiate into a single tissue type, a critical step in the development of a range of organs including the tooth, cartilage, bone, muscle, and lung.[79] Recently it was reported that externally-applied mechanical compression of mesenchymal stem cells (MSCs) was sufficient to drive tooth organ formation.[79] In this condensed phase cells change shape and size, which has been correlated with changes in cell fate; therefore, mechanical stimuli which provide a route to alter cell shape or size have the potential to influence subsequent organ formation.[80] Interestingly, it was discovered that compression-induced changes in cell shape were highly important to tooth development, and that even externally-applied mechanical compression (such as between sheets of PDMS) was able to induce similar changes in cell shape and subsequent differentiation that normally occur within a tightly condensed mesenchyme.

Therefore, we propose the use of a temperature-responsive hydrogel, PNIPAAm, to serve as both the scaffold and as the means by which to compress cells and induce tooth

differentiation. Such scaffolds must fulfill several requirements: 1) the hydrogel LCST must be at or below 37°C, 2) the hydrogel must support cell viability both below *and* above the LCST, so that cells can spread on the gel at a lower temperature (when the hydrogel is swollen) and be subsequently compacted via hydrogel contraction, and 3) the hydrogel must have a sufficiently large swelling ratio to compress cells enough as to induce differentiation. While it is not unusual to use functionalized PNIPAAm as a scaffold in the contracted state (above the LCST), PNIPAAm scaffolds in their swollen state (below the LCST) are typically neither used to culture cells nor used as a means to mechanically compress cells.

Design of GRGDS-modified PNIPAAm Hydrogels for Cell Compression

Our approach to the design of PNIPAAm scaffolds was to first generate a base recipe consisting of 10% NIPAAm and 1% BIS w/v in water for fabrication of PNIPAAm hydrogels with a large swelling ratio and mechanical stability (meaning high enough crosslinking density so that the scaffolds maintain structural integrity in the swollen state and are not fluid). We then added to this base recipe an adhesion-promoting peptide monomer, acrylate-GRGDS, in an approach more commonly used to modify poly(ethylene glycol) hydrogels.[81] To synthesize the GRGDS monomer, the peptide was reacted with *N*-acryloxysuccinimide (NAS) (Figure 52) and purified by dialysis.

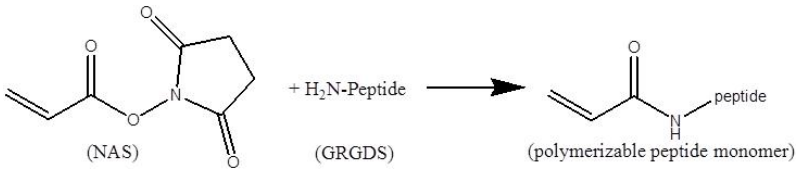

Figure 52. Reaction scheme for synthesis of the GRGDS peptide monomer.

Because the LCST of the PNIPAAm hydrogel is very sensitive to the addition of monomers that change the relative hydrophobicity of the polymer, addition of the peptide significantly increased the LCST of the gel. Therefore, just enough peptide monomer was added to bring the LCST to ~36-37°C. Although the exact concentration of the GRGDS within the PNIPAAm scaffold is unknown, the LCST (as measured by differential scanning calorimetry, DSC) serves as a proxy for peptide concentration for purposes of reproducibility and consistency. The swelling ratio was still quite large even after addition of peptide (Figure 53). The swelling ratio, defined as $(M_{34°C} - M_{37°C})/M_{37°C}$, was measured to be 0.8±0.1.

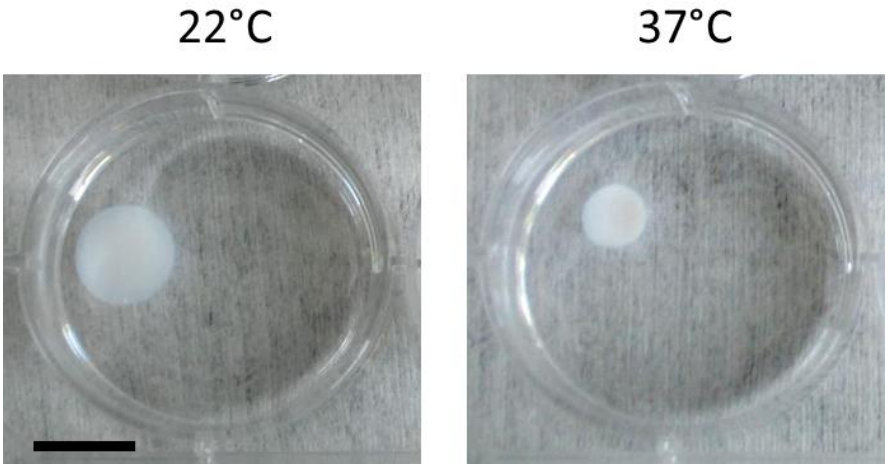

Figure 53. Photographs of a peptide-modified PNIPAAm hydrogel at room temperature and 37°C. Scale = 1 cm.

The dry, lyophilized gels were imaged by SEM. Images of the lyophilized hydrogel reveal pores with a large size distribution (tens to hundreds of microns), but the interconnectivity of the pores is unclear. There is also a non-porous "skin" layer over parts of the scaffold which may hamper cells from migrating into the scaffold. Such a skin is a typical result of hydrogel lyophilization.[82]

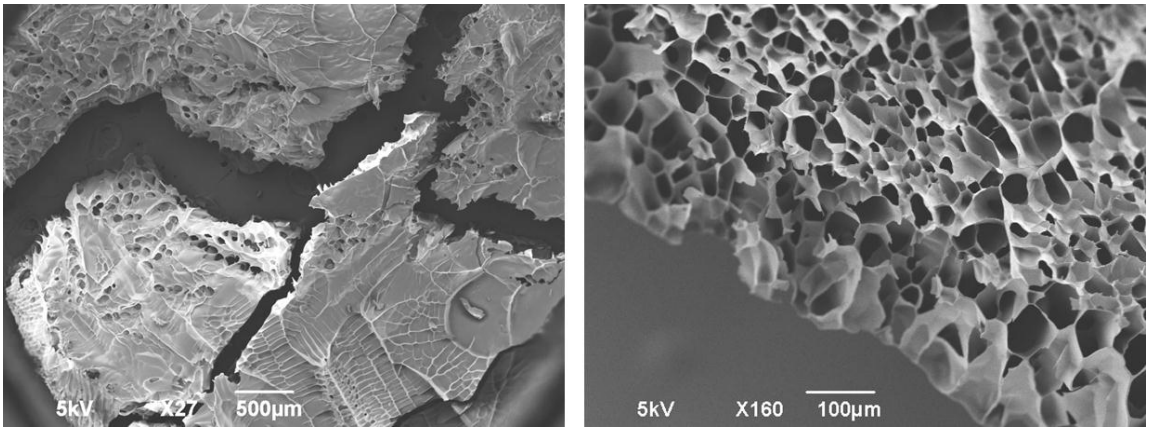

Figure 54. SEMs of the surface (left) and cross section (right) of a peptide-modified PNIPAAm hydrogel after lyophilization.

Determination of biocompatibility and efficacy of hydrogel compression on cell compaction and differentiation is still underway. Preliminary results indicate good viability of cells on the hydrogels at 37°C, with 90% viability after 3 weeks.

Experimental

NAS, NIPAAm, and BIS were purchased from Sigma Aldrich. Ammonium persulfate (APS) was purchased from Mallinckrodt, tetramethylethylenediamine (TEMED) was purchased from Calbiochem, and GRGDS peptide was purchased from Bachem Biosciences. All were used as received except for the NIPAAm, which was recrystallized from hexane.

Peptide Modification: GRGDS was modified with an acrylate moiety on the N-terminus to allow copolymerization into the hydrogel scaffolds. 25 mg of GRGDS was divided into 4 aliquots of 1 mL each using sodium bicarbonate buffer (pH=8.2) as the solvent. One aliquot (6.25 mg of GRGDS) was diluted to 6 mL with sodium bicarbonate buffer and stirred in a round bottom flask while a solution of NAS (0.02g NAS in 3 mL of sodium bicarbonate buffer) was

added dropwise. The solution was stirred in the dark for 2.5 hours at room temperature. The solution was dialyzed for 3 days at 4°C against deionized water with frequent bath changes (Spectra/Por Float-A-Lyzer G2, 10 mL, 0.1-0.5 kD MWCO cellulose ester membrane) to remove unreacted NAS and hydrolysis byproducts. The product was frozen at -80°C and lyophilized. The product was verified by mass spectrometry.

Hydrogel Synthesis: The lyophilized acrylate-modified GRGDS was redistributed in hydrogel precursor solution (10% NIPAAm, 1% BIS w/v in deionized water). This dilution factor was chosen by experimental trial and error to determine what concentration of peptide yielded a hydrogel with an LCST near 36-37°C. To make a hydrogel scaffold, 50 µL of the peptide/gel precursor was placed in the 1 cm diameter well of a MatTek glass bottom dish, then 4 µL of a 10% w/v aqueous APS solution was added, followed by 0.5 µL of tetramethylethylenediamine and mixing. Gelation occurred within a minute. Gels were transferred to a water bath where they were left for 3 days at 4°C to allow any unreacted monomers and initiators to diffuse out of the gel. Each hydrogel was then transferred individually to a 15 mL centrifuge tube filled partially with water, frozen at -80°C, and lyophilized.

Hydrogel Characterization: Differential scanning calorimetry (DSC) was performed (TA Instruments DSC Q200) for a few hydrogels from each batch. The gels were only used if the LCST fell within the target range of 36-37°C. The swelling ratio was defined as $(M_{34°C} - M_{37°C})/M_{37°C}$ and average $M_{37°C}$ and $M_{34°C}$ measurements were done on twelve different gels; six at each temperature (34°C or 37°C). Before weighing, the excess water was removed from the gel using weighing paper.

Conclusions

Dynamic, responsive materials that can autonomously adapt to environmental pressures in functional ways are proving to be essential components in future materials technology. Responsive hydrogels in particular, with their highly tunable and customizable chemo-mechanical properties, have proven transformative in applications[1a, 83] ranging from drug delivery[71] to self-regulating microfluidics[84] and sensors[85] and actuators.[24, 86] Hybrid materials, which take advantage of the unique properties generated by the interplay between multiple materials integrated into a coherent functional system, can allow for the development of tunable chemo-mechanical responses otherwise unachievable by a single material alone. Indeed, by exploring various approaches to the combination of just two simple and well-characterized materials, an array of structures and a responsive hydrogel, a far more complex set of chemo-mechanical actuation mechanisms has emerged. The hydrogel, which has a reversibly responsive volume change, acts as the "muscle" that provides force to reconfigure flexible HAR structures; by varying the HAR structure geometry, the chemistry of the hydrogel, and the topography, location, and pattern of the gel as well as the spatial presentation and combination of stimuli, we access a few fundamental mechanisms identified herein which provide routes to higher complexity of chemo-mechanical actuation.

Taking these systems a step further, we have developed an approach to not only translate a chemical signal into the mechanical movement of microstructures, but to then translate that mechanical movement into a coupled chemical output. Therefore, such actuators can switch system/surface properties through both chemo-mechanical means (such as using the structures' reconfiguration to alter adhesion, wetting behavior, or optical properties) as well as through mechano-chemical means, creating outputs of light, heat, biomolecules, gas, etc.

Such materials, which can sense changes in their environment and functionally respond to those external pressures via chemo-mechano-chemical processes, will provide the foundation for next-generation self-regulating, self-sustaining, and autonomously adaptive "smart" systems. While so fundamentally critical to the adaptive mechanisms and robustness of living systems, the ability to interchange mechanical and chemical inputs and outputs has proven difficult to replicate in artificial materials. While biology makes use of multi-step cascades, complex feedback processes, and ultra-sensitive chemical and mechanical receptors, we are still in the early stages of developing materials which can exhibit comparatively simple chemo-mechanical responses. However, the great promise of such adaptive systems, applied to make clothes that self-camouflage, actuating surfaces that prevent biofouling, or buildings that help save energy by self-regulating temperature or light, continues to drive research in the field of smart, chemo-mechanical materials.

Part II: Site-specific Catalysis within 3D Microenvironments

Introduction

The ability to pattern the location of target chemical reactions, interactions, and integration of moving components within "micromachines" is critical to achieving the desired properties and functions within chemo-mechanical systems. Whether such systems are nanoscale boxes built out of DNA that require highly localized, specific sequences to serve as a lock and key system[87] or micro-rotors that turn in programmable directions due to asymmetric chemical modification of each tooth,[88] it is clear that the intricate nano and microsystems of the future will be heavily reliant upon complex chemo-mechanical interactions between multiple materials within 3D organizations. A large area of research focuses on the use of catalytic chemical conversions to drive the directed movement[61c] of nano/microscale structures to create nanomotors and other nano/micromachines.[89] While the mechanisms of chemo-mechanical movement vary (bubble propulsion,[90] interfacial tension gradients,[91] etc.), to induce directional movement there should be specific, asymmetric placement of the catalyst within the microsystem.

One technique well suited to intricate 3D microscale fabrication is multiphoton lithography;[48] however, relatively little work has focused on the use of the technique for depositing metals,[92] especially for catalysis. We explore in the following sections the use of multiphoton lithography to integrate catalysts, in particular platinum and palladium, within 3D microenvironments.

Chapter 9: Multiphoton Deposition of Platinum and Palladium Catalysts

Parts of this section have been adapted from: L. D. Zarzar, B. S. Swartzentruber, J. C. Harper, D. R. Dunphy, C. J. Brinker, J. Aizenberg and B. Kaehr, "Multiphoton lithography of nanocrystalline platinum and palladium for site-specific catalysis in 3D microenvironments." *Journal of the American Chemical Society*, **134**, 4007-4010 (2012).

Collaborators: Brian Swartzentruber, Jason Harper, Darren Dunphy, C. Jeffrey Brinker, Joanna Aizenberg, Bryan Kaehr

Introduction

Platinum and palladium catalysts are crucial for a broad range of existing and emerging chemical, biological, and technological applications; consequently, substantial recent work has been aimed at understanding and improving their function and efficiency and reducing their consumption/utilization via nano-structuring.[93] Despite progress towards directed synthesis of a wide variety of platinum and palladium nanostructures and alloys, there are few reported strategies for integration of these catalysts within nano or micro-scale platforms. Specifically, the ability to dictate catalysis within microfluidic systems is crucial for the success of lab-on-chip devices which rely on well-defined catalyst/substrate interactions for improved efficiency, portability, and cost.[94] Increasingly, microfluidic designs incorporate 3D channel geometries[95]; therefore, the development of a strategy to precisely position catalysts within 3D microfluidics should enable a wide range of technologies, including autonomously powered microfluidics,

diagnostics, microreactors, and sensors, as well as energy generation, conversion, and storage applications.[61c, 89, 96]

Platinum, palladium, and rhodium have been incorporated into a microfluidic hydrogenation reactors via processes such as sputtering,[97] and recently Xu *et al.* used direct laser writing to pattern catalytic and SERS active silver microflowers within a microfluidic channel.[98] Despite these examples, the scope of catalyst printing for microreactors remains limited, and successful integration of catalysts such as Pt and Pd within 3D microfluidics has not been demonstrated.

Here we describe a straightforward procedure to integrate arbitrary micropatterns of nanostructured Pt and Pd within 3D fluidic architectures using multiphoton lithography (MPL),[99] an intrinsically 3D direct-write technique.[53, 100] These MPL-deposited Pt and Pd materials are composed of polycrystalline metallic nanoparticles that show excellent electronic, electrochemical, and catalytic properties. We show that site-specific H_2O_2 decomposition catalyzed by MPL-directed Pt can be used to drive directed fluid flow in three dimensions upon integration within appropriately designed 3D structural components. We envision similar approaches can be applied broadly for site specific catalysis in microfluidic environments, for instance, toward the design and testing of catalytic micro-pumps and motors.[90-91, 101]

Platinum and Palladium Photoreduction

The use of MPL to form conductive metallic structures has been explored;[92c, 102] however, reports on MPL of catalytic materials are scant,[98, 103] and the use of MPL to form Pt and Pd materials has not been reported. Previously, photoreduced Pt and Pd nanomaterials have been synthesized using methods often requiring the use of chemical stabilizers in order to generate

nanoparticles or nanowires.[104] To adapt the synthesis of Pd and Pt nanocrystals for MPL conditions, we explored the use of precursors often used in platinotype/palladiotype photographic processes first developed in the late 19th century[105] and recently adapted by Jiang and Miller for fuel cell applications.[106] In one such printing method, paper (serving as the support matrix) is embedded with $(NH_4)_3[Fe(C_2O_4)_3]$ and either $(NH_4)_2[PtCl_4]$ or $(NH_4)_2[PdCl_4]$; it is then exposed to UV light, which induces a photochemical reduction of the iron to form a strong reducing agent which can then reduce, for instance, Pt(II) to Pt(0), as described in the following the reactions:

$$h\nu + 2[Fe(C_2O_4)_3]^{3-} \rightarrow 2[Fe(C_2O_4)_2]^{2-} + C_2O_4^{2-} + 2CO_2$$

$$[PtCl_4]^{2-} + 2[Fe(C_2O_4)_2]^{2-} \rightarrow Pt\downarrow + 2[Fe(C_2O_4)_2]^{-} + 4Cl^{-}$$

To investigate MPL of Pt and Pd by adapting this photographic process, we mixed a 1:1 precursor solution comprised of 0.7 M of either the $(NH_4)_2[PtCl_4]$ or the $(NH_4)_2[PdCl_4]$ and 1.0 M of the $(NH_4)_3[Fe(C_2O_4)_3]$ and tested Pt/Pd direct-writing using a mode-locked Ti:sapphire laser centered at 750 nm. If the laser was focused into the solution, metal particles could be seen emanating from the focal point. If the laser was focused upon the surface of a glass cover slip, adherent Pt and Pd structures could be printed sequentially on un-modified (or ITO coated) glass with arbitrary shapes and intrinsic registration using a scanning laser, dynamic-mask based approach (Figure 55, Figure 56).[53] Bubbles were observed emanating from the opaque structure at the point of laser focus/fabrication, indicating solution boiling with likely contribution of evolution of CO_2 from ferric oxalate reduction.

The $(NH_4)_2[PtCl_4]$, $(NH_4)_2[PdCl_4]$ and $(NH_4)_3[Fe(C_2O_4)_3]$ precursors display no significant absorbance above ~550 nm (Figure 57),[105] and excitation of the charge-transfer band of $[Fe(C_2O_4)_3]^{3-}$, which is required for its subsequent photolysis, is achieved in the range of ~200

- 500 nm.[107] Thus, as expected, no initial deposition was observed when 5 mW continuous wave (CW) 750 nm light was employed.

Interestingly, we observed that further deposition of chemically and structurally identical Pt or Pd could be extended from an existing metallic structure using 750 nm CW laser light and the same precursor solutions. These observations indicate that the heat generated at the point of focus at the glass/metal interface leads to localized thermal decomposition/reduction of the ferric oxalate into an iron (II) reducing agent. The mechanism of metal oxalate thermal decomposition and resulting intermediates is highly dependent on experimental and environmental conditions,[108] but extensive heating can result in the reduction of iron (III) to iron (II) with FeC_2O_4 as a possible intermediate.[109] FeC_2O_4 has also been shown to reduce platinum and palladium precursors salts.[105] Moreover, this mechanism provides an avenue to explore direct-writing of metals using widely available and less costly CW light sources.

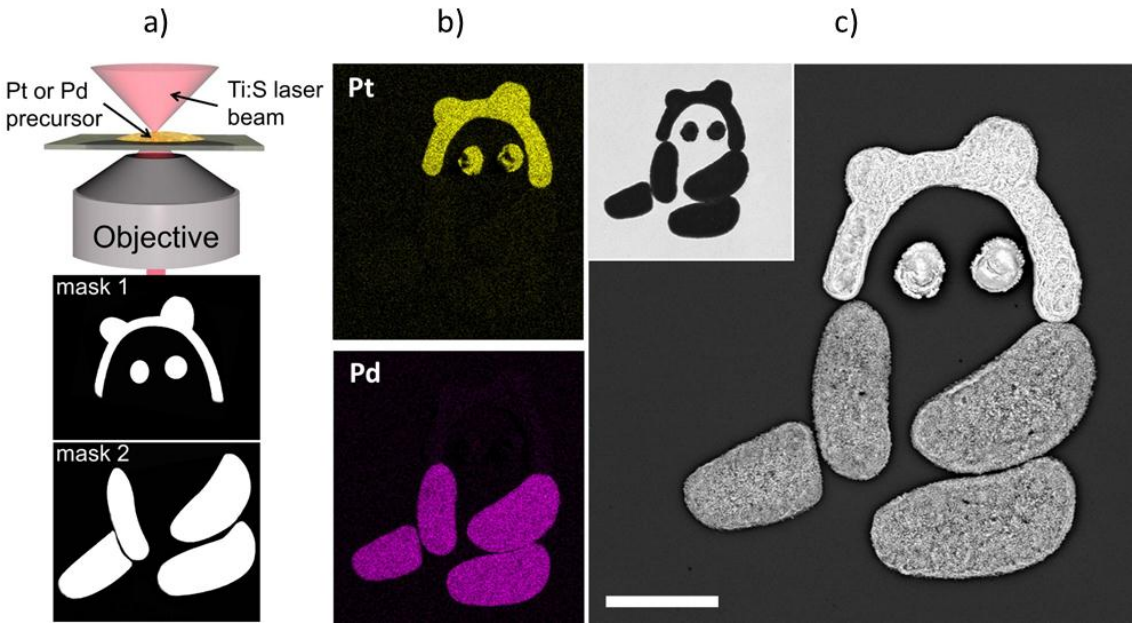

Figure 55. a) Fabrication schematic showing the two digital masks used to define Pt and Pd. b) EDS image maps indicating regions of Pt and Pd. c) Backscatter SEM. Inset is an optical micrograph. Scale = 20 μm.

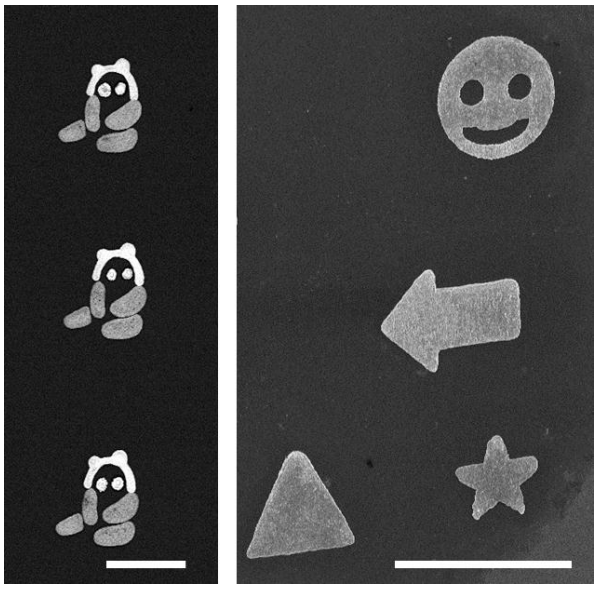

Figure 56. A series of Pt and Pd pandas (left) and various Pd shapes (right) printed on ITO coated glass. Scale = 50 μm.

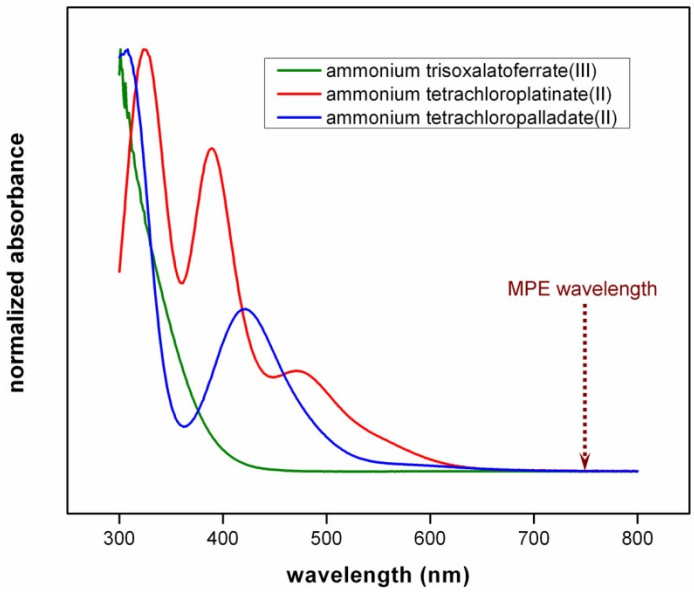

Figure 57. Absorbance spectra of all precursors. None absorb near the multiphoton excitation (MPE) wavelength of 750 nm.

Characterization of Deposited Pt and Pd

After MPL deposition on glass, structures could be rinsed rigorously post-fabrication without any detectible delamination or degradation. Figure 55b shows energy-dispersive X-ray spectrographs (EDS) and backscatter scanning electron micrographs (SEM) respectively demonstrating the fabrication of well-defined patterns of pure (i.e., no iron oxide contaminant detected with EDS) Pt and Pd. High resolution SEMs (Figure 58a,b) show that the metallic patterns are comprised of small metallic granules, indicating that the rate of photoreduction within the focal volume is limited by the diffusion of metallic precursors.[48, 92d, 110] SEM cross-sectional analysis of an exemplary Pd structure revealed that the granular surface, in large part, is continuous throughout the structure interior, down to the glass/metal interface, at which point the structure appears solidified, indicating thermal melting/annealing at the interface—a consequence of heating via light absorption by the metallic pads. We estimated the steady state

temperature rise (ΔT) at the laser focal point of the glass/metal interface using the solution for the low frequency limit (essentially CW) of the laser modulation:[111]

$$\Delta T = \frac{A_0}{2\sqrt{\pi} w_0 \Lambda}$$

where A_0 is the average power (~5 mW) multiplied by the percentage of light absorbed by the metal at 750 nm (~30% for Pt and Pd), w_0 is the $1/e^2$ radius of the focused laser spot (~350 nm), and Λ is the thermal conductivity of the glass (1.3 $Wm^{-1}K^{-1}$). These values give a maximum steady state temperature rise of ~930K under these conditions, which is substantially higher than the annealing point for borosilicate cover glass (557°C).

Using our direct write set-up, we observed a reproducible minimum line width of ca. 2 μm, with gap width resolutions of ca. 200 nm (Figure 58a). The discrepancy between minimum line width and laser spot size (~700 nm) is attributed to heating at the laser focal point, as discussed, which degrades resolution by increasing the size of the effective volume where precursors are reduced. Further characterization of the crystallinity and electrochemical properties of MPL-Pt was carried out using transmission electron microscopy (TEM) and cyclic voltammetry (CV). TEM analysis of the MPL-deposited Pt scraped from glass substrates showed clusters with crystallites ranging in diameter from 4 - 8 nm (Figure 58c), and distinct crystallographic planes could be resolved in the electron diffraction pattern of crystallites located at cluster edges (Figure 58c inset). CV was used to characterize MPL-Pt (Figure 58d), and we measured an electroactive surface area to geometric surface area ratio of ~36. We characterized the electrical properties of MPL-Pt and Pd lines written on glass substrates using an *in situ* nanoprobe technique (Figure 59) and measured resistivity values of 4.2 ± 0.5 and 2.3 ± 0.3 (μΩ·m) for Pt and Pd respectively which is approximately one order of magnitude higher than those for bulk metals (Figure 60).

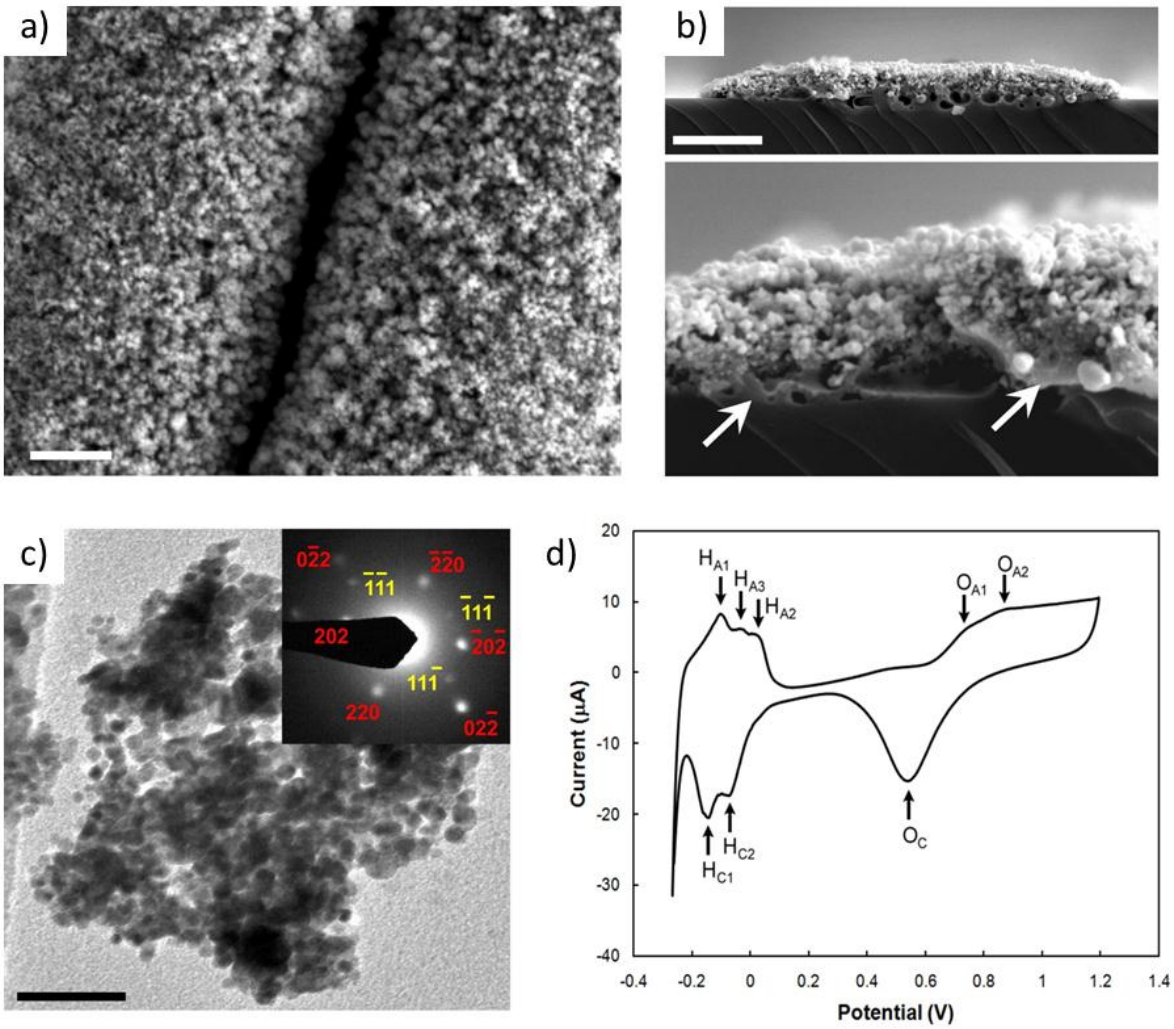

Figure 58. a) Two Pd structures separated by a ~200 nm gap. Scale = 1 μm. b) Cross section of a MPL-Pd line showing melting/annealing of the glass (left arrow) and Pd (right arrow). Scale = 5 μm. c) TEM of MPL-Pt crystallites and electron diffraction pattern obtained from the edge of a cluster (corresponding to two crystallites). Scale = 50 nm. d) CV of an MPL-Pt working electrode in 1.0 M H_2SO_4 shows hydrogen adsorption (cathodic peaks; H_C) and desorption (anodic peaks; H_A) and formation ($O_{A1,2}$) and subsequent reduction (O_C) of an oxide layer.

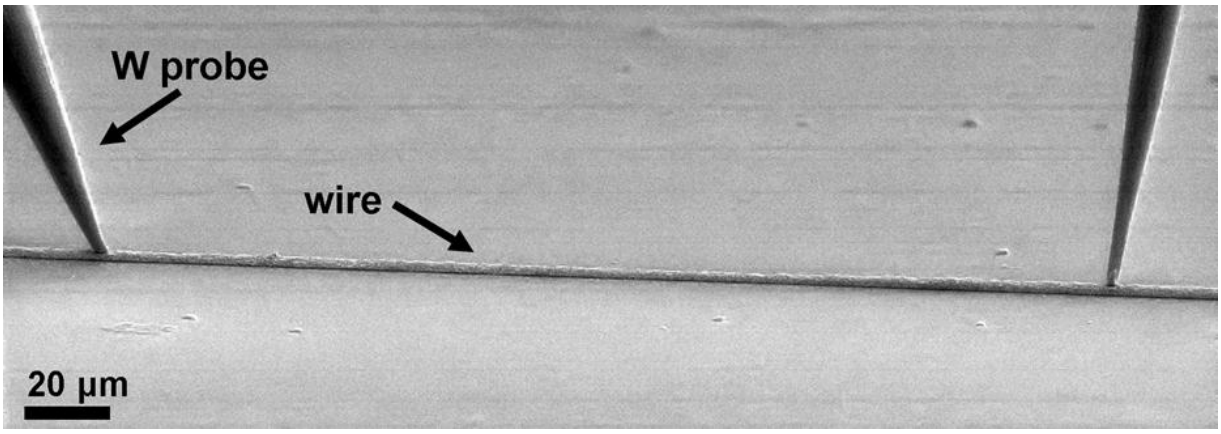

Figure 59. SEM images showing the tungsten nanoprobes in contact with an MPL-generated wire fabricated onto a glass cover slip.

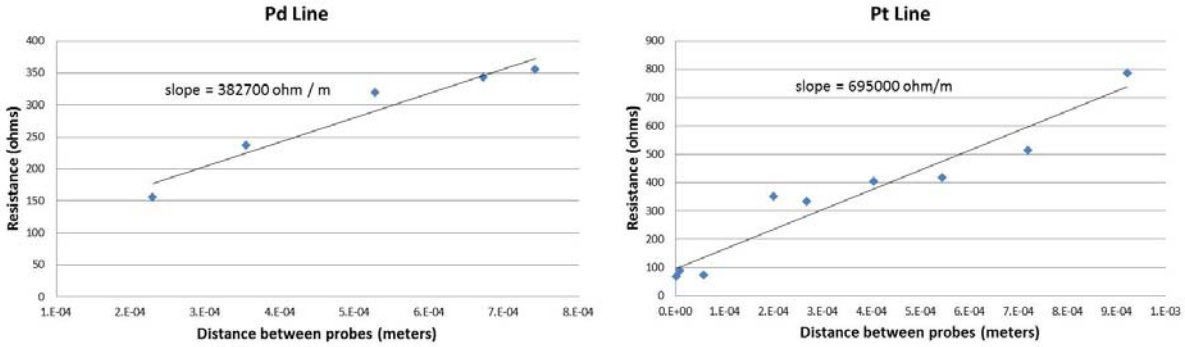

Figure 60. Graphs show the measured resistance versus distance between probes for a Pt and a Pd line drawn on glass. Resistivity was calculated by multiplying the slope by the cross sectional area of the line (2 µm x 3 µm).

Incorporation of Pt and Pd Catalysts into 3D Microenvironments

The emerging field of synthetic catalytic nanomotors and pumps provides an exciting testbed to explore nanomaterials with life-like energy conversion strategies.[61c, 89, 96, 112] To achieve the work necessary to directionally power such devices generally requires asymmetric placement of the catalyst in relation to the surrounding environment in order to generate net

directional motion and flow.[101b, c, 113] MPL enables arbitrary 3D structures to be readily designed and fabricated, allowing functional/asymmetric geometries to be rapidly prototyped. We explored Pt catalyzed decomposition of hydrogen peroxide to generate directed fluid and particulate flow within 3D micro-chambers and channels.

In Figure 61a, a Pt pad was patterned onto glass and then encased within a photo-crosslinked protein chamber containing a self-crossing spiral outlet. Addition of 1% H_2O_2 resulted in continuous and directed flow of oxygen through the spiral as the peroxide substrate could be replenished at the catalytic site, for the most part, via diffusion across the protein hydrogel chamber walls and ceiling, thereby allowing the majority of the spiral channel to maintain constant O_2 pressure. In contrast, directing the oxygen outflow into an asymmetric channel (Figure 61b) resulted in a peristalsis-like effect on the channel, with the channel fluid periodically compressed and released by the oxygen bubble evolution and resultant negative pressure developed upon outflow. Pumping is illustrated by the directional transport of microspheres at relatively high velocities (up to ca. 60 μm s^{-1}) through the channel (Figure 61b). Importantly, this approach offers greater flexibility versus existing techniques[101a, 101c] in the design of autonomously powered microfluidics.

Finally, we explored Pt patterning within a preformed 3D microenvironment. Unfortunately, formation of metallic pads on protein substrates resulted in deformation of the protein support. However, this challenge was overcome by developing a silica composite[114] which provided sufficient mechanical reinforcement of the structural surfaces defined by the protein template to withstand the subsequent heat generated during metal deposition. We designed a geometry where gas flow is forced downward, underneath the catalyst, to exit into the surrounding fluid (Figure 61c and Figure 62). Traversing the imaging plane through the

structure shows that the gas generated from the top chamber is directed underneath the Pt catalyst, demonstrating high resolution integration of a metallic component that is otherwise unachievable without 3D lithographic control.

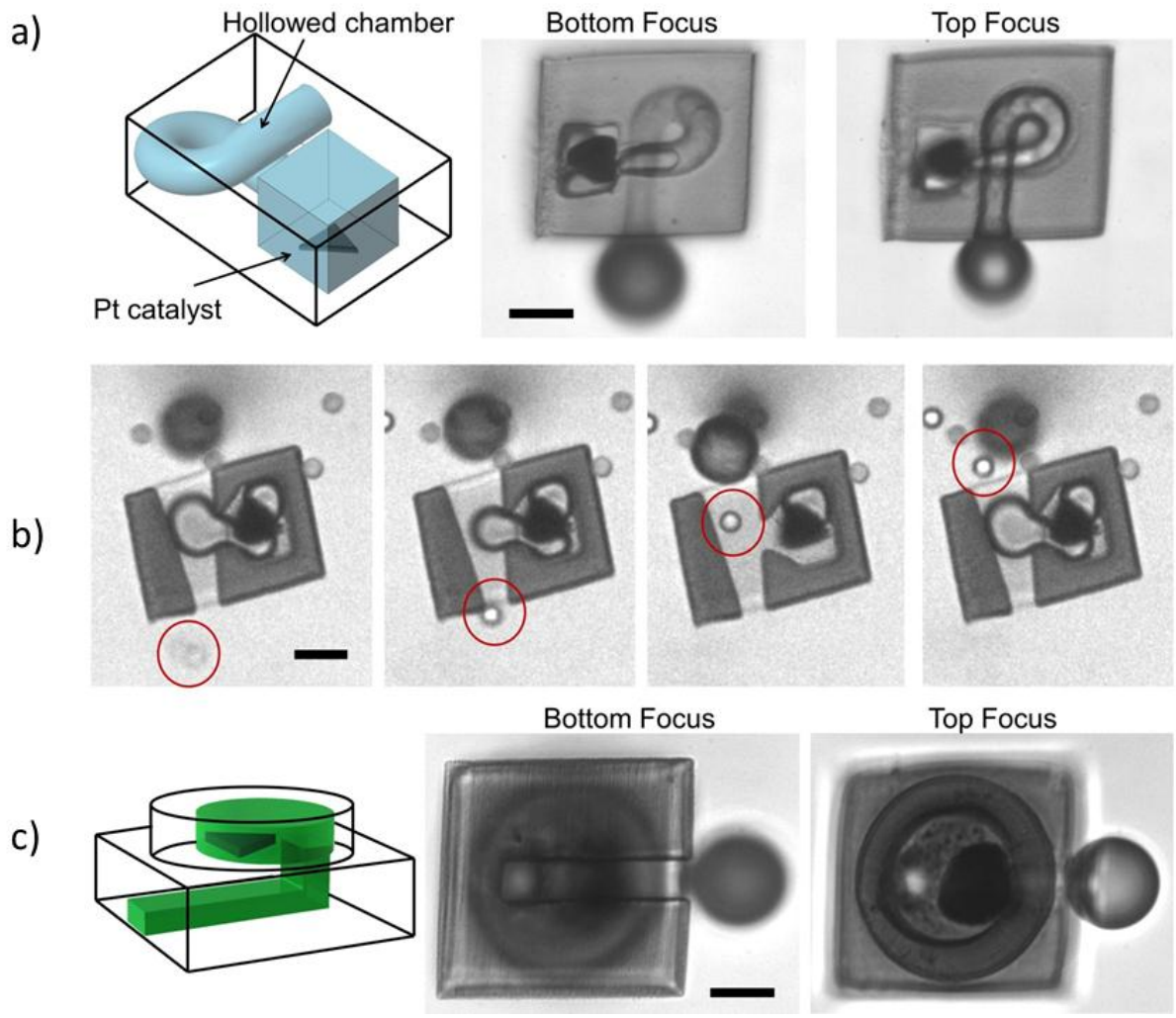

Figure 61. a) A Pt catalyst contained in a protein chamber directs gas through a self-crossing spiral channel. b) The directional outflow of gas produced at an MPL-Pt catalyst contained in a microchamber pumps a 5 µm particle (circled in red) through the asymmetric channel over approximately 1 second. c) An MPL-Pt catalyst printed inside the upper chamber of a 3D microchamber directs gas flow downwards underneath the catalyst. Scale = 10 µm.

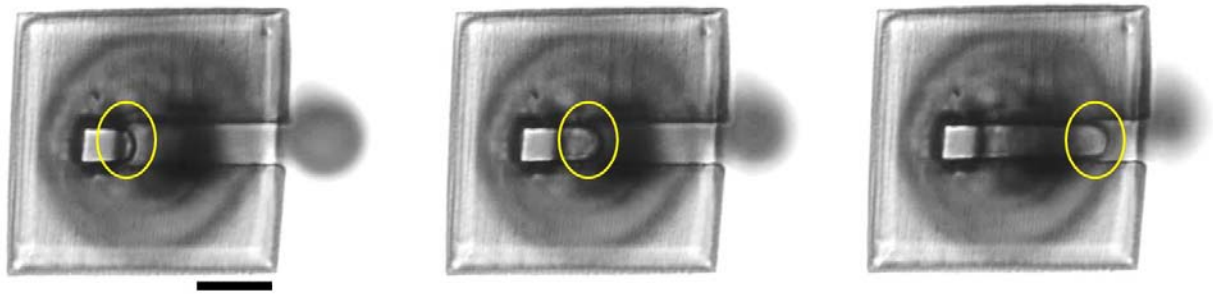

Figure 62. Images showing the meniscus of an air bubble (circled in yellow) traveling underneath the catalyst. This structure is the same as the one shown in Figure 61c, but the series of frames proves that the bubbles are indeed exiting the structure below the catalyst, which is out of focus. Scale = 10 μm.

Experimental

Instrumentation and Laser Fabrication: A Ti:sapphire laser (Tsunami, Spectra Physics) centered at 750 nm with a 60 fs pulse width and 80 MHz repetition rate was used as the light source for multiphoton excitation induced photoreduction. Structures were defined using mask-directed MPL as previously described.[100] Briefly, the laser focus was raster scanned with an X/Y open frame scan head (Nutfield Technology) across a digital micromirror device that served as a reflectance mask. The laser beam was adjusted to fill the back aperture of an oil-immersion objective (Nikon 100× Fluar, 1.3 NA) situated on a Nikon inverted microscope. Typically powers of 5 mW (following the focusing objective) were used. The X and Y frequencies of the laser scanner were set at 0.1 and 180 Hz respectively with a driving voltage of 0.7 V to produce a scan area of ~ 50 x 50 μm and thus a dwell time of 2.0 ms/μm^2. To fabricate wires and electrodes spanning hundreds of microns, the sample was translated axially at 10 μm/sec using a motorized stage (Applied Scientific Instrumentation). Microchambers were fabricated from

solution between two cover slips spaced by a 50 μm thick Teflon spacer. 3D structures described by a series of 2D images were fabricated from the top inner surface using 1 μm z-plane steps per image (15-40 images per structure), controlled with a nano-positioner (Mad City Labs). All aspects of laser fabrication were controlled via Labview software.

Pt and Pd Precursor Solutions and Sample Fabrication: Ammonium trisoxalatoferrate(III) trihydrate, ammonium tetrachloroplatinate(II), and ammonium tetrachloropalladate(II) were purchased from Sigma Aldrich and used as received. $(NH_4)_3[Fe(C_2O_4)_3]\cdot 3H_2O$ (1 M), $(NH_4)_2[PtCl_4]$ (0.7 M), and $(NH_4)_2\ [PdCl_4]$ (0.7 M) were prepared and stored in the dark at room temperature. A few hours prior to use, the Pt precursor solution (1:1 by volume $(NH_4)_3[Fe(C_2O_4)_3]$: $(NH_4)_2[PtCl_4]$) and Pd precursor solution (1:1 by volume $(NH_4)_3[Fe(C_2O_4)_3]$: $(NH_4)_2[PdCl_4]$) were prepared. 20 μL of precursor solution was placed on a glass cover slip and the laser focus was scanned through the solution. If the focus was set within the solution, free floating metal particles were generated, but if the laser was scanned near the surface of the glass cover slip, a solid, well adhered metal layer was written on the glass. Concentrations of Pt(II) or Pd(II) down to 0.0035 M and 0.007 M respectively were also sufficient for deposition, but required longer laser dwell times (~25 ms/μm^2) to form structures.

Fabrication of Protein and Silica Reinforced Structures: 3D protein structures were fabricated from bovine serum albumin via a method described elsewhere.[53] In short, 200 mg/mL BSA was dissolved in PBS and methylene blue (10 mM) was used as the photosensitizer. For catalyst deposition such as that shown in Figure 61c, structures were reinforced with a mechanically stable silica network using a recently described method.[114] Briefly, structures were heated to 45°C in phosphate buffered saline for 8 hours and subsequently incubated in a solution of 100 mM silicic acid, pH 3, 45°C, for 16 hours followed by rinsing in water.

Optical, SEM, EDS, and TEM Characterization: Optical imaging was done with the same Nikon inverted microscope setup used for MPL. Optical images and movies were captured using an Andor Ixon EMCCD. Structures that were to be imaged with SEM were produced on ITO coated cover slips and images were recorded using an FEI Quanta series SEM. This instrument was equipped with an EDS from EDAX which was used in imaging mode for elemental analysis of Pt and Pd. TEM was performed on a JEOL 2010, operating at an accelerating voltage of 200 kV and equipped with a Gatan slow scan CCD camera. TEM samples were prepared by scraping a MPL-Pt structure off a glass substrate and transferring the particles to a carbon-coated copper grid.

Electrical characterization: The resistivity of Pd and Pt wires (2 μm thick and 3 μm wide) fabricated on an insulating glass surface were measured using a two-probe nanomanipulator retro-fit inside of a JEOL 6701F scanning electron microscope. Current and voltage were measured and controlled using an Agilent B1500A Semiconductor Device Analyzer. Probe tips were polycrystalline tungsten wire electrochemically etched to an end radius of curvature of less than 250 nm. I-V curves were collected at different points across the length of the wire. The resistance at each point was then plotted and the resistivity was calculated using the slope of the linear fit.

Electrochemical Characterization: A several millimeter long Pt line was fabricated by MPL and electrochemically interrogated. Silver paint (SPI 05001-AB, SPI Supplies) provided an electrical contact to the potentiostat. Electrochemical measurements were performed on a PalmSens hand-held potentiostat (Palm Instruments BV, The Netherlands) or on a PGZ 100 Voltalab potentiostat (Radiometer Analytical, Lyon, France) and were measured versus an Ag/AgCl reference electrode (3 M) and a Pt coil counter electrode from Bioanalytical Systems

(West Lafayette, IN). MPL generated Pt electrodes were electrochemically cleaned by potential cycling from -0.265 to 1.2 V vs. Ag/AgCl in 1 M H_2SO_4 until a stable voltammogram was obtained (typically 20 cycles). For bulk Pt heterogeneous electron transfer rate measurements, 1.6 mm diameter Pt electrodes (Bioanalytical Systems) were first polished in 0.05 μm alumina slurry, followed by successive sonication in acetone and nanopure water. This was followed by electrochemical cleaning in 1 M H_2SO_4, as described above, with the exception that the lower potential limit was -0.2 V.

Conclusions

We have demonstrated that MPL of Pt and Pd facilitates the design of dynamic microsystems based on harnessing localized catalysis within 3D microenvironments to generate directed fluid and gas flow. These autonomous pumps and fluidics may be useful for flow generation, fluid mixing, propulsion, collection and transport. Additionally, MPL-Pt and Pd materials display excellent electronic and catalytic functionality; further enhancement is expected by exploring alloyed systems and controlling resolution and particle morphology using structure-directing agents[92b, 93, 110, 115] or electroplating techniques.[48] Fabrication of Pt and Pd structures with free-form, 3D architectures is currently being investigated through judicial variation of the chemical and environmental parameters in an effort to overcome the low structure fidelity incurred via laser heating.[102a, b, 110] The ability to prototype arbitrary 3D microscale electroactive and catalytic surfaces provides a new toolset with which to fabricate dynamic, 3D nano/microscale systems.

References

1. (a) Stuart, M. A. C.; Huck, W. T. S.; Genzer, J.; Müller, M.; Ober, C.; Stamm, M.; SukhorukovI, G. B.; Szleifer, I.; Tsukruk, V. V.; Urban, M.; Winnik, F.; Zauscher, S.; Luzinov, I.; Minko, S., Emerging applications of stimuli-responsive polymer materials. *Nature Materials* **2010,** *9*, 101-113; (b) Mather, P., Soft answers for hard problems. *Nature Materials* **2007,** *6*, 93-94; (c) Nelson, A., Stimuli-responsive polymers: engineering interactions. *Nature Materials* **2008,** *7*, 523-525.

2. Sambongi, Y.; Iko, Y.; Tanabe, M.; Omote, H.; Iwamoto-Kihara, A.; Ueda, I.; Yanagida, T.; Wada, Y.; Futai, M., Mechanical rotation of the c subunit oligomer in ATP synthase (F0F1): direct observation. *Science* **1999,** *286* (5445), 1722-1724.

3. Monod, J.; Changeux, J.-P.; Jacob, F., Allosteric proteins and cellular control systems. *Journal of Molecular Biology* **1963,** *6*, 306-329.

4. Christie, J. M.; Reymond, P.; Powell, G. K.; Bernasconi, P.; Raibekas, A. A.; Liscum, E.; Briggs, W. R., Arabidopsis NPH1: a flavoprotein with the properties of a photoreceptor for phototropism. *Science* **1998,** *282* (5394), 1698-1701.

5. Manson, M. D.; Tedesco, P.; Berg, H. C.; Harold, F. M.; Van Der Drift, C., A protonmotive force drives bacterial flagella. *Proceedings of the National Academy of Sciences* **1977,** *74* (7), 3060.

6. Alon, U.; Surette, M. G.; Barkai, N.; Leibler, S., Robustness in bacterial chemotaxis. *Nature* **1999,** *397* (6715), 168-171.

7. Fratzl, P.; Barth, F. G., Biomaterial systems for mechanosensing and actuation. *Nature* **2009,** *462*, 442-448.

8. Satir, P., The physiology of cilia and mucociliary interactions. *Annual Review of Physiology* **1990,** *52*, 137-155.

9. Ghyoot, M.; Ridder, C. D.; Jangoux, M., Fine structure and presumed functions of the pedicellariae of Echinocardium cordatum (Echinodermata, Echinoida). *Zoomorphology* **1987,** *106*, 279-288.

10. Sutherland, R. L.; Mäthger, L. M.; Hanlon, R. T.; Urbas, A. M.; Stone, M. O., Cephalopod coloration model. I. Squid chromatophores and iridophores. *Journal of the Optical Society of America* **2008,** *25* (3), 588-599.

11. Jiang, F. X. a. L., Bio-inspired, smart, multiscale interfacial materials. *Advanced Materials* **2008,** *20*, 2842-2858.

12. Zhou, Z.-g.; Liu, Z.-w., Biomimetic cilia based on MEMS technology. *Journal of Bionic Engineering* **2008,** *5*, 358-365.

13. Evans, B. A.; Shields, A. R.; Carroll, R. L.; Washburn, S.; Falvo, M. R.; Superfine, R., Magnetically actuated nanorod arrays as biomimetic cilia. *Nano Letters* **2007,** *7*, 1428-1434.

14. (a) Tabata, O.; Hirasawa, H.; Aoki, S.; Yoshida, R.; Kokufuta, E., Ciliary motion actuator using self-oscillating gel. *Sensors and Actuators A* **2002,** *95*, 234-238; (b) Watanabe, T.; Akiyama, M.; Totani, K.; Kuebler, S. M.; Stellacci, F.; Wenseleers, W.; Braun, K.; Marder, S. R.; Perry, J. W., Photoresponsive hydrogel microstructure fabricated by two-photon initiated polymerization. *Advanced Functional Materials* **2002,** *12*, 611-614.

15. (a) Jeong, B.; Gutowska, A., Lessons from nature: stimuli-responsive polymers and their biomedical applications. *Trends in Biotechnology* **2002,** *20*, 305-311; (b) Liu, F.; Urban, M. W., Recent advances and challenges in designing stimuli-responsive polymers. *Progress in Polymer Science* **2010,** *35* (1-2), 3-23.

16. Schild, H. G., Poly(*N*-isopropylacrylamide): experiment, theory, and application. *Progress in Polymer Science* **1992,** *17*, 163-249.

17. Zhou, X.; Weng, L.; Chen, Q.; Zhang, J.; Shen, D.; Li, Z.; Shao, M.; Xu, J., Investigation of pH sensitivity of poly(acrylic acid-co-acrylamide) hydrogel. *Polymer International* **2003,** *52*, 1153-1157.

18. Jochum, F. D.; Theato, P., Temperature-and light-responsive smart polymer materials. *Chemical Society Reviews* **2013**.

19. (a) Kataoka, K.; Miyazaki, H.; Bunya, M.; Okano, T.; Sakurai, Y., Totally synthetic polymer gels responding to external glucose concentration: their preparation and application to on-off regulation of insulin release. *Journal of the American Chemical Society* **1998,** *120*, 12694-12695; (b) Yang, H.; Liu, H.; Kang, H.; Tan, W., Engineering target-responsive hydrogels based on aptamer-target interactions. *Journal of the American Chemical Society* **2008,** *130*, 6320-6321.

20. (a) Zhao, B.; Moore, J. S., Fast pH- and ionic strength-responsive hydrogels in microchannels. *Langmuir* **2001,** *17*, 4758-4763; (b) Kozlovskaya, V.; Kharlampieva, E.; Mansfield, M. L.; Sukhishvili, S. A., Poly (methacrylic acid) hydrogel films and capsules: Response to pH and ionic strength, and encapsulation of macromolecules. *Chemistry of Materials* **2006,** *18* (2), 328-336.

21. Satarkar, N. S.; Hilt, J. Z., Magnetic hydrogel nanocomposites for remote controlled pulsatile drug release. *Journal of Controlled Release* **2008,** *130* (3), 246-251.

22. Yoshida, R.; Takahashi, T.; Yamaguchi, T.; Ichijo, H., Self-oscillating gel. *Journal of the American Chemical Society* **1996,** *118*, 5134-5135.

23. De, S. K.; Aluru, N. R., Equilibrium swelling and kinetics of pH-responsive hydrogels: models, experiments, and simulations. *Journal of Microelectromechanical Systems* **2002,** *11*, 544-555.

24. Sidorenko, A.; Krupenkin, T.; Taylor, A.; Fratzl, P.; Aizenberg, J., Reversible switching of hydrogel-actuated nanostructures into complex micropatterns. *Science* **2007,** *315*, 487-490.

25. Sidorenko, A.; Krupenkin, T.; Aizenberg, J., Controlled switching of the wetting behavior of biomimetic surfaces with hydrogel-supported nanostructures. *Journal of Materials Chemistry* **2008,** *18*, 3841-3846.

26. Kim, P.; Zarzar, L. D.; Zhao, X.; Sidorenko, A.; Aizenberg, J., Microbristle in gels: toward all-polymer reconfigurable hybrid surfaces. *Soft Matter* **2010,** *6*, 750-755.

27. Pokroy, B.; Epstein, A. K.; Persson-Gulda, M. C. M.; Aizenberg, J., Fabrication of bioinspired actuated nanostructures with arbitrary geometry and stiffness. *Advanced Materials* **2009,** *21*, 463-469.

28. Kim, P.; Epstein, A. K.; Khan, M.; Zarzar, L. D.; Lipomi, D. J.; Whitesides, G. M.; Aizenberg, J., Structural transformation by electrodeposition on patterned substrates (STEPS): a new versatile nanofabrication method. *Nano Letters* **2012,** *12*, 527–533.

29. Sumaru, K.; Ohi, K.; Takagi, T.; Kanamori, T.; Shinbo, T., Photoresponsive properties of poly(*N*-isopropylacrylamide) hydrogel partly modified with spirobenzopyran. *Langmuir* **2006,** *22*, 4353-4356.

30. (a) Yoshida, R., Self-oscillating polymer and gels as novel biomimetic materials. *Bulletin of the Chemical Society of Japan* **2008,** *81*, 676-688; (b) Shiraki, Y.; Yoshida, R., Autonomous intestine-like motion of tubular self-oscillating gel. *Angewandte Chemie International Edition* **2012,** *51*, 6112–6116.

31. Dhanarajan, A. P.; Misra, G. P.; Siegel, R. A., Autonomous chemomechanical oscillations in a hydrogel/enzyme system driven by glucose. *Journal of Physical Chemistry A* **2002,** *106*, 8835-8838.

32. (a) Tom N. Krupenkin; J. Ashley Taylor; Schneider, T. M.; Yang, S., From rolling ball to complete wetting: the dynamic tuning of liquids on nanostructured surfaces. *Langmuir* **2004,** *20*, 3824-3827; (b) McAuley, S. A.; Ashraf, H.; Atabo, L.; Chambers, A.; Hall, S.; Hopkins, J.; Nicholls, G., Silicon micromachining using a high-density plasma source. *Journal of Physics D: Applied Physics* **2001,** *34*, 2769–2774.

33. Zarzar, L. D.; Kim, P.; Aizenberg, J., Bio-inspired design of submerged hydrogel-actuated polymer microstructures operating in response to pH. *Advanced Materials* **2011,** *23*, 1442-1446.

34. Hong, W.; Zhao, X.; Suo, Z., Drying-induced bifurcation in a hydrogel-actuated nanostructure. *Journal of Applied Physics* **2008,** *104*, 084905.

35. He, X.; Aizenberg, M.; Kuksenok, O.; Zarzar, L. D.; Shastri, A.; Balazs, A. C.; Aizenberg, J., Synthetic homeostatic materials with chemo-mechano-chemical self-regulation. *Nature* **2012,** *487* (7406), 214-218.

36. May, E. L.; Hillier, A. C., Rapid and reversible generation of a microscale pH gradient using surface electric fields. *Analytical Chemistry* **2005,** *77*, 6487-6493.

37. Hong, W.; Liu, Z.; Suo, Z., Inhomogeneous swelling of a gel in equilibrium with a solvent and mechanical load. *International Journal of Solids and Structures* **2009,** *46*, 3282-3289.

38. Wilson, S. A.; Jourdain, R. P. J.; Zhang, Q.; Dorey, R. A.; Bowen, C. R.; Willander, M.; Wahab, Q. U.; Al-hilli, S. M.; Nur, O.; Quandt, E.; Johansson, C.; Pagounis, E.; Kohl, M.; Jatovic, M.; Samel, B.; van der Wijngaart, W.; Jager, E. W. H.; Carlsson, D.; Djinovic, Z.; Wegener, M.; Moldovan, C.; Iosub, R.; Abad, E.; Wendlandt, M.; Rusu, C.; Persson, K., New materials for micro-scale sensors and actuators:: an engineering review. *Materials Science and Engineering: R: Reports* **2007,** *56* (1-6), 1-129.

39. Hong, Y.; Blackman, N. M. K.; Kopp, N. D.; Sen, A.; Velegol, D., Chemotaxis of nonbiological colloidal rods. *Physical Review Letters* **2007,** *99* (17), 178103.

40. Yoshida, R., Design of functional polymer gels and their application to biomimetic materials. *Current Organic Chemistry* **2005,** *9*, 1617-1641.

41. Yoshida, R., Self-oscillating polymer gel as novel biomimetic materials exhibiting spatiotemporal structure. *Colloid and Polymer Science* **2011**.

42. Zarzar, L. D.; Liu, Q.; He, X.; Hu, Y.; Suo, Z.; Aizenberg, J., Multifunctional actuation systems responding to chemical gradients. *Soft Matter* **2012,** *8*, 8289-8293.

43. Marcombe, R.; Cai, S.; Hong, W.; Zhao, X.; Lapusta, Y.; Suo, Z., A theory of constrained swelling of a pH-sensitive hydrogel. *Soft Matter* **2010,** *6* (4), 784-793.

44. Bryant, S. J.; Hauch, K. D.; Ratner, B. D., Spatial patterning of thick poly(2-hydroxyethyl methacrylate) hydrogels. *Macromolecules* **2006,** *39*, 4395-4399.

45. Yu, T.; Ober, C. K., Methods for the topographical patterning and patterned surface modification of hydrogels based on hydroxyethyl methacrylate. *Biomacromolecules* **2003,** *4*, 1126-1131.

46. Wong, D. Y.; Griffin, D. R.; Reed, J.; Kasko, A. M., Photodegradable hydrogels to generate positive and negative features over multiple length scales. *Macromolecules* **2010,** *431*, 2824–2831.

47. Zarzar, L. D.; Kim, P.; Kolle, M.; Brinker, C. J.; Aizenberg, J.; Kaehr, B., Direct writing and actuation of 3D-patterned hydrogel pads on micropillar supports. *Angewandte Chemie International Edition* **2011,** *50*, 9356-9360.

48. LaFratta, C. N.; Fourkas, J. T.; Baldacchini, T.; Farrer, R. A., Multiphoton fabrication. *Angewandte Chemie International Edition* **2007,** *46*, 6238-6258.

49. Baldacchini, T.; LaFratta, C. N.; Farrer, R. A.; Teich, M. C.; Saleh, B. E. A.; Naughton, M. J.; Fourkas, J. T., Acrylic-based resin with favorable properties for three-dimensional two-photon polymerization. *Journal of Applied Physics* **2004,** *95*, 6072-6076.

50. (a) Campagnola, P. J.; Delguidice, D. M.; Epling, G. A.; Hoffacker, K. D.; Howell, A. R.; Pitts, o. D.; Goodman, S. L., 3-Dimensional submicron polymerization of acrylamide by multiphoton excitation of xanthene dyes. *Macromolecules* **2000,** *33*, 1511-1513; (b) Li, S.; Li, L.; Wub, F.; Wang, E., A water-soluble two-photon photopolymerization initiation system: Methylated-β-cyclodextrin complex of xanthene dye/aryliodonium salt. *Journal of Photochemistry and Photobiology A: Chemistry* **2009,** *203*, 211-215; (c) Jhaveri, S. J.; McMullen, J. D.; Sijbesma, R.; Tan, L.-S.; Zipfel, W.; Ober, C. K., Direct three-dimensional microfabrication of hydrogels via two-photon lithography in aqueous solution. *Chemistry of Materials* **2009,** *21*, 2003-2005.

51. Kaehr, B.; Shear, J. B., Multiphoton fabrication of chemically responsive protein hydrogels for microactuation. *Proceedings of the National Academy of Sciences* **2008,** *105*, 8850-8854.

52. Maruo, S.; Fourkas, J. T., Recent progress in multiphoton microfabrication. *Laser and Photonics Reviews* **2008,** *2*, 100-111.

53. Nielson, R.; Kaehr, B.; Shear, J. B., Microreplication and design of biological architectures using dynamic-mask multiphoton lithography. *Small* **2009,** *5*, 120-125.

54. Behkam, B.; Sitti, M., Bacterial flagella-based propulsion and on/off motion control of microscale objects. *Applied Physics Letters* **2007,** *90*, 023902-1-3.

55. Motoi Oishi, H. H., Teppei Uno, Takehiko Ishii, Michihiro Iijima,; Nagasaki, Y., One-pot synthesis of pH-responsive PEGylated nanogels containing gold nanoparticles by autoreduction of chloroaurate ions within nanoreactors. *Macromolecular Chemistry and Physics* **2007,** *208*, 1176-1182.

56. Heredia, K. L.; Tolstyka, Z. P.; Maynard, H. D., Aminooxy end-functionalized polymers synthesized by ATRP for chemoselective conjugation to proteins. *Macromolecules* **2007,** *40*, 4772-4779.

57. Lin, D. C.; Yurke, B.; Langrana, N. A., Inducing reversible stiffness changes in DNA-crosslinked gels. *Journal of Materials Research* **2005,** *20*, 1456-1464.

58. Okeyoshi, K.; Yoshida, R., Oxygen-generating gel systems induced by visible light. *Advanced Functional Materials* **2010,** *20*, 708-714.

59. Podual, K.; III, F. J. D.; Peppas, N. A., Glucose-sensitivity of glucose oxidase-containing cationic copolymer hydrogels having poly(ethylene glycol) grafts. *Journal of Controlled Release* **2000,** *67*, 9-17.

60. He, X.; Friedlander, R. S.; Zarzar, L. D.; Aizenberg, J., Chemo-mechanically regulated oscillation of an enzymatic reaction. *Chemistry of Materials* **2013,** *25* (4), 521-523.

61. (a) Fritz, J.; Baller, M.; Lang, H.; Rothuizen, H.; Vettiger, P.; Meyer, E.; Güntherodt, H.-J.; Gerber, C.; Gimzewski, J., Translating biomolecular recognition into nanomechanics. *Science* **2000,** *288* (5464), 316-318; (b) Lahann, J.; Langer, R., Smart materials with dynamically controllable surfaces. *MRS Bulletin* **2005,** *30* (03), 185-188; (c) Paxton, W. F.; Sundararajan, S.; Mallouk, T. E.; Sen, A., Chemical locomotion. *Angewandte Chemie International Edition* **2006,** *45* (33), 5420-5429.

62. (a) Ariga, K.; Mori, T.; Hill, J. P., Control of nano/molecular systems by application of macroscopic mechanical stimuli. *Chemical Science* **2011,** *2* (2), 195-203; (b) Todres, Z. V., Organic mechanochemistry and its practical applications. *CRC / Taylor & Francis* **2006**.

63. Philippova, O. E.; Hourdet, D.; Audebert, R.; Khokhlov, A. R., pH-Responsive gels of hydrophobically modified poly(acrylic acid). *Macromolecules* **1997,** *30*, 8278-8285.

64. Alvarez, S. G.; Alvarez, M. T., A Practical procedure for the synthesis of alkyl azides at ambient temperature in dimethyl sulfoxide in high purity and yield. *ChemInform* **1997,** *28* (39).

65. Bates, C. G.; Saejueng, P.; Murphy, J. M.; Venkataraman, D., Synthesis of 2-arylbenzo[*b*]furans via copper(I)-catalyzed coupling of *o*-iodophenols and aryl acetylenes. *Organic Letters* **2002,** *4* (26), 4727-4729.

66. Mammoto, T.; Ingber, D. E., Mechanical control of tissue and organ development. *Development* **2010,** *137* (9), 1407-1420.

67. Chen, C. S.; Mrksich, M.; Huang, S.; Whitesides, G. M.; Ingber, D. E., Geometric control of cell life and death. *Science* **1997,** *276* (5317), 1425-1428.

68. Maniotis, A. J.; Bojanowski, K.; Ingber, D. E., Mechanical continuity and reversible chromosome disassembly within intact genomes removed from living cells. *Journal of Cellular Biochemistry* **1997,** *65* (1), 114-130.

69. Farge, E., Mechanical induction of Twist in the *Drosophila* foregut/stomodeal primordium. *Current Biology* **2003,** *13* (16), 1365-1377.

70. Brown, T. D., Techniques for mechanical stimulation of cells in vitro: a review. *Journal of Biomechanics* **2000,** *33* (1), 3-14.

71. Qiu, Y.; Park, K., Environment-sensitive hydrogels for drug delivery. *Advanced Drug Delivery Reviews* **2012**.

72. Shimizu, S.; Yamazaki, M.; Kubota, S.; Ozasa, T.; Moriya, H.; Kobayashi, K.; Mikami, M.; Mori, Y.; Yamaguchi, S., In nitro studies on a new method for islet microencapsulation using a thermoreversible gelation polymer, *N*-Isopropylacrylamide-based copolymer. *Artificial Organs* **1996,** *20* (11), 1232-1237.

73. Stile, R. A.; Burghardt, W. R.; Healy, K. E., Synthesis and characterization of injectable poly (N-isopropylacrylamide)-based hydrogels that support tissue formation in vitro. *Macromolecules* **1999,** *32* (22), 7370-7379.

74. (a) Okano, T.; Yamada, N.; Sakai, H.; Sakurai, Y., A novel recovery system for cultured cells using plasma-treated polystyrene dishes grafted with poly(*N*-isopropylacrylamide). *Journal of Biomedical Materials Research* **2004,** *27* (10), 1243-1251; (b) Akiyama, Y.; Kikuchi, A.; Yamato, M.; Okano, T., Ultrathin poly (N-isopropylacrylamide) grafted layer on polystyrene surfaces for cell adhesion/detachment control. *Langmuir* **2004,** *20* (13), 5506-5511.

75. Stile, R. A.; Healy, K. E., Thermo-responsive peptide-modified hydrogels for tissue regeneration. *Biomacromolecules* **2001,** *2* (1), 185-194.

76. Wang, J.; Chen, L.; Zhao, Y.; Guo, G.; Zhang, R., Cell adhesion and accelerated detachment on the surface of temperature-sensitive chitosan and poly(*N*-isopropylacrylamide) hydrogels. *Journal of Materials Science: Materials in Medicine* **2009,** *20* (2), 583-590.

77. Ohya, S.; Kidoaki, S.; Matsuda, T., Poly(*N*-isopropylacrylamide)(PNIPAM)-grafted gelatin hydrogel surfaces: interrelationship between microscopic structure and mechanical property of surface regions and cell adhesiveness. *Biomaterials* **2005,** *26* (16), 3105-3111.

78. Kim, M. R.; Jeong, J. H.; Park, T. G., Swelling induced detachment of chondrocytes using RGD-modified poly (*N*-isopropylacrylamide) hydrogel beads. *Biotechnology Progress* **2002,** *18* (3), 495-500.

79. Mammoto, T.; Mammoto, A.; Torisawa, Y.; Tat, T.; Gibbs, A.; Derda, R.; Mannix, R.; de Bruijn, M.; Yung, C. W.; Huh, D.; Ingber, D. E., Mechanochemical control of mesenchymal condensation and embryonic tooth organ formation. *Developmental Cell* **2011,** *21*, 758-769.

80. Oster, G. F.; Murray, J. D.; Harris, A., Mechanical aspects of mesenchymal morphogenesis. *Journal of Embryology and Experimental Morphology* **1983,** *78* (1), 83-125.

81. Hern, D. L.; Hubbell, J. A., Incorporation of adhesion peptides into nonadhesive hydrogels useful for tissue resurfacing. *Journal of Biomedical Materials Research* **1998,** *39* (2), 266-276.

82. Annabi, N.; Nichol, J. W.; Zhong, X.; Ji, C.; Koshy, S.; Khademhosseini, A.; Dehghani, F., Controlling the porosity and microarchitecture of hydrogels for tissue engineering. *Tissue Engineering Part B: Reviews* **2010,** *16* (4), 371-383.

83. (a) Das, M.; Zhang, H.; Kumacheva, E., Microgels: old materials with new applications. *Annual Review of Materials Research* **2006,** *36*, 117-142; (b) Howse, J. R.; Topham, P.; Crook, C. J.; Gleeson, A. J.; Bras, W.; Jones, R. A. L.; Ryan, A. J., Reciprocating Power Generation in a Chemically Driven Synthetic Muscle. *Nano Letters* **2005,** *6* (1), 73-33.

84. (a) Beebe, D. J.; Moore, J. S.; Bauer, J. M.; Qing Yu; Liu, R. H.; Devadoss, C.; Jo, B.-H., Functional hydrogel structures for autonomous flow control inside microfluidic channels. *Nature* **2000,** *404*, 588-590; (b) David T. Eddington, D. J. B., Flow control with hydrogels. *Advanced Drug Delivery Reviews* **2004,** *56*, 199-210.

85. (a) Aguirre, C. I.; Reguera, E.; Stein, A., Tunable colors in opals and inverse opal photonic crystals. *Advanced Materials* **2010,** *20*, 2565–2578; (b) Tellis, J. C.; Strulson, C. A.; Myers, M. M.; Kneas, K. A., Relative humidity sensors based on an environment-sensitive fluorophore in hydrogel films. *Analytical Chemistry* **2010**; (c) Richter, A.; Paschew, G.; Klatt, S.; Lienig, J.; Arndt, K.-F.; Adler, H.-J. P., Review on hydrogel-based pH sensors and microsensors. *Sensors* **2008,** *8* (1), 561-581.

86. (a) Bassil, M.; Davenasb, J.; Tahchia, M. E., Electrochemical properties and actuation mechanisms of polyacrylamide hydrogel for artificial muscle application. *Sensors and Actuators B: Chemical* **2008,** *134*, 496–501; (b) Gerlach, G.; Arndt, K.-F., *Hydrogel sensors and actuators: engineering and technology*. Springer: 2009; Vol. 6.

87. Andersen, E. S.; Dong, M.; Nielsen, M. M.; Jahn, K.; Subramani, R.; Mamdouh, W.; Golas, M. M.; Sander, B.; Stark, H.; Oliveira, C. L. P., Self-assembly of a nanoscale DNA box with a controllable lid. *Nature* **2009,** *459* (7243), 73-76.

88. Catchmark, J. M.; Subramanian, S.; Sen, A., Directed Rotational Motion of Microscale Objects Using Interfacial Tension Gradients Continually Generated via Catalytic Reactions. *Small* **2005,** *1*, 202-206.

89. Wang, J., Can man-made nanomachines compete with nature biomotors? *ACS Nano* **2009,** *3* (1), 4-9.

90. Ismagilov, R. F.; Schwartz, A.; Bowden, N.; Whitesides, G. M., Autonomous movement and self-assembly. *Angewandte Chemie* **2002,** *114* (4), 674-676.

91. Paxton, W. F.; Kistler, K. C.; Olmeda, C. C.; Sen, A.; Angelo, S. K. S.; Cao, Y.; Mallouk, T. E.; Lammert, P. E.; Crespi, V. H., Catalytic nanomotors: Autonomous movement of striped nanorods. *Journal of the American Chemical Society* **2004,** *126* (41), 13424-13431.

92. (a) Baldacchini, T.; Pons, A.-C.; Pons, J.; LaFratta, C. N.; Fourkas, J. T., Multiphoton laser direct writing of two dimensional silver structures. *Optics Express* **2005,** *13*, 1275-1280; (b)

Cao, Y.-Y.; Dong, X.-Z.; Takeyasu, N.; Tanaka, T.; Zhao, Z.-S.; Duan, X.-M.; Kawata, S., Morphology and size dependence of silver microstructures in fatty salts-assisted multiphoton photoreduction microfabrication. *Applied Physics A* **2009,** *96*, 453–458; (c) Maruo, S.; Saeki, T., Femtosecond laser direct writing of metallic microstructures by photoreduction of silver nitrate in a polymer matrix. *Optics Express* **2008,** *16*, 1174-1179; (d) Kaneko, K.; Sun, H.-B., Two-photon photoreduction of metallic nanoparticle gratings in a polymer matrix. *Applied Physics Letters* **2003,** *83*, 1426-1428.

93. Chen, A.; Holt-Hindle, P., Platinum-based nanostructured materials: synthesis, properties, and applications. *Chemical Reviews* **2010,** *110*, 3767–3804.

94. Haeberle, S.; Roth, G.; von Stetten, F.; Zengerle, R., Microfluidic lab-on-a-chip platforms: requirements, characteristics and applications. *Chemical Society Reviews* **2010,** *39* (3), 1153-1182.

95. (a) Liao, Y.; Song, J.; Li, E.; Luo, Y.; Shen, Y.; Chen, D.; Cheng, Y.; Xu, Z.; Sugioka, K.; Midorikawa, K., Rapid prototyping of three-dimensional microfluidic mixers in glass by femtosecond laser direct writing. *Lab on a Chip* **2012,** *12* (4), 746-749; (b) Ke, K.; Hasselbrink Jr, E. F.; Hunt, A. J., Rapidly prototyped three-dimensional nanofluidic channel networks in glass substrates. *Analytical Chemistry* **2005,** *77* (16), 5083-5088.

96. Mei, Y.; Solovev, A. A.; Sanchez, S.; Schmidt, O. G., Rolled-up nanotech on polymers: from basic perception to self-propelled catalytic microengines. *Chemical Society Reviews* **2011,** *40*, 2109-2119.

97. (a) Iles, A.; Habgood, M.; de Mello, A. J.; Wootton, R. C., A Simple technique for microfluidic heterogeneous catalytic hydrogenation reactor fabrication. *Catalysis Letters* **2007,** *114* (1), 71-74; (b) Urakawa, A.; Trachsel, F.; von Rohr, P. R.; Baiker, A., On-chip Raman analysis of heterogeneous catalytic reaction in supercritical CO2: phase behaviour monitoring and activity profiling. *Analyst* **2008,** *133* (10), 1352-1354.

98. Xu, B. B.; Zhang, R.; Liu, X. Q.; Wang, H.; Zhang, Y. L.; Jiang, H. B.; Wang, L.; Ma, Z. C.; Ku, J. F.; Xiao, F. S., On-chip fabrication of silver microflower arrays as a catalytic microreactor for allowing in situ SERS monitoring. *Chemical Communications* **2012**.

99. Zarzar, L. D.; Swartzentruber, B. S.; Harper, J. C.; Dunphy, D. R.; Brinker, C. J.; Aizenberg, J.; Kaehr, B., Multiphoton lithography of nanocrystalline platinum and palladium for site-specific catalysis in 3D microenvironments. *Journal of the American Chemical Society* **2012,** *134*, 4007-4010.

100. Kaehr, B.; Shear, J. B., Mask-directed multiphoton lithography. *Journal of the American Chemical Society* **2007,** *129*, 1904-1905.

101. (a) Kline, T. R.; Paxton, W. F.; Wang, Y.; Velegol, D.; Mallouk, T. E.; Sen, A., Catalytic micropumps: Microscopic convective fluid flow and pattern formation. *Journal of the American Chemical Society* **2005,** *127* (49), 17150-17151; (b) Solovev, A. A.; Mei, Y.; Uren˜a, E. B. d.;

Huang, G.; Schmidt, O. G., Catalytic microtubular jet engines self-propelled by accumulated gas bubbles. *Small* **2009,** *5*, 1688–1692; (c) Solovev, A. A.; Sanchez, S.; Meiz, Y.; Schmidt, O. G., Tunable catalytic tubular micro-pumps operating at low concentrations of hydrogen peroxide. *Physical Chemistry Chemical Physics* **2011,** *13*, 10131–10135.

102. (a) Tanaka, T.; Ishikawa, A.; Kawata, S., Two-photon-induced reduction of metal ions for fabricating three-dimensional electrically conductive metallic microstructure. *Applied Physics Letters* **2006,** *88*, 081107-1-3; (b) Ishikawa, A.; Tanaka, T.; Kawata, S., Improvement in the reduction of silver ions in aqueous solution using two-photon sensitive dye. *Applied Physics Letters* **2006,** *89*, 113102-1-3; (c) Xu, B.-B.; Xia, H.; Niu, L.-G.; Zhang, Y.-L.; Sun, K.; Chen, Q.-D.; Xu, Y.; Lv, Z.-Q.; Li, Z.-H.; Misawa, H.; Sun, H.-B., Flexible nanowiring of metal on nonplanar substrates by femtosecond-laser-induced electroless plating. *Small* **2010,** *6*, 1762-1766.

103. Allen, R.; Nielson, R.; Wise, D. D.; Jason, B., Catalytic three-dimensional protein architectures. *Analytical Chemistry* **2005,** *77* (16), 5089-5095.

104. (a) Einaga, H.; Harada, M., Photochemical preparation of poly (N-vinyl-2-pyrrolidone)-stabilized platinum colloids and their deposition on titanium dioxide. *Langmuir* **2005,** *21* (6), 2578-2584; (b) Bai, L.; Zhu, H.; Thrasher, J. S.; Street, S. C., Synthesis and electrocatalytic activity of photoreduced platinum nanoparticles in a poly(ethylenimine) matrix. *ACS Applied Materials and Interfaces* **2009,** *1*, 2304-2311; (c) Harada, M.; Saijo, K.; Sakamoto, N., Characterization of metal nanoparticles prepared by photoreduction in aqueous solutions of various surfactants using UV–vis, EXAFS and SAXS. *Colloids and Surfaces A: Physicochemical and Engineering Aspects* **2009,** *349* (1), 176-188; (d) Sakamoto, Y.; Fukuoka, A.; Higuchi, T.; Shimomura, N.; Inagaki, S.; Ichikawa, M., Synthesis of platinum nanowires in organic-inorganic mesoporous silica templates by photoreduction: formation mechanism and isolation. *The Journal of Physical Chemistry B* **2004,** *108* (3), 853-858.

105. Ware, M., An Investigation of Platinum and Palladium Printing. *The Journal of Photographic Science* **1986,** *34*, 165-177

106. (a) Jiang, J.; Hall, T. D.; Tsagalas, L.; Hill, D. A.; Miller, A. E., Photographic production of metal nano-particles for fuel cell electrodes. *Journal of Power Sources* **2006,** *162*, 977-984; (b) Redjala, T.; Apostolecu, G.; Beaunier, P.; Mostafavi, M.; Etcheberry, A.; Uzio, D.; Thomazeaud, C. c.; Remita, H., Palladium nanostructures synthesized by radiolysis or by photoreduction. *New Journal of Chemistry* **2008,** *32*, 1403-1408.

107. (a) Porter, G. B.; Doering, J. G.; Karanka, S., Photolysis of transition metal oxalato complex ions. *Journal of the American Chemical Society* **1962,** *84* (21), 4027-4029; (b) Chen, J.; Zhang, H.; Tomov, I. V.; Rentzepis, P. M., Electron transfer mechanism and photochemistry of ferrioxalate induced by excitation in the charge transfer band. *Inorganic Chemistry* **2008,** *47* (6), 2024-2032.

108. Dollimore, D., The Thermal decomposition of oxataltes. a review. *Thermochimica Acta* **1987,** *117*, 331-363.

109. Gallagher, P. K.; Kurkjian, C. R., A Study of the thermal decomposition of some complex oxalates of iron (III) using the mössbauer effect. *Inorganic Chemistry* **1966,** *5*, 214-219.

110. Cao, Y.-Y.; Takeyasu, N.; Tanaka, T.; Duan, X.-M.; Kawata, S., 3D metallic nanostructure fabrication by surfactant-assisted multiphoton-induced reduction. *Small* **2009,** *5*, 1144–1148.

111. Cahill, D. G., Analysis of heat flow in layered structures for time-domain thermoreflectance. *Review of Scientific Instruments* **2004,** *75* (12), 5119-5122.

112. Paxton, W. F.; Baker, P. T.; Kline, T. R.; Wang, Y.; Mallouk, T. E.; Sen, A., Catalytically induced electrokinetics for motors and micropumps. *Journal of the American Chemical Society* **2006,** *128* (46), 14881-14888.

113. Kaehr, B.; Brinker, C. J., Using bacterial cell growth to template catalytic asymmetry. *Chemical Communications* **2010,** *46* (29), 5268-5270.

114. Khripin, C. Y.; Pristinski, D.; Dunphy, D. R.; Brinker, C. J.; Kaehr, B., Protein-directed assembly of arbitrary three-dimensional silica architectures. *ACS Nano* **2011,** *5*, 1401-1409.

115. Zhang, Y.-L.; Chen, Q.-D.; Xia, H.; Sun, H.-B., Designable 3D nanofabrication by femtosecond laser direct writing. *Nano Today* **2010,** *5*, 435-448.